# Towards global irrigation networks: from OpenStreetMap and elevation data plus the hydrological effects

Cases from the Netherlands, the Nile delta, the Indus basin and the Citarum basin

Ian van Zaanen
Student number: 5960819
MSc thesis, Utrecht University
Master Earth, Surface and Water, track Hydrology
Utrecht, May 2018

First supervisor: Dr. M.W. Straatsma
Second supervisor: Dr. L.P.H. van Beek

# Abstract

Water is essential for human life. Due to the increasing imbalance in freshwater availability and water demand, water scarcity is becoming a big problem. Irrigation accounts for 69% of the global water withdrawal and, therefore, global hydrological models are widely used to map water demand for irrigation. These models assume that surface water is taken from its nearest source and if there is no surface water available, it is taken from groundwater. Due to the absence of irrigation networks in these models, there is no explicit spatial link between irrigated areas and their surface water source. The aim of this study was to extract irrigation networks from OpenStreetMap (OSM) data and a global digital elevation model to create the link between rivers and irrigated areas. The method included three main steps: (1) processing the OSM water data (waterways and open water shapefiles), whereupon the OSM data was linked to a river, (2) subtracting urban areas and (3) excluding higher located areas with an elevation threshold. Thereafter individual irrigation networks were created. These networks were created on a 30 arcseconds resolution. Four different study areas were described, which are the Netherlands, the Nile delta, the Indus basin and the Citarum basin. Furthermore, the definition of the river source has been analysed. The OSM based irrigation networks were created on three minimum discharges, 100, 50 or 5 $m^3/s$, and the effects on the networks were analysed. Moreover, the irrigation networks were compared to the area equipped for irrigation reported by the Global Map of Irrigated Areas (GMIA). Finally, the networks were created for inclusion in a global hydrological model and therefore the hydrological effects of the irrigation networks were evaluated. The created networks were compared to raster-based irrigation networks with 60', 30' and 5' irrigated areas and evaluated for the water demand, actual evapotranspiration, discharges at the river mouth and water allocation fractions simulated by the global hydrological model PCR-GLOBWB. These water allocation fractions were compared to the fractions reported by the GMIA.

This specific method has successfully created irrigation networks. OSM data seems to be a good source for constructing irrigation networks. The definition of the river discharge as source affected the created irrigation networks. Smaller discharges created more and smaller networks. The choice of an irrigation network influenced several hydrological parameters. Total water withdrawal increased for the OSM and 60'networks compared to the 30' and 5' networks due to the increasing ability of allocating surface water. This indicated that the water demands for the 30' and 5' networks were not met. Actual evapotranspiration showed a more reliable spatial distribution for the OSM based irrigation networks compared to the 30' and 5' irrigated areas. This was best seen in arid regions, such as the Nile delta. Discharge at the river mouth was highly overestimated using the 30' and 5' networks and slightly overestimated using the 60' and OSM based irrigation networks. In general, water allocations fractions per water source were probably overestimated using the 60' networks due to the cell size of the 60' cells and were better computed using the OSM data, except for the Indus. The simulated water allocation fractions were spatially in line with the fractions reported by the GMIA. However, the validation statistics (Pearson correlation coefficient, Nash-Sutcliffe efficiency and the Percentage Bias) were in severe disagreement. This is probably due to the variability in irrigation extent between our irrigation networks and the ones created by the GMIA. So, OSM data can be used to create irrigation networks in future studies, however the OSM data needs to be improved.

# Table of contents

Abstract ..... 1
Acknowledgements ..... 4
1. Introduction ..... 5
1.1 Background ..... 5
1.2 Aim and objectives ..... 6
1.3 Approach ..... 6
1.4 Thesis outline ..... 7
2. Literature study ..... 8
2.1 Basic structure of an irrigation network ..... 8
2.1.1 Surface water availability ..... 8
2.1.2 Elevation ..... 9
2.2 Current implementation of irrigation networks within GHMs ..... 10
2.3 Model input data ..... 11
2.3.1 Digital elevation model ..... 11
2.3.2 Hydrological model PCR-GLOBWB2 ..... 11
2.4 Global Map of Irrigated Areas and its uncertainties ..... 14
3. Study areas ..... 16
3.1 The Netherlands ..... 17
3.2 Nile delta ..... 18
3.3 Indus basin ..... 19
3.4 Citarum basin (Java) ..... 20
4. Materials and methods ..... 21
4.1 OpenStreetMap and country data ..... 21
4.2 Developing irrigation network ..... 22
4.3 Definition of source of surface water for irrigation networks ..... 25
4.4 Comparison of irrigation networks to GMIA ..... 26
4.5 PCR-GLOBWB model setup and its hydrological effects of the choice of an irrigation network 27
4.5.1 Model run setup ..... 27
4.5.2 Hydrological effects ..... 27

4.6 Comparison of water allocation fractions to Global Map of Irrigated Areas ..... 28
5. Results ..... 30
5.1 Developed irrigation networks ..... 30
5.2 Effect of the definition of the surface source water for irrigation networks ..... 33
5.3 Compare developed irrigation networks to GMIA ..... 35
5.4 Hydrological effects of the choice of irrigation network ..... 37
5.4.1 Water demand ..... 37
5.4.2 Actual evapotranspiration ..... 37
5.4.3 Discharge at river mouth ..... 40
5.5 Comparison water allocation fractions ..... 40
5.5.1 Fraction of water allocation maps ..... 41
5.5.2 OSM and 60' networks ..... 43
5.5.3 Accuracy of OSM simulated water allocation ..... 43
6. Discussion & limitations ..... 45
6.1 Analyzing OSM irrigation networks ..... 45
6.1.1 Performance irrigation networks ..... 45
6.1.2 Limitations and inaccuracies of irrigation networks ..... 46
6.2 Effect of the definition of the source of surface water on irrigation networks ..... 48
6.3 Evaluating OSM networks to GMIA ..... 48
6.4 Estimation of the effect of the choice of irrigation networks ..... 49
6.4.1 Water demand ..... 49
6.4.2 Actual evapotranspiration ..... 50
6.4.3 Discharge at river mouth ..... 50
6.5 Evaluating the comparison water fractions against Global Map Irrigated Areas ..... 51
6.5.1 Fraction of water allocation maps ..... 51
6.5.2 OSM and 60' networks ..... 52
6.5.3 Accuracy of fraction of water allocation ..... 53
7. Conclusions ..... 54
8. Recommendations ..... 55
9. References ..... 56
Appendix A ..... 62
Appendix B ..... 63
Appendix C ..... 64

# Acknowledgements

I am using this opportunity to express my gratitude to my first supervisor Dr. Menno Straatsma, who provided me with insightful comments and suggestions during this MSc research project in the field of global irrigation modelling. Furthermore, I would to thank Dr. Rens van Beek who helped me understanding the PCR-GLOBWB model and I am gratefully indebted to his for his very valuable comments on this thesis. Last but not least, I would like to thank Chris Kerklaan and Danny do Quang for their valuable suggestions and overall help during this thesis and Lennart Verhoog and Harro Boven for peer-reviewing my thesis.

# 1. Introduction

## 1.1 Background

Water is the most essential resource for humans and society (Hanasaki *et al.*, 2008). The imbalance in freshwater availability and water demand causes water scarcity to be one of the biggest problems nowadays (UNEP, 2000; Wada, Van Beek and Bierkens, 2012). Water requirements, which are mainly for irrigation, have been increasing rapidly for the last five decades (Wada, van Beek, & Bierkens, 2011). Current estimates of the gross global water demand for irrigation range from 2400 to 2600 $km^3$/year around the year 2010 ( Wada, Wisser and Bierkens, 2014; FAO, 2016; Hanasaki *et al.*, 2018), which is 70% of the global water use from surface water (Siebert *et al.*, 2013). Considering the occurring global warming, altering the global water cycle (Kabat *et al.*, 2004), the low efficiency of many irrigation techniques (Brouwer *et al.*, 1988) and the rapid population growth, water scarcity is expected to become worse (United Nations, 2013; IPCC, 2014).

Surface water is one of the most easily available resources to meet the demand for irrigation water (van Beek, Wada and Bierkens, 2011). Given the pressure irrigation puts on global water resources and its prominent position in the food production, global hydrological models (GHMs) are widely used to evaluate projections of climate change and socio-economic developments on the global water demand. In absence of reliable global data on irrigation networks, such models usually follow a simple approach. First, to link water supply to water demand for irrigated crops: water is taken from the nearest source, such as (1) a river if a river is close by (blue water), (2) from local precipitated water that is temporarily stored in the ground (green water), and (3) in case there is no surface water available, it is taken from groundwater (Vorosmarty *et al.*, 2005; Wada, Van Beek and Bierkens, 2012). Most GHMs assume that an agriculture field within a cell is served by the river passing through it; it cannot receive water resources from a neighboring cell. This assumption works satisfactorily at coarser spatial resolutions, such as 1 or 0.5 arc-degrees (Wada, Van Beek and Bierkens, 2012). At these resolutions a two cell distance would allow a maximum distance of 111 km, or 55 km between river and irrigated area at the equator. However, this assumption no longer holds when moving towards finer spatial resolutions, such as 10 km, 1 km or 100 m. Irrigation networks can be large. Some of the networks, for example the Indus River in Pakistan, can be up to 200 km long and as a consequence 200 km away from their river source (Qureshi *et al.*, 2008). Hence, with the increasingly higher resolution of GHMs, representing the hydrological system in more detail, irrigation networks have to be defined explicitly to avoid inaccuracies in global (irrigation) water requirements.

Independent of the GHMs, only a few studies are known that determine irrigated areas globally (Thenkabail *et al.*, 2008; Siebert *et al.*, 2013; Salmon *et al.*, 2015). In 2009 a Global Irrigated Area Map (GIAM) was developed by the International Water Management Institute (IWMI). It was mainly based on satellite sensor data, and validated on Google Earth images and ground truth data (Thenkabail *et al.*, 2008). GIAM simulates data for 28 different crop types to ensure varying seasonality on a 10 km spatial resolution. More recently a Global Map of Irrigated Areas (GMIA) version 5 has been created by Siebert *et al.* (2013). They computed irrigation extent and fraction of irrigated volume per water source (surface water, groundwater and non-conventional) on 5 arcminutes (henceforth referred to as ’) cells. This map is based on ground truth information, literature, national reports (from provinces, districts and governates), online databases, together with reports from the Food and Agriculture Organization of the United Nations (FOA-AQUASTAT) database and the World Bank. Lately, the Global Rain-fed, Irrigated and Paddy Croplands (GRIPC) was published by Salmon *et al.*, (2015). This map depicts three agricultural land use classes: irrigated, rain-fed and paddy croplands at a 500 meter (m) spatial resolution. It is mainly based on the MODIS Land Cover Type database, yet it combines climate data and statistics. Due to large uncertainties within these maps, large differences in total area used for irrigation are computed. Thenkabail *et al.*

(2008) estimated 43% more globally irrigated area compared to Siebert *et al.*, (2013). Salmon *et al.* (2015) also showed a greater irrigated area compared to the national statistics. Latterly Meier, Zabel and Mauser (2017) constructed a new map called "downscaled GMIA". This study simply downscaled the GMIA map to a map of 30 arcseconds. 22% more irrigated area was estimated than the original GMIA. While such maps are widely used in GHMs to determine irrigation water demand, these maps do not link the source of the surface water to the area that is irrigated from that source. Therefore a new method is needed, since there is no digitized irrigation network database available (Haddeland *et al.*, 2014) and not all irrigated areas are officially registered.

Data to create the link between rivers and irrigated area is available on a global scale. First, OpenStreetMap (OSM) data can be used for information on local water distribution. OSM is an open-source database that provides information on waterways and free water (Weber and Haklay, 2008), which can be used for information on local canals or rivers. Furthermore, digital elevation models (DEMs), such as SRTM (Farr *et al.*, 2007) and MERIT DEM (Yamazaki *et al.*, 2017), are widely implemented in hydrological studies and are free available. DEMs can be used to determine local flow directions and the area that is available for irrigation. Moreover, global permanent water maps are available. These permanent water maps can be derived from the HydroSHEDS (Lehner, Verdin and Jarvis, 2008), HydroLAKES (Lehner and Messager, 2017) or from average discharge maps simulated by GHMs, such as PCR-GLOBWB (Sutanudjaja *et al.*, 2017) and H08 (Hanasaki *et al.*, 2018). They provide information on the location of surface water that can act as a source for irrigation networks. While these data is available, they are not yet providing the irrigation networks for use in GHMs.

## 1.2 Aim and objectives

The aim of this study was to develop a new method to create irrigation networks based on OpenStreetMap data together with a global digital elevation model. To assess the hydrological effects a GHM was used. The minor objectives were:

1. Develop irrigation networks that are connected to a river based on OpenStreetMap data and a global DEM.
2. Determine the sensitivity of the network shape, area and length to the definition of the surface water source.
3. Compare created irrigation networks to the area equipped for irrigation reported by the Global Map of Irrigated Areas.
4. Assess water demand, actual evapotranspiration, discharge as simulated with GHM PCR-GLOBWB for the OSM network and compare to raster-based irrigation networks of 60, 30 and 5'.
5. Compare simulated fraction of irrigated volume per water source for each cell for the OSM networks to the 60' networks and validate against the Global Map of Irrigated Areas.

## 1.3 Approach

To link a river to irrigated areas and to make GHMs independent of their scale this study used OSM data. In combination with a global DEM, irrigation networks were created and these networks were connected to their main river source. OSM was used to access the local water distribution and to determine the areas fed by the river source. However, some areas are also fed by groundwater and therefore there existed no link with surface water. The DEM was used as a threshold to define the area that is available for irrigation. Furthermore, urban area data from OSM were used as a second threshold. The sensitivity of the networks to the definition of the river source was performed using three different minimum river discharges. This river source was derived from an average river discharge map simulates by the PCR-GLOBWB model (Sutanudjaja *et al.*, 2017). The created irrigation

networks were in compared to the reported irrigated areas by the GMIA. To assess the hydrological effects of the created irrigation networks, the GHM PCR-GLOBWB was used at a spatial resolution of 5'. Four different irrigation networks have been used as input for surface water distribution and the effects have been evaluated for water demand, actual evapotranspiration, average discharge at the river mouth and water allocation per source (surface water and groundwater). The latter has been compared to the irrigated volume per source reported by the GMIA.

This study presents results of the Netherlands, an area that has little actually irrigated area, yet much OSM data available. Furthermore, two large irrigation networks, the Nile delta and the Indus Basin, are presented. Finally, the Citarum basin in Java is presented, which is interesting due to many small irrigation systems and limited availability in OSM data.

## 1.4 Thesis outline

First, this study presents a brief literature study about the structure of irrigation networks and their current implementation in GHMs, together description of an existing global irrigation map (Chapter 2). Second, the study areas are described in Chapter 3. Furthermore, the methods for creating the irrigation networks as well as the methods for the PCR-GLOBWB simulation and validation are described in Chapter 4. The results for both created irrigation networks and the analysis of the hydrological effects are provided in Chapter 5. Chapter 6 presents the discussion of the results and conclusions are drawn in Chapter 7. Chapter 8 suggests recommendations for further research.

# 2. Literature study

In this chapter the basic structure of irrigation networks is presented. Then, two main parameters (surface water availability and elevation) that determine size, length and shape of irrigation networks are reviewed. Subsequently, the current implementation of irrigation networks in GHMs is discussed. Furthermore, the used DEM is described and an description of the GHM PCR-GLOBWB, which is used for implementation of the created irrigation networks, is given as well as some of its evaluated hydrological parameters affected by the surface water distribution. Finally, The Global Map of Irrigated Area developed by Siebert *et al.*, (2013) is described together with its limitations.

## 2.1 Basic structure of an irrigation network

Most of the irrigation networks are fed by river water (Siebert *et al.*, 2010). In general these networks consist of many channels, which can be classified in different ways. Irrigation networks often consist of channel hierarchy, the biggest channel as the main channel, followed by the branch channel, major distributaries, minor distributaries and watercourse as the smallest channel (figure 2.1) (Asawa, 2008; NPTEL, 2016). The main channel receives its water supplies from the river and redirects the water to branch and secondary channels. The branch channels receive their water from the main canal and moves water towards the major distributaries. The major distributaries supply water to the minor distributaries and the water courses. These watercourses transport the water to the area to be irrigated (Asawa, 2008). In general, the structure and extent of an irrigation system is dependent on many factors, such as water availability and elevation.

### 2.1.1 Surface water availability

Rivers have been the prevailing surface water source for humans (Hanasaki *et al.*, 2018). 60 to 70 percent of the irrigation water is met by surface water (Siebert *et al.*, 2013) and therefore surface water availability is very important for irrigation. One of the main factors that determine surface water availability is discharge. Higher discharges are associated with higher surface water availability and thus more water is available for irrigation purposes. This influences the length of the irrigation canal and thereby the size of an irrigation network (FAO, 2016). Higher discharges are able to distribute more water towards the branch channels and thus the irrigated fields (Gaafar, El-agha and Rap, 2016). There is a huge variety in lengths of irrigation canals. Large irrigation canals are found along rivers with high average discharges, such as the Nile, the Indus and the Mississippi (Siebert *et al.*, 2015; FAO, 2011). In these networks, the length of an individual irrigation canal can be up to 200 km (Qureshi *et al.*, 2008). Within these large irrigation systems, such as the Nile delta, the branch channel receives its water often at a minimum average annual discharge of 5 $m^3/s$ from the main channel (Asawa, 2008). This is required to buffer for lower discharges during drier periods (Asawa, 2008). Lower discharges might not able to distribute enough water towards the fields (Gaafar, El-agha and Rap, 2016).

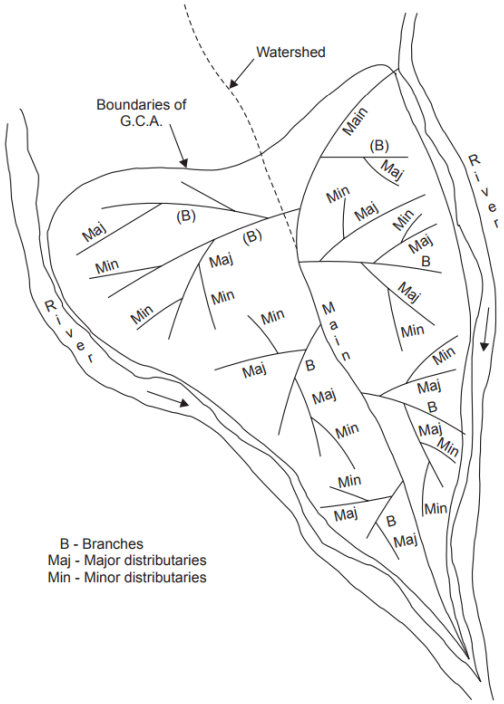


Figure 2.1: Layout of an irrigation canal network. The channel in the middle is the main channel. Bs are the branches, Majs are the major distributions and the Mins are the minor distributions (NPTEL, 2016).

### 2.1.2 Elevation

Elevation determines the shape and extent of an irrigation network. The typical shape of an irrigation system is often created due to channel alignment. In general, irrigation systems are built perpendicular on the contour lines, to enable the use of gravity to move water towards the crops without any costs for construction of pumps (figure 2.2a) (Brouwer *et al.,* 1988). The main channels are often built on a watershed divide between two valleys. This allows a larger irrigable area for the same canal, since water moves from the watershed towards the networks, as shown in the figure 2.2b. This results in an efficient as well as economic system. Concave shaped networks are expected to be created (Brouwer *et al.,* 1988). However in reality there are more factors that determine the shape of an irrigation system, since systems are, besides geography, also shaped by the society (such as urban areas). Both the human and the physical dimension of irrigation system have to be accounted for (Khanal, 2003). In mountainous areas the conditions are different, because the slope of the area is greater. In these situations, so called contour channels are built. These channels follow the contour lines while accounting for the slope of the channels (Asawa, 2008). Due to these higher elevation differences and the channels following the contour lines, v- shaped irrigation networks are often created (Delrieu *et al.*, 2005).

Elevation also determines the area that is suitable for irrigation. For optimal efficiency the slope may not be too high and very large slopes will make irrigation impossible (Brouwer *et al.,* 1988). Surface irrigation (furrow, basin and border) is the most dominant type of irrigation. Its prevalence around the world is 86% (FAO, 2016). It allows a maximum slope of 8%, whereas the slope can be up to 25% when terraces are built (Brouwer et al, 1988).

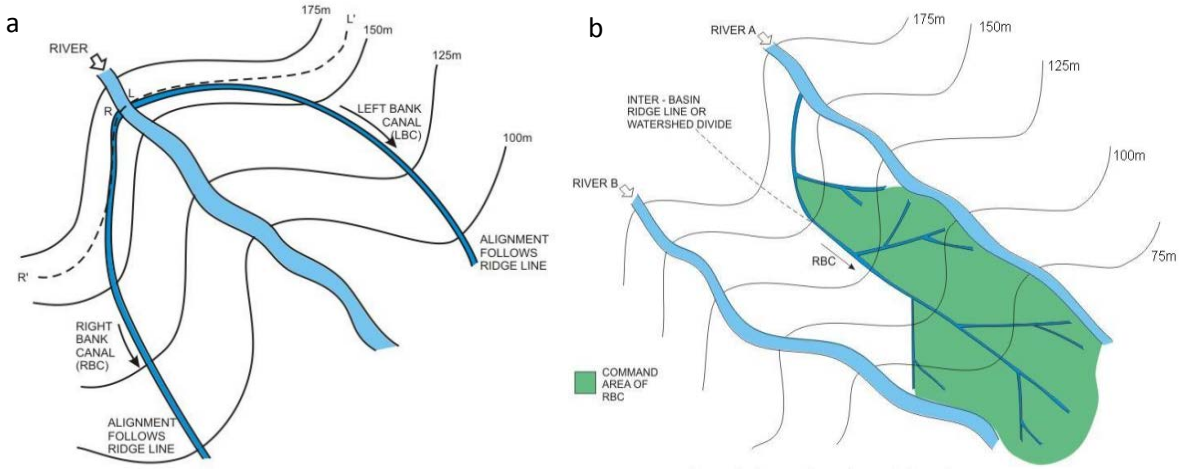


Figure 2.2: (a) Practical alignment of the irrigation canals. Irrigation canals are often aligned perpendicular on the contour lines. However due to practical issues they sometimes are partly aligned along them. (b) Irrigated area for canal system, whenever the canal is built up to a watershed divide (Kharagpur, 2012).

## 2.2 Current implementation of irrigation networks within GHMs

Currently, GHMs do not account for the shape and size of irrigation networks. Digitized irrigation networks are not yet available and therefore surface water distribution is based on allocation schemes or hypothetical algorithms. Different types of these algorithms are widely implemented in different hydrological models. PCR-GLOBWB, for example, implemented a dynamic allocation scheme that distributes surface water based on latitude-longitude extraction areas (figure 2.3a) (De Graaf *et al.*, 2014). Three different sizes of these schemes are available within the model, namely based on 60', 30' and 5' areas. At these resolutions these cells have sizes of 111 by 111 km, 55 by 55 km and 9 by 9 km at the equator. In the current version of PCR-GLOBWB, water availability is pooled over zones of approximately 60' around 5' cells, clipped by basin and country borders (Sutanudjaja *et al.*, 2017) (figure 2.3b). Rivers passing through this area feed the entire area; yet water exchange between 60' areas is not allowed and therefore surface water is restricted within a 60' area. As a consequence cells do not always have access to its nearest surface water source if this is situated outside the 60' area. Therefore the main disadvantage of this scheme is that it is fixed and that it does not reflect local networks (Sutanudjaja *et al.*, 2017),

In contrast to the prescribed allocation scheme, other GHMs, such as LPJ (Lund-Postdam-Jena) (Schaphoff *et al.*, 2018) and WaterGAP Global Hydrology Model (WGHM) (Hunger and Doll, 2008), have incorporated hypothetical algorithms. LPJ use fixed areas centred on the cell with demand (Sitch *et al.*, 2003). These grid cells are divided into fractional coverages of vegetation types, which determine the water demand (Schaphoff *et al.*, 2018). WGHM allows allocation from a neighbouring cell, whenever water requirements cannot be satisfied within a certain cell. Adjacent cells with the highest actual water storage are used as source (Hunger and Doll, 2008).

However, these algorithms are a highly conceptional approach and therefore H08, developed by Hanasaki *et al.* (2008), recently updated their scheme. They modelled water transfer from rivers towards further afield cells via aqueducts (Hanasaki *et al.*, 2018). The existence of aqueducts were confirmed from literature or were created when there was a major river present that would allocate water to cells nearby (if necessary). This partly solves the problem of not having access to neighbour or further located cells. However, the downside of this method is that only large water aqueducts are indicated and smaller systems are not yet accounted for (Hanasaki *et al.*, 2018).

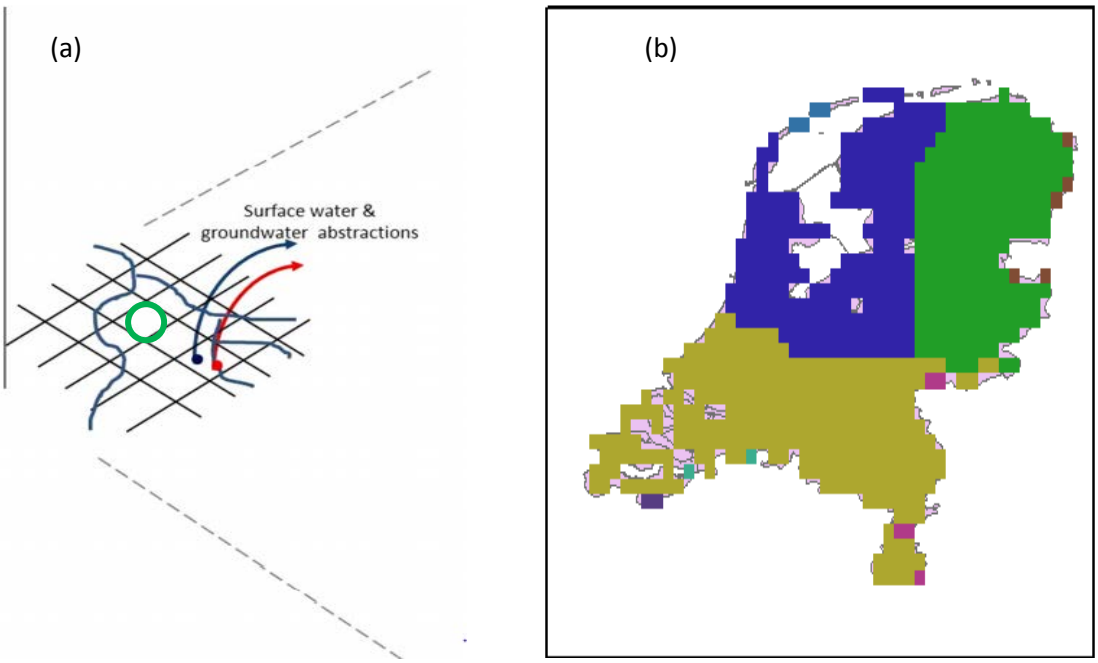


Figure 2.3: (a) The described allocation scheme by De Graaf *et al.* (2014). The green circle highlights a cell that is not connected with a main river source and therefore groundwater is abstracted. (b) Example of the 60' square extraction areas subdivide into 5' cells for the Netherlands. Each different colour indicates an individual irrigation network.

## 2.3 Model input data

### 2.3.1 Digital elevation model

River water distribution and its created irrigation networks are dependent on elevation (Brouwer *et al.,* 1988). To obtain elevation differences a DEM can be used. However, the quality (accuracy and resolution) vary substantially around DEMs. Recently, a new DEM was developed; the Multi-Error-Removed Improved-Terrain (MERIT DEM). Currently, it is the best available DEM for hydrological purposes. It is a combination of different DEMs and was optimized for global hydrodynamic models. For detailed information see Yamazaki *et al.* (2017). This DEM has a resolution of 3 arc seconds, which represents cells of approximately 90 by 90 m at the equator. To create a baseline for this new DEM, both SRTM3 DEM (Farr *et al.* 2007) (below N60° lat) and the AW3D-30 m DEM (above N60° lat) are used. However these DEMs contain some errors and observation gaps. These observation gaps were filled with the VFP-DEM (Viewfinder Panoramas DEM) developed by Gesch *et al.* (2014). To account for reference ground level errors, satellite data, such as the Ice, Cloud, and land Elevation Satellite (ICESat) was used (Harding and Carabajal, 2005). A combination of these DEMs removed the four major height errors in space borne DEMs. These errors are stripe noise, speckle noise, tree height bias and absolute bias (Yamazaki *et al.*, 2017). The accuracy of MERIT DEM has therefore been increased resulting in an error of only ± 2m. Data were provided in WGS 84 geographic coordinate system.

### 2.3.2 Hydrological model PCR-GLOBWB2

The GHM PCRaster GLOBal Water Balance model (PCR-GLOBWB 2) (Sutanudjaja *et al.*, 2017) is a grid-based model that describes the global water cycle. It is coded in PCRaster and can be implemented in Python with the PCRaster Python extension (Karssenberg *et al.*, 2010). For more detailed information see van Beek and Bierkens (2008). The current finest resolution is 5'. It calculates the water storage

for two vertical soil layers with a maximum depth of, respectively, 0.3 m and 1.2 m and with the underlying groundwater layer on a cell-by-cell basis for each time step, which is a day (Sutanudjaja *et al.*, 2017) ($S_1$+$S_2$ in figure 2.4). Water can exchange between the reservoirs, due to capillary rise and percolation ($S_3$ in figure 2.4) and between the top layer and de atmosphere, due to precipitation, evaporation and snowmelt. These vertical fluxes between the layers ($S_1$,$S_2$ and $S_3$) are mainly towards the groundwater layer. However, during dry periods with low soil moisture contents, the water can move upwards due to the forcing of capillary rise (Wada *et al.*, 2010). Water can also leave a cell laterally, by baseflow, overland flow and interflow. The sum of these three is the total runoff, which discharged towards lakes or the ocean following the selected river networks (Sutanudjaja *et al.*, 2017). Current global climate data containing precipitation, potential evaporation and temperature are used to force the model and to make future estimates (e.g. Climate Research Unit (CRU)) or with predicted parameters for from Global Climate models (van Beek, 2008). Actual evapotranspiration (AET) is calculated from potential evapotranspiration (PET). The AET is mainly based on the vegetation covers and crop factors. Furthermore, PCR-GLOBWB has many hydrological functions. It can calculate surface and groundwater availability, human water use and water withdrawals from surface water and groundwater (van Beek and Bierkens, 2008; Sutanudjaja *et al.*, 2017).

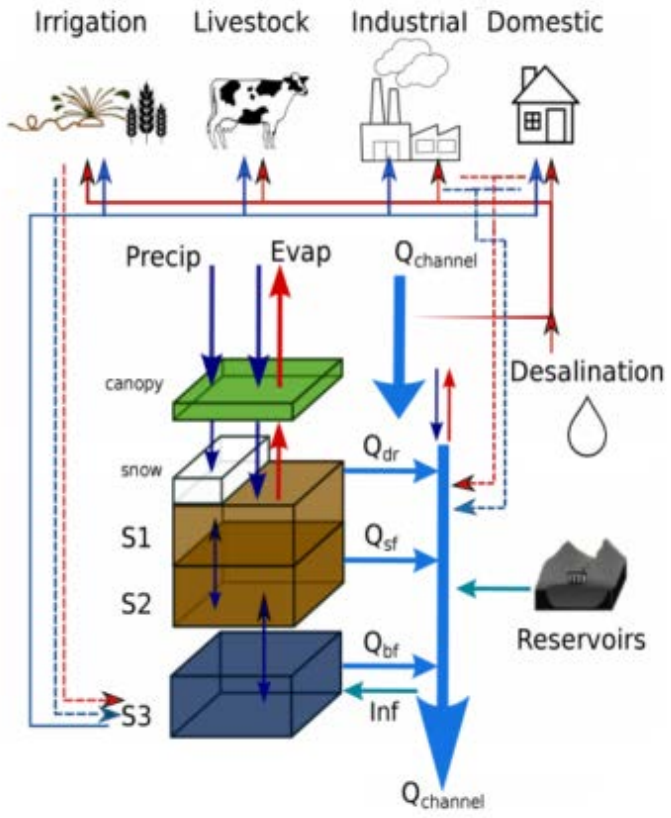


Figure 2.4: Schematic framework of cell within the PCR-GLOBWB 2 model with the modelled fluxed. The model contains four vertical layers: canopy layer, S1&S2 (soil moisture storage) and S3 (groundwater storage). The red lines indicate surface water abstraction and the blue lines groundwater abstraction (Sutanudjaja *et al.*, 2017).

PCR-GLOBWB consists of a water demand model (Wada *et al.*, 2012). Water demands, which vary with time, are estimated for livestock, industry, household and irrigation. The first three are a function of the population, electricity demand and gross domestic product (GDP) per capita. In addition, livestock water demand is the combination of livestock densities and add the drinking

water requirements to the densities (FAO, 2007), industrial demand is based on gridded industrial water demand data (water for manufacturing and energy production) obtained from Shiklomanov (2000) and domestic water demand is based on drinking water requirements per capita derived from the FAO AQUASTAT (Wada *et al.*, 2014).

Irrigation water demand is estimated according to the FOA guidelines: in case of paddy irrigation, paddies are simulated with 50 mm surface water depth to represent flooding irrigation over the crops. For each daily time step the water balance is assessed and therefore the water requirements equal the sum of evaporation and percolation minus the precipitation (Wada, Wisser and Bierkens, 2014). In case of non-paddy irrigation, water requirements are calculated by the difference between Total Available Water (TAW) and Readily Available Water (RAW) in the first and second layer (Allen *et al.*, 1998). Whereas TAW is the total soil moisture available to irrigated crops. Water can be extracted until wilting point is reached and therefore TAW [mm] is based on the difference between field capacity ($\theta_f$) and wilting point ($\theta_w$) and multuplied by the rooting depth (d) [mm]:

$$\mathrm{TAW} = (\theta_f - \theta_w) * d \quad (1)$$

RAW is the actual soil moisture available in the second layer (no surface water available) (Wada, Wisser and Bierkens, 2014). The deficit (TAW-RAW) is the amount of water applied to the crops. Irrigation efficiency is accounted for in the model, by increasing the irrigation water demand by 40%. This give you the the irrigation gross demand (resulting in a efficiency of 71%). However, irrigation water demand is only dependent on these crop factors and irrigation maps of Siebert *et al.* (2015). Therefore it is invariant, regardless of the water distribution by, for example, irrigation networks (Wada, Wisser and Bierkens, 2014).

Surface water and groundwater allocation are determined by surface water availability which is based on local and upstream reservoirs and readily extractable groundwater reserves. Surface water is distributed over 60's irrigated areas, discussed in chapter 2.2. However, it is also possible to use another scheme, since the prescribed scheme is not always in accordance with local water distributions. The distribution of surface water in urban areas is based on data from McDonald *et al.* (2014). For irrigation, the dataset of Siebert *et al.* (2013) is used for areas where it is reliable. For areas that are not reliable the prescribed allocation scheme is used (figure 2.3).

Water withdrawal is determined by the water demand and therefore is equivalent to the total gross demand (De Graaf *et al.*, 2014; Wada, Wisser and Bierkens, 2014). If there is insufficient water available, water withdrawal is shortened to the available amount. Within PCR-GLOBWB2 a dynamic allocation scheme is implemented to supply water for irrigation, industry, livestock's and households (figure 2.3a) (De Graaf *et al.*, 2014). Two year running mains of river discharges and groundwater recharge are used to determine surface and groundwater availabilities. (De Graaf *et al.*, 2014). Ideally, the total water withdrawal would be fulfilled by surface water and renewable groundwater. Within PCR-GLOBWB, first the surface water is withdrawn and as soon as it falls below ten percent of the long term average it stops and the resulting gap is then met by groundwater. Firstly, renewable groundwater is abstracted and, when absent, fossil groundwater is abstracted. The amount of groundwater which can be abstracted is based on the international Groundwater Resources Assessment Centre (IGRAC)(see www.igrac.net). They gathered a large database of global groundwater resources (Global Groundwater Information System, GGIS) (Wada, Wisser and Bierkens, 2014). The model works in such way that in every grid cell the total abstractions are changeable. The demands are total demands and sector independently. This means that all demands are received from local available surface or groundwater and that local preferences are not covered. The Abstraction rates from surface water and groundwater, however, are dependent on the distance of

the cell to the main river or surface water source. it assumes that it is more likely that areas close to the main river source abstract more surface water than groundwater. Farther away from the main river, groundwater abstractions are probably more than surface water abstractions. For irrigation water withdrawal the model has its own routine based on crops calendars which ensure optimal crops growth. The map of irrigated areas based on the MIRCA2000 dataset (Portmann, Siebert and Döll, 2010) that separates two different crop groups, paddy and non-paddy, and assembled 26 different crop classes (Wada, Wisser and Bierkens, 2014). This is combined with crop growing season lengths and crop factors based on the Global Crop Water Model (Siebert and Döll, 2008).

Daily crop evapotranspiration is calculated combining potential evapotranspiration calculated with the Penman–Monteith equation and transpiration from specific crops and open soil evaporation, put together to a crop coefficient (Allen *et al.*, 1998; Wada, Wisser and Bierkens, 2014). The actual evapotranspiration (AET) is the combination of evaporation of water from the soil and plant surfaces that is actually evaporated and transpired via stomata (Martel *et al.*, 2018). The AET is dependent on the water availability and the solar radiation. In arid conditions the potential evapotranspiration (PET) is very high due to high solar radiations, however due to limited amount of surface water the AET is relatively low. The irrigation water consumption is determined by the evaporation and transpiration (Sutanudjaja *et al.*, 2017) and is therefore used to evaluate the irrigation networks. Higher AET suggests higher surface water availability to irrigate the plants with (Martel *et al.*, 2018).

Discharge is calculated from the kinematic wave approximation based on the Saint-Venant Equation. The local drain direction (LDD) is determined by an 8-point gradient algorithm across the land surface. This means that for each 8 neighbouring points, the cell with the lowest elevation is determined, resulting in a flow of water towards this cell. However is has to follow a selected drainage network, that is convergent. Flow velocity is calculated for each cell individually based on discharge and Manning's equation (Sutanudjaja *et al.*, 2017). Hereafter, this velocity is used to move the volume of water in a cell along the selected drainage network, following the local drain directions, resulting in discharge. The defined drainage network is obtained from the HydroSHEDS database (Lehner, Verdin and Jarvis, 2008).

## 2.4 Global Map of Irrigated Areas and its uncertainties

Five different studies created a global irrigation map, independent on GHMs. Most global irrigation maps are based on remote sensing and statistical data (Thenkabail *et al.*, 2008; Portmann, Siebert and Döll, 2010; Siebert *et al.*, 2013; Salmon *et al.*, 2015; Meier, Zabel and Mauser, 2017). One of these global irrigation maps, the Global Map of Irrigated Areas (Siebert *et al.* 2013), is widely used in GHMs, in order to estimate irrigation water demand. GMIA is based on a combination of irrigation statistics for 26909 sub-national units (mostly derived from FAO AQUATAT (FAO, 2016)) and geo-spatial information on the location and the extent of irrigated areas. Information of different countries, such as provinces and districts, were used as input for the model together with reports from the FAO and the World Bank. It presents the area equipped for irrigation (AEI) and the fraction of AEI with water from the different sources (surface water, ground water and desalinized water) at 5' resolution.

Because it is based on national census data, the GMIA provides accurate information in countries with lots of data available. However, this is also one of the main limitations of the GMIA. Information is often very dense in developed countries; yet, it lacks in developing countries (Siebert *et al.*, 2013). A lack of nation census data has influence on the reported area equipped for irrigation.

The presence of unrecorded wells and irrigation canals might result in underestimated irrigation some regions for the GMIA (Salmon *et al.,* 2015). Especially the information on the water source for irrigation is limited. Many countries do not provide specific information of the source of irrigated water. When statistics on water use were unknown, the percentage AEI per water source water was estimated on other information, such as the availability of water resources. Therefore the map quality between these maps differ a lot. The AEI assigned 93% of the countries with excellent to good map quality; only 42% for the data layer on the water source of irrigation. This may lead to unrealistic estimates in certain countries.

# 3. Study areas

In this chapter, the four study areas are described. These areas are the Netherlands, the Nile delta, the Indus basin and the Citarum basin on Java, Indonesia (figure 3.1). The Nile delta and the Indus basin are the densest irrigated areas in the world while along the Citarum river many small irrigation networks are situated. The Netherlands does not have many area equipped for irrigation (FAO, 2016). it was selected due to the extensive amount of OSM data available. There is huge variety in completeness of the OSM data. Whereas the Netherlands is relatively complete, the Nile and the Indus are well represented and the Citarum has little data available. The study areas are ordered according to the completeness of data available.

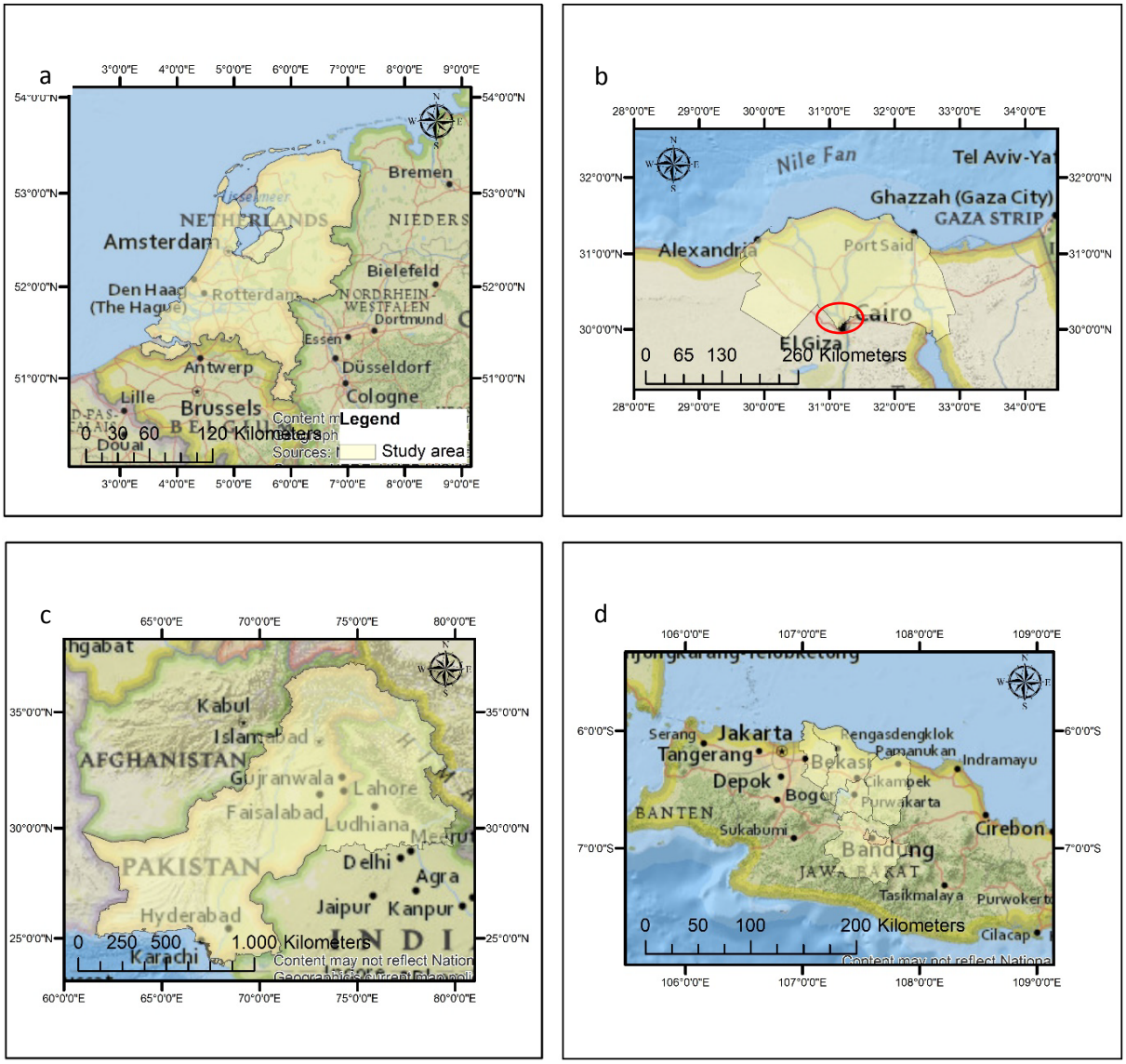


Figure 3.1: The study area are situated in the Netherlands (a), the Nile delta (b), the Indus basin (c) and the Citarum basin (d). The red circle indicates the Apex of the delta, which is assumed as the beginning of the delta.

## 3.1 The Netherlands

The first case study is the Netherlands (figure 3.1a). It is covering a surface area of 42,000 $km^3$. It has a temperate maritime climate and an average precipitation of 800 mm/year (KNMI, 2017). The average evaporation is 530 mm/year.

The Netherlands has two main rivers: 1) the Rhine, which enters the country at Lobith and 2) the Meuse that enters the country in the south at Maastricht (figure 3.2). Most of the water of the rivers is drained into the North Sea and discharges partly via the IJsselmeer (from the IJssel). Downstream of Lobith the Rhine splits into the northern branch, the Lower Rhine, and the southern branch, the Waal (Arnold, 2009). About 10 km downstream the northern branch, the IJssel branches off towards the IJsselmeer. The Lower Rhine flows to the western part of the country and discharges into the North Sea. The Waal, also flows towards to western part of the country and feeds a large estuary together with the Meuse (Arnold, 2009). The Rhine is the biggest river with an average discharge of 2300 $m^3/s$ compared to 230 $m^3/s$ of the Meuse river (averaged 1901 to 2000) (van der Most *et al.*, 2009). About 70% of the discharge of the Rhine flows into the Waal and 30% into the Lower Rhine (van der Most *et al.*, 2009). According to the Dutch government the IJsselmeer and the IJssel are the main freshwater suppliers for the Northern part of the Netherlands (Arnold, 2009). The western part of the Netherlands is fed by the Rhine that carries water to North-Holland via the Amsterdam Rhine Canal (Arnold, 2009). The Meuse feeds the southern part of the Netherlands. Besides these main rivers the Netherlands is knows of its large density of small canals (Arnold, 2009).

One of the main factors that influence the water distribution is a dam at Driel (figure 3.2). This dam determines the amount of water towards the IJssel or the Lower Rhine. This is mainly for safety and agricultural purposes. It distributes the water, such that every branch of the Rhine has the same flood risk (Arnold, 2009). Moreover, water quality is important for the distribution. Surface water is often used for extracting drinking water. Due to salt intrusion from the North sea, a minimum river discharge is required to guarantee good quality of the surface water (Arnold, 2009). Good water quality is also required for agriculture in the western part of the Netherlands, due to cultivation of tulips. Water is not pumped uphill in The Netherland.

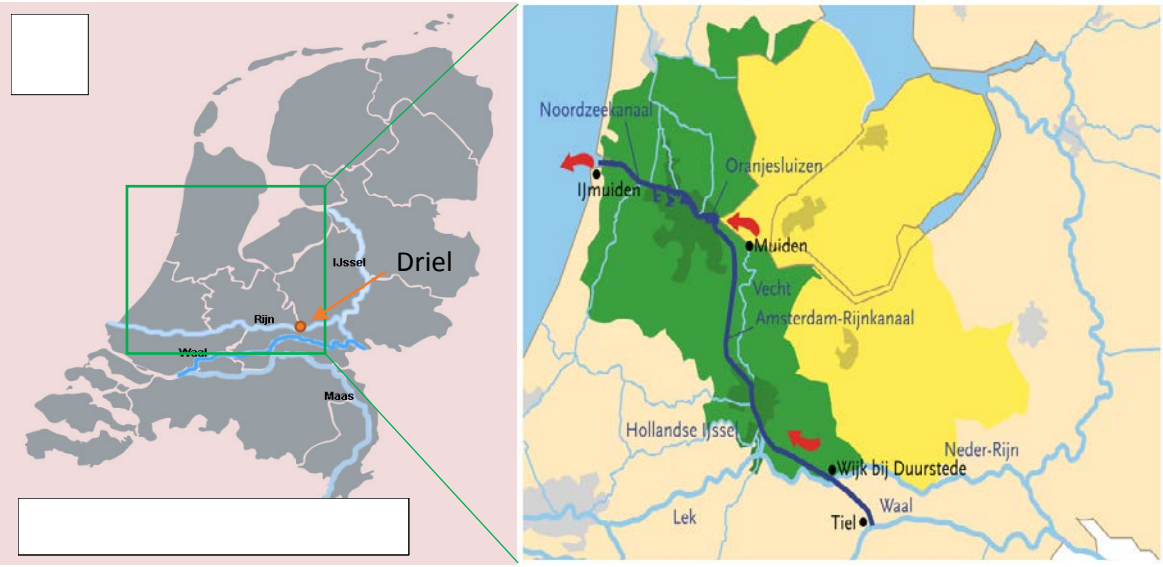


Figure 3.2: (a) The main rivers of the Netherlands, the Meuse (Maas) in the South and the Rhine (Rijn) splits into the Waal (dark blue) and the IJssel (source: van der Most *et al.*, 2009). The green and the yellow area in figure 3.2b (Arnold, 2009), represent the area fed by the Amsterdam Rhine Canal.

## 3.2 Nile delta

The second study area is the Nile delta (figure 3.1b). The Nile delta contains one of the biggest irrigation networks of the world (Allam M.N., El Gamal F., 2005) and it is covering a surface area of about 38,000 $km^2$ (240 by 160 km) (Roest, 1999). The average discharge is 2,830 $m^3/s$ (FAO, 2016) and the total length of the Nile river is 6,900 km. The Nile originates from the Blue Nile (Ethiopia) and the White Nile (Great lakes region in Uganda) and flows through eleven countries, starting in Uganda and Ethiopia towards Egypt (Oloo, 2010). However, this study is focussed on the delta that is located in Egypt. Because of the arid conditions, the Nile river is the only available source of fresh surface water in the delta (Roest, 1999). The delta has an annual precipitation of 100-200 mm, mainly during the winter season (Droogers *et al.*, 2012).

The land surface of Nile delta has a little slope from the apex, at Cairo, towards the Mediterranean Sea (Roest, 1999), resulting in a northwards flow direction. This study assumes that the Nile delta starts north of Cairo, where the Nile bifurcates into two main streams, one flowing into Mediterranean Sea at Rosetta (western branch) and the other stream in Damietta (eastern branch) (figure 3.3). At this location, the apex, irrigation water is regulated and distributed over the irrigation canals. Six major irrigation canals are constructed within the delta (figure 3.3). From these canals a dense irrigation network is created (Allam M.N., El Gamal F., 2005). The network divides 380 $m^3/s$ out of the main river towards the irrigation channels that feeds the approximate 27,000 $km^2$ of irrigated area (Allam M.N., El Gamal F., 2005). The system of the irrigation network is built such that water lost from one point upstream the delta is reused downstream, either by gravity or pumping. This substantially increases the overall water efficiency (Gaafar, El-agha and Rap, 2016). However, due to sea water intrusion in the northern part of the delta, irrigation is limited at the fringes of the delta (Nofal *et al.*, 2015).

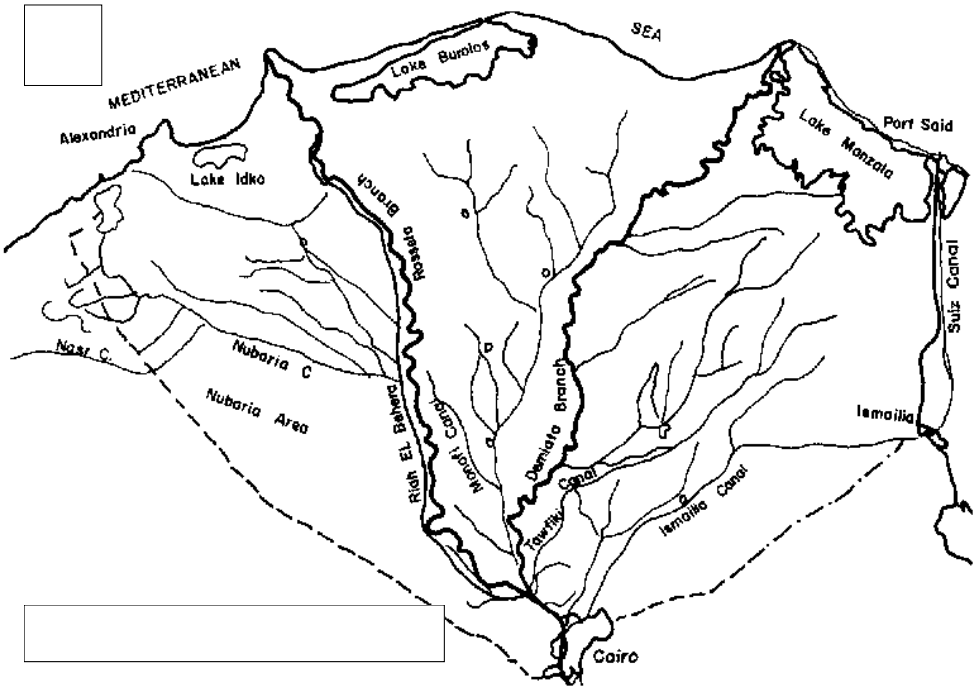


Figure 3.3: The two main branches of the Nile (Demietta in the east and Rosetta in the west). Furthermore, the main canals of the Nile delta are shown (Biswas, 1983).

## 3.3 Indus basin

The Indus is the fifteenth largest river in Asia with respect to mean annual discharge. It flows through Pakistan, India and China (figure 3.1c). It has a length of 3,180 km and the total drainage area of the river is 1.15 million km$^2$ (FAO, 2016). Meltwater is de main water source and the average discharge downstream is 1955 m$^3$/s (Memon and Thapa, 2011).

The climate differs over the entire Indus basin. It varies from cold mountain highlands in the north, to semi-arid and temperate climates on the plains downstream. The annual precipitation is also different over de basin, it varies from 2000 mm on mountain slopes in the north to 100-500 mm in the plains, downstream (FAO, 2011). The precipitation varies during the year, since the climate is heavily influenced by the monsoon, when most precipitation occurs (FAO, 2016).

The Indus is fed by seven rivers that originate from glacier water (figure 3.4). The Indus river itself flows through the northern part of India towards north Pakistan. After it connects with the Panjnad river in the middle of Pakistan, it flows towards the south, along the entire length of Pakistan and discharges in the Arabic Sea near city of Karachi.

The Indus is extremely important for Pakistan's food production. It irrigates 80% of Pakistan's agricultural land (FAO, 2011). Many dams are constructed across the Indus (figure 3.4). These dams were made for water distribution for irrigation purposes and flood control (Magsi and Salman, 2012; FAO, 2011b). These dam projects have led to extensive irrigation systems that can be up to 200 km in length (Swain, 2004). Large irrigation networks have been installed throughout the basin. The main irrigation canals are shown in figure 3.4. Within the Indus basin, about 263,000 km$^2$ is equipped for irrigation (FAO, 2011).


Figure 3.4: The Indus basin, with its seven rivers: Sutlej, Jhelum, Chenab, Ravi, Beas, Panjnad and the Indus river. The main (irrigation) canals are provided with dark blue. The built barrages are indicated as dark blue triangles (Memon and Thapa, 2011).

## 3.4 Citarum basin (Java)

The fourth study area is the Citarum basin, which is located east of Jakarta (figure 3.1d). The Citarum river originates from a mountain range south of Bandung. It flows through a couple of lakes, such as the Saguling, the Cirata and the Julanda. These lakes are important water reservoirs for irrigation purposes (MPWI, 2007). The total area of the basin is 11,500 $km^2$ and therefore it is the largest river of West – Java. The total length is 300 km and the average discharge is 80 $m^3/s$ (Fulazzaky, 2010). The southern part of the area is located in a mountain range, resulting in high slopes. The downstream area, in the north, mainly consists of flat alluvial plains (Fulazzaky, 2010). The climate of the basin is tropical and is characterised by specific wet and dry season. The annual precipitation is 2300 mm (Fulazzaky, 2010).

This study area was chosen, because it is the food production area for the big metropole Jakarta and Bandung, which represents a population of 30 and 2.5 million people, respectively (WPR, 2017). Most of its river water is used for irrigation and to distribute the water properly, many irrigation dams are constructed across this river. Most irrigation occurs downstream, whereas the irrigated areas contain small rice paddies (Xiao *et al.*, 2006) and a total of 3900 $km^2$ irrigated fields is reported (Fulazzaky, 2010). While surface irrigation (basin and border) is the most dominant type downstream, upstream near the city Bandung many terraces are built (MPWI, 2007).

# 4. Materials and methods

This chapter provides a concise overview of the modelling framework (figure 4.1). To create the spatial link between rivers and irrigation networks a GIS routine based on OpenStreetMap data and a global DEM is developed. The method consists of different steps: (1) creation of irrigation networks based on OSM and elevation data, (2) evaluation of the choice of the river discharge as source, 3) comparison of OSM irrigation networks to the area equipped for irrigation reported by the GMIA, (4) using the PCR-GLOBWB model to determine the effects of using different irrigation networks and (5) comparison of simulated volume fractions per water source by the PCR-GLOBWB model to GMIA. ArcGIS 10.5, the PCRaster package within Python programming language and PCR-GLOBWB2 are used. For detailed cryptic modelling steps within ArcGIS and Python see Appendix B & C.

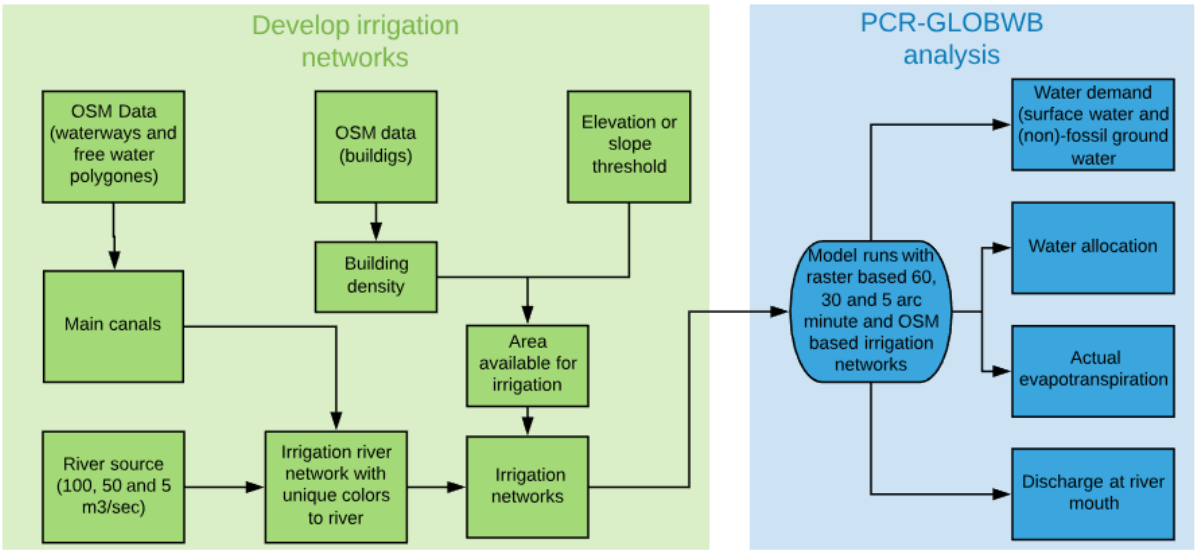


Figure 4.1: The processing steps of this study. The first part: develop the potential irrigation networks, is presented on the left side (green) and on the right side the implementation in PCR-GLOBWB (blue). The model run have been evaluated for total water demand, water allocation, actual evapotranspiration and discharge at the river mouth.

## 4.1 OpenStreetMap and country data

The GIS routine to spatially link rivers and irrigation networks used OpenStreetMap data as input. OSM is a community that provides user-generated maps (Haklay, 2010). It has the advantage that OSM exists of free, editable maps of the entire planet. It is a so called open-source content, which means that access to geographical information, such as map images and map data is free (OSM, 2015). Country data is available for download as shapefile and is categorized in different layers, such as roads, buildings, land use, infrastructure, free water and waterways. This study focussed on surface water and therefore only the shapefiles of open water (containing polygons) and waterways (containing lines) were used. This data is visualised in figure 4.2. The free water and waterways shapefiles were merged together and clipped to the area of interest. The area of interest is country (for the Netherlands and the Indus basin) and province (for the Nile delta and the Citarum basin) based (GADM, 2017).

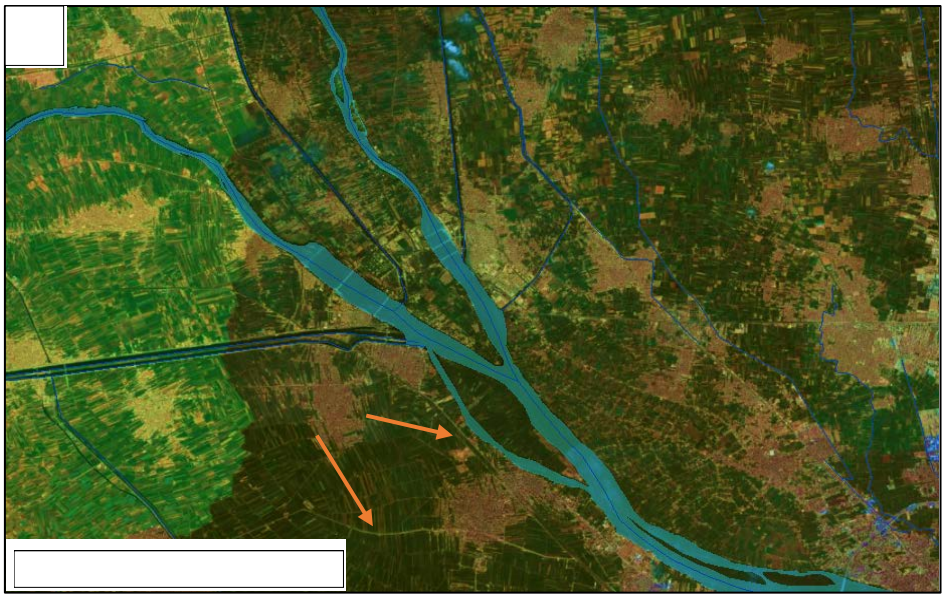

Figure 4.2: Visualisation of the used OSM open water (light blue) and waterways (blue) data on an aerial picture for the apex of the Nile delta near Cairo. Note that the brightness of the picture is adjusted to clearly show the OSM data representing most of the existing canals. The orange arrows indicate the existing canals that are not yet mapped by the OSM community. The blue polygons in the middle represent the Nile river.

To ensure the accuracy of OSM data, the OSM community verifies everything that is edited and therefore major mistakes are corrected (Weber and Haklay, 2008). However, due to the excessive amount of work that is done worldwide, 3 million edits per day (OSM, 2015), not all data can be checked properly. Consequently, the main disadvantage of OSM is the variation in accuracy and completeness of the maps (Haklay, 2010; Barrington-Leigh and Millard-Ball, 2017). In figure 4.2 an example of completeness in OSM data at the apex of the Nile is displayed. However, there exists no global map that shows the completeness of the OSM water data. It is assumed that maps of developing countries are less accurate than developed countries with good internet access (Barrington-Leigh and Millard-Ball, 2017). Second, completeness is to a large extent determined by the interest of people in area. Since many studies focus on the Nile delta and the Indus basin it is assumed that after the Netherlands (indicated as developed country), the Nile delta and the Indus basin follow in terms of the level of completeness. The Citarum basin, however, has very limited water data available.

Incomplete data has have adverse consequences during creation of irrigation networks. Incomplete water data may cause incomplete irrigation canals that result in sub optimally constructed irrigation networks due a lack of data or loose line segments (Haklay, 2010). These loose line segments are visualized in figure 4.3 and need to be accounted for in this study.

## 4.2 Developing irrigation network

To link irrigation networks to a river, pre-processing of OSM data was required. This included buffering waterways and filtering the smallest irrigation canals. To be able to filter small irrigation canals, waterways had to be buffered to create an area around these lines. They were buffered with 15 m on both sides. Here we assumed irrigation canals have an average width of 30 m, which concurs with recent studies, like Ghazaw (2011) and Kharagpur (2012). In order to cope with conflicts in overlapping (buffered) polygons at canal confluences, overlapping canals were dissolved into one polygon. However, there still be small canals within the OSM data that needed to be filtered (figure

4.3). To filter these small canals, polygons with an area less than 30,000 $m^2$ were left out. As a consequence each canal had to be at least 1000 m in length to be included ($\frac{30{,}000 \text{ area}}{30 \text{ m buffer}} = 1000 \text{ m}$). As a result, networks consisting of major canals were created (figure 4.4).

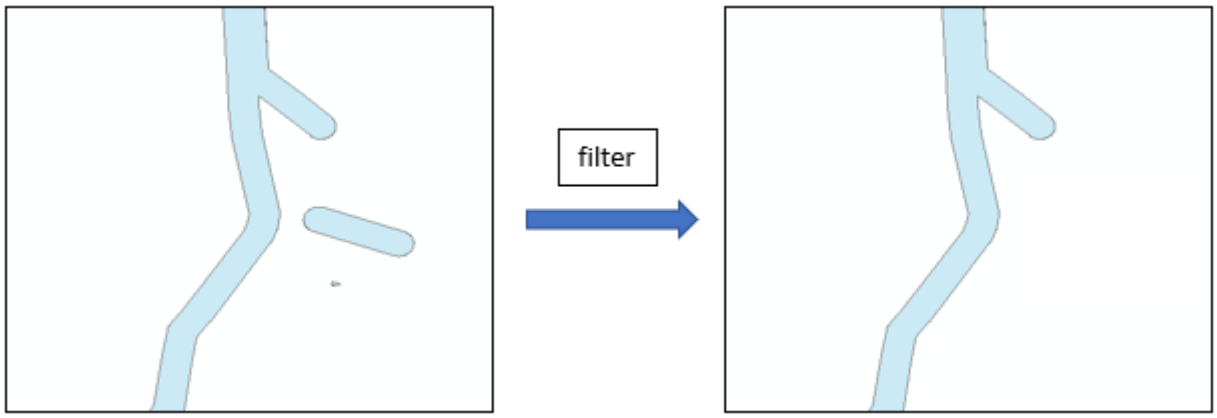


Figure 4.3: Left-hand side: example of a loose segment. The lines are already buffered. Lines that are not connected are filtered to avoid loose segments. Right-hand side: additional lines arranged as a filter.

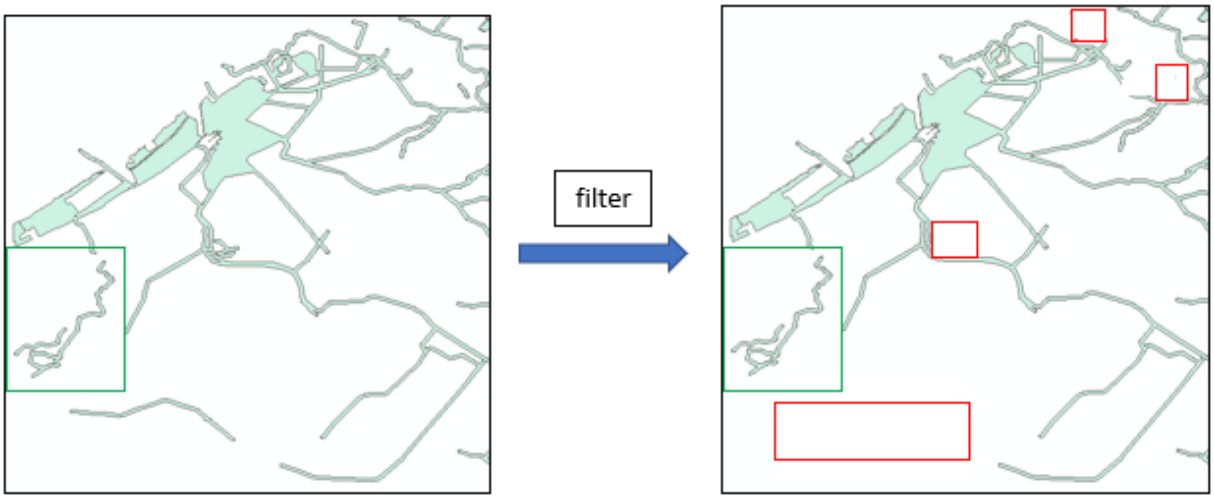


Figure 4.4: Left-hand side: example of the OSM waterways and open water data for small part of the Nile delta. The figure shows loose segments within the OSM data. Right-hand side: red squares show which lines are filtered by the threshold of 30,000 $m^2$. The green highlighted squares show segments that are not connected with the river source, however the polygons have an area bigger than 30,000 $m^2$.

Subsequently, the rivers were linked to the OSM irrigation canals. These rivers are defined as average river discharges, consisting of one-pixel widening river area, simulated by the PCR-GLOBWB model (Sutanudjaja *et al.*, 2017) based on a 5' resolution. The irrigation networks were created by defining a river as those cells with a minimum average discharge of 100, 50 or 5 $m^3/s$. For each study area a default river discharge was chosen as water source for the irrigation network. The chosen river discharge that functioned as source of the irrigation network was based on the discharges used in the literature. A minimum river discharge of 100 $m^3/s$ was used to only assess the main rivers in the Netherlands, Nile delta and Indus basin. This included the Rhine (2300 $m^3/s$) and the Meuse (230 $m^3/s$) (van der Most *et al.*, 2009), the Nile (2900 $m^3/s$) (FAO, 2016) and the Indus (1955 $m^3/s$) (Memon and Thapa, 2011). A minimum discharge of 50 $m^3/s$ was selected for the Citarum basin, considering the average discharge of the Citarum river is 80 $m^3/s$ (Fulazzaky, 2010). Using a minimum discharge of 100 $m^3/s$ for the Citarum basin would have removed the upstream part of the river and

created unrealistic irrigation networks. Each river cell was assigned with a unique ID (identifier) (number). This number was also assigned to the canal segment that overlapped the river cell by using a spread zone operator (figure 4.5). This operator started from the river cells, which calculated the shortest friction distance path over the canals. Additionally, a second spread zone operator, starting from an irrigation canal, was used to interpolate between irrigation canals. A maximum spreading of 30 km from a canal towards the fields was allowed. As a result, a network with different numbers that clearly identifies the river source of an irrigation network was created. It must be noted that this spread was not dependent on the slope of the area. For visualisation each number got an individual colour.

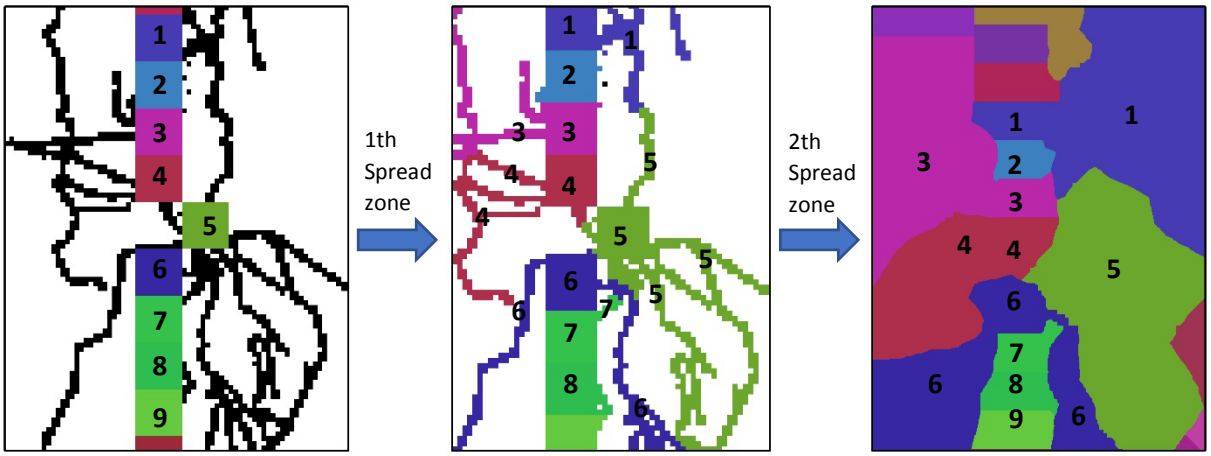


Figure 4.5: Left-hand side: river cells with unique number for each cell and irrigation canals. Each number is assigned with a colour. Middle: after the first spread zone operator. Each irrigation canal that overlaps a river cell is assigned by the same number (colour) Right-hand side: created irrigation networks after the second spread zone operator. Spreading started from irrigation canal to create an irrigation network.

The different networks do not yet represent the irrigation networks. Irrigation networks are dependent on elevation (FAO, 1985) and urbanization (Khanal, 2003) and therefore they had to be accounted for. To determine the areas possibly irrigated from surface water, a global DEM and the OSM shapefiles of buildings were used. Regarding the DEM, MERIT DEM by Yamazaki *et al.* (2017) was used, which is prescribed in chapter 2.3.1. The DEM was used to set a maximum height difference between two adjacent cells. For flat areas, in this study the Netherlands and the Nile delta, the elevation threshold was chosen to be maximum 10 m higher compared to the elevation of the point where the river enters the country (Most *et al.,* 2009). This assumed that irrigation systems can use pumping systems to pump the water to a higher location. A maximum of 10 m was used, since the pumping costs would increase rapidly (FAO, 1985; Fipps and Dainello, 2015). In these study areas, the height of Lobith (the city where the Rhine enters the Netherlands) is 10 m above sea level and the height of the apex of the Nile delta is 20 m above sea level. This implies that areas with an elevation higher than 20 and 30 m, respectively, are omitted. In mountain areas, which are in this case the Indus basin and the Citarum basin, a difference of 10 m between two adjacent 3 arcsecond cells was used as a maximum difference in height. This applied a slope of $\frac{10}{90} \approx 0{,}07$, which is 7% at the equator. This is approximately the maximum slope for surface irrigation (FAO, 1985). Accuracy of the DEM has been taken into account. Yamazaki *et al.* (2017) estimated an average error of ±2m, which means a maximum difference of 8 – 12m. This range indicates a range in the slope of ≈6.5% to 8% at the equator. Note that this threshold probably underestimates the irrigated areas in mountain areas,

where terraced irrigation is most common (Xiao *et al.*, 2006). This type of irrigation allows for slopes of 25% (FAO, 1985).

Second, the OSM buildings shapefile was used. To only include urban areas; a building density is performed using the OSM analytics tool created by the Humanitarian OpenStreetMap Team (HOT). The OSM analytics tool provides building densities based on OSM data (HOT, 2016). However, they do not support downloading files of these data. This study therefore used OSM building polygons. These polygons were converted to points and hereafter a point density function was applied to them. Twenty buildings per 30 arcseconds cell were used as a threshold, which is in line with used density for urban areas determined by the HOT (2016) (figure 4.6). Urban areas were left out from the areas possibly irrigated from surface water. Due to the subtraction of these urban areas, some maps may have white spots within the area. Hereafter, the irrigation networks were created on a 30 arcseconds resolution. The created irrigation networks are potential irrigation networks with their potentially irrigated areas. This means that these areas are not necessarily irrigated (Doll and Siebert, 2002). Regardless, they are henceforth indicated as irrigation networks.

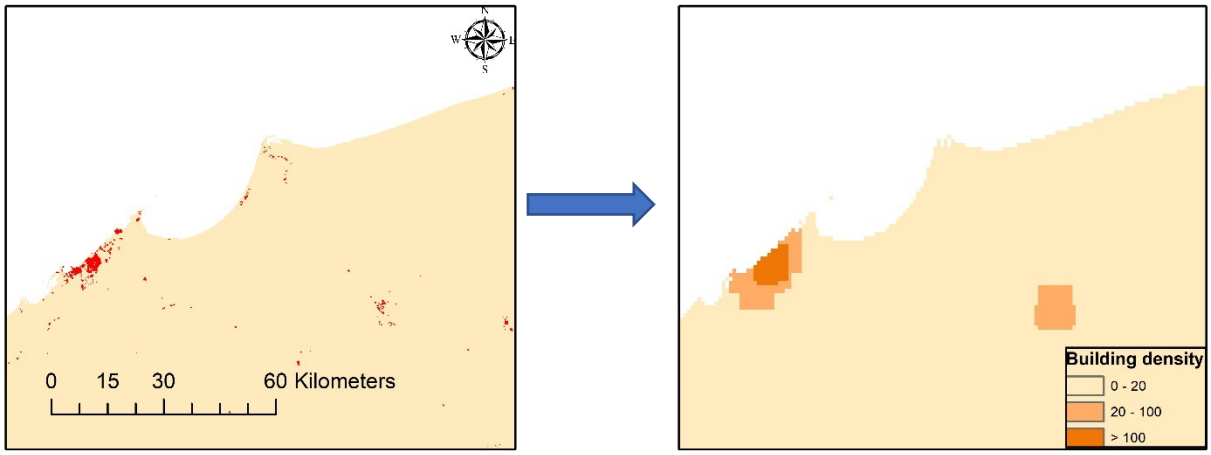

Figure 4.6: Left-hand side: OSM building shapefile data for the northwestern part of the Nile delta. Right-hand side: map after using building density operator. The dark orange colours represent higher building densities (>20 buildings per 30 arcseconds)

## 4.3 Definition of source of surface water for irrigation networks

Irrigation networks link surface water to irrigated areas, which makes the definition of where the surface water is highly important. Default discharges have been chosen to act as river source. However, whenever the definition changes, the location of the source for an irrigation network changes with it. For example, defining river discharges with minimum discharge of 100 $m^3/s$ as source, instead of 5 $m^3/s$, excludes smaller rivers (< 100 $m^3/s$) to be a source. This may lead to increased network areas and length, since the access to a source becomes limited. In order to get an idea what the consequences are for choosing a default discharge, three different thresholds of minimum average river discharges were used to determine its effects on the irrigation networks: 100, 50 and 5 $m^3/s$. The river discharges are henceforth referred to as Q100, Q50 or Q5. Figure 4.7 represents these river classes for each study area based on average annual discharges. The average area, total irrigated area, average length and maximum distance to the boundary of the networks are evaluated to determine the sensitivity of the network to definition of the surface water source. Please note that only rivers are taken as water source for an irrigation networks and that lakes are omitted.

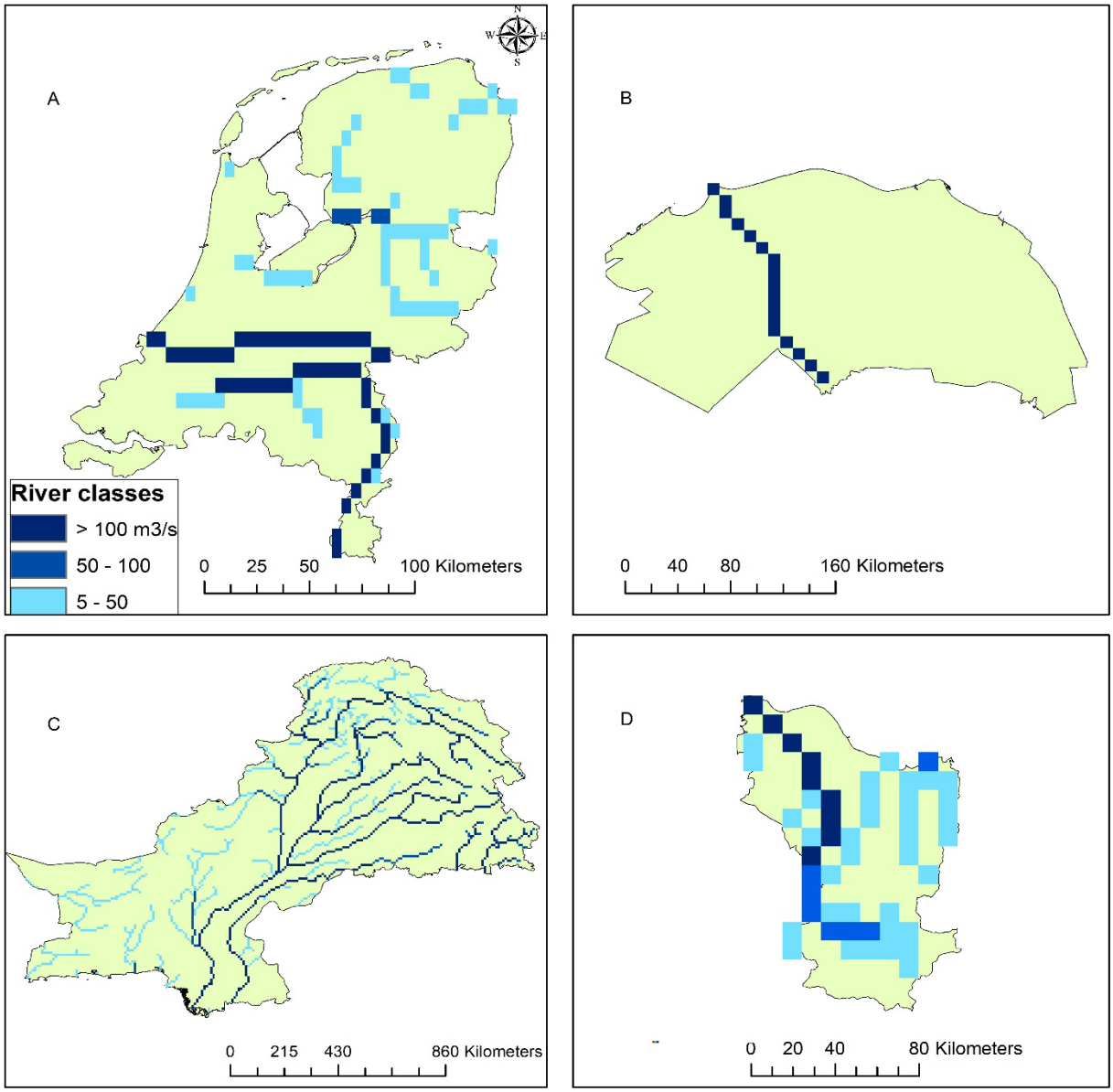


Figure 4.7: Resulting river discharges for (a) the Netherlands, (b) the Nile delta, (c) the Indus basin and (d) the Citarum basin using minimum discharge 100, 50 and 5 $m^3/s$ as threshold.

## 4.4 Comparison of irrigation networks to GMIA

In order to validate the created irrigation networks, the extent of the irrigation networks is compared to the extent of the AEI reported by the GMIA (Siebert *et al.*, 2013). By extent, this study refers to the size rather than the calculated area. The AEI is available in a raster reporting the irrigated surface area extent on a 5' resolution. Next, the total irrigated surface area is calculated for the irrigation networks. The total number of cells was multiplied by the area of a 30 arcseconds cell. Each study area accounted for differences in longitude and latitude. The estimated area is compared to the reported AEI by the GMIA.

## 4.5 PCR-GLOBWB model setup and its hydrological effects of the choice of an irrigation network

The choice of an irrigation network influences the water distribution and therefore affects several hydrological parameters, such as water withdrawal, actual evapotranspiration and discharge at the river mouth. PCR-GLOBWB was used to estimate the hydrological effects of the irrigation networks simulating these three parameters for each study area.

### 4.5.1 Model run setup

Within PCR-GLOBWB, the networks at which allocations of surface and groundwater are performed was changed. Additionally, PCR-GLOBWB was run at standard parameterization at 5' spatial resolution to simulate hydrology at a daily resolution for the year 2010. Outputs were reported as yearly averages. A spin-up time of 9 years was used (2000-2009). Four different maps were implemented, based on four different irrigation networks that indicate these zones: OSM networks and the raster-based 60', 30' and 5' irrigated areas(reviewed in chapter 2.2). This is done for each study area. Consequently, a total of sixteen runs have been performed.

### 4.5.2 Hydrological effects

**Water demand**

To estimate water demand, water withdrawal was evaluated. Water demand is invariant, regardless of the water distribution and therefore water withdrawals are simulated. Water withdrawal is based on two year running means of river discharges and groundwater recharges (Sutanudjaja *et al.*, 2017). Change of water distribution by using a different irrigation network is likely to affect the river discharges and groundwater recharges and thus the surface water withdrawal. Total water, surface water and (non)-renewable groundwater withdrawal were calculated using the PCR-GLOBWB model. The annual total withdrawals per 5' cell were summed up and divided by the area to get the average withdrawals in mm/year for each study area. Surface water and groundwater withdrawals were calculated as percentage of total withdrawal.

**Actual evapotranspiration**

The effect on the AET distribution was evaluated. After precipitation, the actual evapotranspiration is the most important determinant of water balance. Both evaporation and transpiration show crop extent and compose irrigation water consumption (Sutanudjaja *et al.*, 2017). AET is dependent on water availability, which is influenced by the irrigation networks. AET distribution maps were assessed for each network and compared with each other. Furthermore the average AET is calculated for each network.

**Discharge at the river mouth**

To analyse the cumulative effect on a river's water balance, discharges at the river mouth have been simulated. Discharges at the river mouth are dependent on water distribution and withdrawals upstream, which indicates that they are likely to be affected by the choice of an irrigation network. Discharges for all networks were simulated and compared to discharges at the river mouth reported by the literature.

## 4.6 Comparison of water allocation fractions to Global Map of Irrigated Areas

The choice of an irrigation network affects the water allocation and therefore the fraction of water allocation was simulated by the PCR-GLOBWB model. A comparison between the OSM and 60' networks is performed to assess the effect of the choice of the irrigation network. First, maps are presented and then these maps were converted to ASCII files to perform a statistical correlation. Both simulations were analysed using RStudios. Calculated fractions were then plotted against each other with a correlation line.

In order to validate the OSM based irrigation networks were compared them to the GMIA. Simulated volume fraction of surface water and renewable groundwater estimated by PCR-GLOBWB for the OSM and 60' networks were compared to the volume fraction per water source for each cell of the reported GMIA data from Siebert *et al.* (2015). First, maps of the GMIA were shown, then the calculated OSM fractions were plotted against the GMIA fractions with a correlation line. Furthermore, within RStudios a Pearson correlation coefficient, Nash-Sutcliffe efficiency and the Percent Bias ($P_{bias}$) was calculated.

**Pearson correlation**

The Pearson correlation coefficient measures the statistical relationship between two datasets. It needs two equal datasets to compare to calculate the correlation coefficient (CC), using formula (2):

$$CC = \frac{n(\sum xy) - (\sum x)(\sum y)}{\sqrt{[n(\sum x^2) - (\sum x)^2][n(\sum y^2) - (\sum y)^2]}} \quad (2)$$

Where x is the GMIA values and the y is the values calculated for the irrigation networks used for the analysis (OSM, 60', 30' and 5'). N is the number of pairs. A perfect positive fit means a CC value of one, whereas a weak linear correlation illustrates a value close to zero (Yuan *et al.*, 2017). Whenever the CC is negative, a negative correlation is observed.

**Nash-Sutcliffe efficiency**

The Nash–Sutcliffe model efficiency (NSE) is defined as one minus the sum of the absolute squared differences between the predicted and observed values, normalized by the variance (Nash and Sutcliffe, 1970). It measures the predictive accuracy of hydrological models. The defined correlation ranges from minus infinity to one. NSE is one implies a perfect match. NSE is zero, indicates that the differences between the model estimations and the observations is as large as the variability in the observed data (Nash and Sutcliffe, 1970) . Minus infinity < NSE < zero, implies the mean value of the observed data is a better predictor than the model. See formula (3).

$$NSE = 1 - \frac{\sum_{i=1}^{n}(y_i - x_i)^2}{\sum_{i=1}^{n}(x_i - x)^2} \quad (3)$$

**Percent bias**

The Percent bias ($P_{bias}$) is defined as the average tendency of the simulated values to be smaller or larger than the validation values, which is in this case the GMIA data (Gupta *et al.*, 2009). Assessing formula (4), the simulated values are the 60' and OSM data points (y) and the validation values are the GMIA database (x). Whenever the $P_{bias}$ is positive an overestimation of the 60' and OSM data is

indicated, whereas a negative value indicates an underestimation. Zero value means no bias. $P_{bias}$ > 30 is assumed to be poor (Samuelsen, Hansen and Wehde, 2015).

$$\mathrm{Pbias} = 100\frac{\sum_{i=1}^{n}(y_i - x_i)}{\sum_{i=1}^{n} x_i} \quad (4)$$

# 5. Results

In this chapter, the outcomes of the four different case studies: the Netherlands, the Nile delta, Indus basin and the Citarum basin were described. First, the created irrigation networks based on OSM data are presented (Chapter 5.1). Second, the influence of the definition of the source of surface water on the irrigation networks was estimated (Chapter 5.2). Third, the OSM based irrigation networks were compared to the area equipped for irrigation reported by the GMIA. Fourth, the effect of the created irrigation networks on water withdrawal, actual evapotranspiration and discharges was compared to the raster based 60', 30' and 5' irrigated areas. Last, the irrigation water fraction volume per cell of the OSM and 60' irrigation networks were validated against the Global Map of Irrigation Areas (GMIA).

## 5.1 Developed irrigation networks

OSM data together with elevation data was used to determine irrigation networks that are fed by a river source. Figures 5.1 and 5.2 represent the created OSM based irrigation networks. Different colours indicate separate irrigation networks, which are fed by an individual river source cell. Areas not connected to the river source, were assigned as red areas. These areas were fed by a water source outside the study area or fed by groundwater or rain water. The Indus basin is enlarged to overlay the OSM data upon the irrigation networks. The OSM data is shown to illustrate the effect on the shape and size of each network. Each OSM network is described individually in terms of size, irrigated surface areas, water distribution and non-irrigated areas. The created irrigation networks of the Netherlands is shown together with its corresponding DEM to show the accuracy of the networks. For each network the total irrigated area (table 5.3), the average size of the irrigation networks (table 5.1) and the maximum length of the networks was estimated (table 5.2).

**The Netherlands**

The irrigation networks for the Netherlands are shown in figure 5.1a. Fifty separate networks were created for the Netherlands. Overall, irrigation networks further away from the river source can be distinguished better as they are more spread out. This is clearly seen in the northern provinces of the Netherlands, such as the green network in figure 5.1a. Within this network, surface water is distributed from the Rhine river towards the northern part of the Netherlands. The yellow line in figure 5.1a represents the IJssel and it is evident that this river feeds the green irrigation network in the north. The northwestern part of the Netherlands is fed by the Rhine (highlighted light blue). The Wadden Islands (north) and Zeeuws Vlaanderen (southwest) are not connected to any river. The Scheldt river is located outside the study area, causing Zeeuws Vlaanderen to be red. The areas not labelled as irrigated areas are in accordance to the higher located areas of the DEM (see figure 5.1b). These areas represent ice-pushed ridges of the Veluwe, and the Hondsrug and the areas in Limburg that contain hills. The northern part of Limburg (Meuse valley) have irrigated areas, however these are mostly fed by groundwater (Deltaris, 2014). The areas in the Drenthe (north), east of the Veluwe and in Noord-Brabant (south), highlighted in figure 5.1a, are probably overestimated. These areas are located at a higher elevation (≥20 m NAP) and are therefore more likely to get their water from another source, since in the Netherlands no water is pumped uphill (Arnold, 2009).

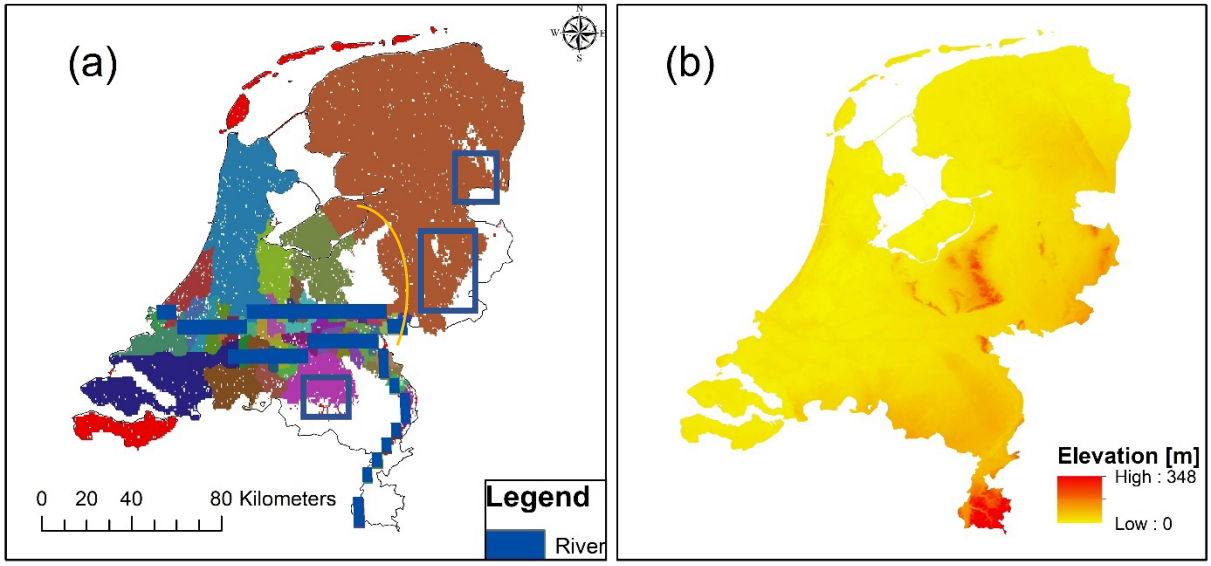

Figure 5.1: (a) The created OSM based irrigation networks for the Netherlands and (b) the corresponding DEM. Each colour represents an individual irrigation network. The areas that have no irrigation network (white areas) concur with higher elevated areas. The blue squares highlight the probably overestimated irrigated areas, since no water is pumped uphill in the Netherlands. The yellow line represents the IJssel.

**Nile delta**

Eighteen large irrigation networks were created for the Nile delta (figure 5.2a). All individual networks are by definition fed by the Nile. Water is distributed along the entire delta and the eastern side is mostly fed by river water from the apex of the Nile. The irrigated areas are spread out, as they shift away from the Nile towards the Mediterranean Sea. The non-irrigated areas are mountain ranges. There is a large red disconnected irrigated area, which extends into the desert where no infrastructure is located in the southwest.

**Indus basin**

701 individual networks were created for the Indus (figure 5.2b). The sizes and shapes of the individual networks vary a lot. Large irrigation networks are created northeast, whereas small networks appear southeast. These small networks have unnatural rectangular shapes (highlighted in in figure 5.2b). These shapes are created due to the absence of OSM data, which is shown in figure 5.2b. Non-irrigated areas are simulated between the networks. These are mainly caused by the maximum spreading.

**Citarum basin**

The Citarum basin is shown in figure 5.2c. The Citarum basin consists of fourteen small irrigation networks with one relatively big (green) network in the middle. Within this network the river water is conspicuously distributed via irrigation canals towards the eastern side of the basin. No irrigation is reported around Bandung and in the mountain range in the south.

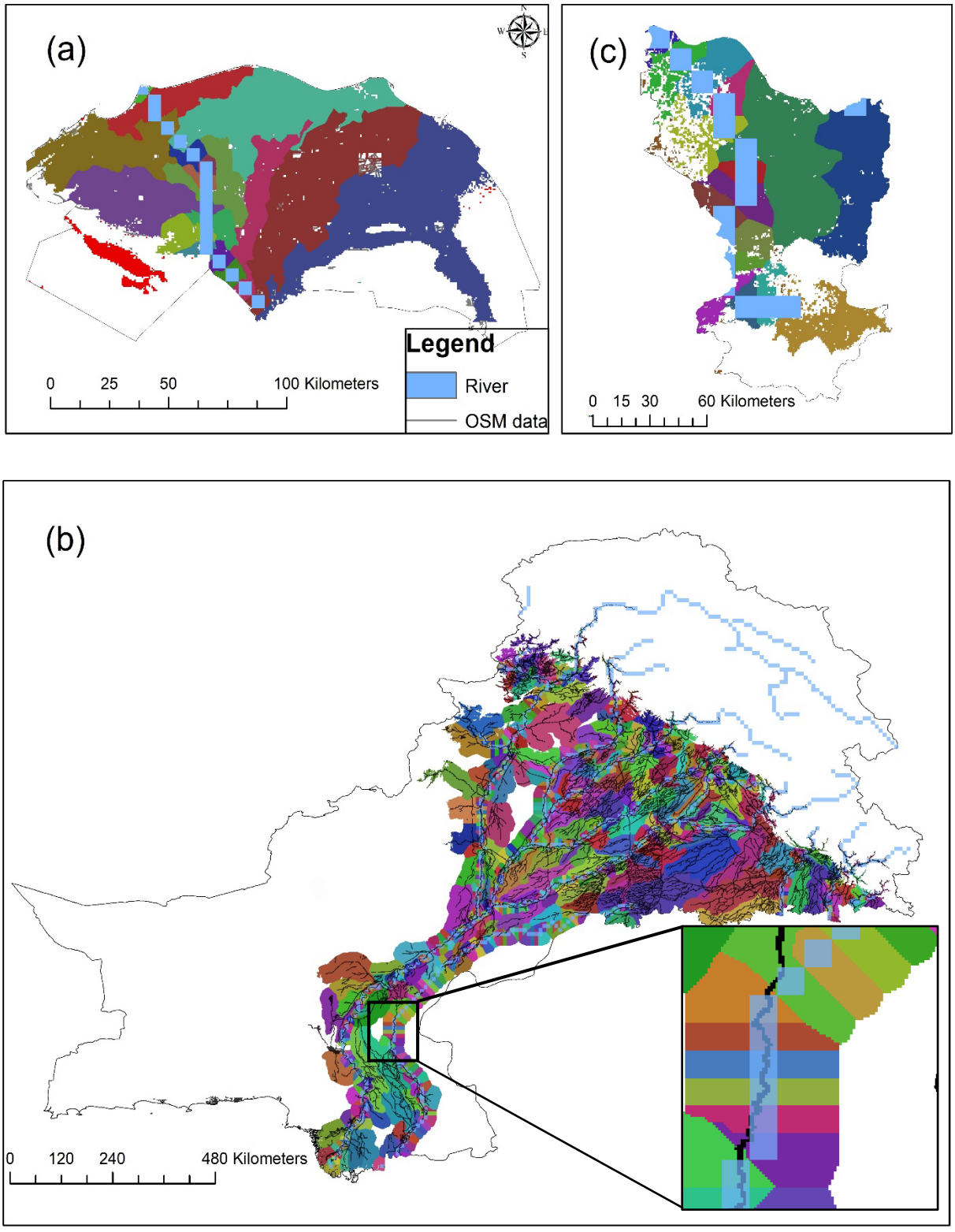


Figure 5.2: The created OSM based irrigation networks for (a) the Nile delta, (b) the Indus basin and (c) the Citarum basin. The blue cells represent river cells, whereas the other colours indicate individual irrigation networks. Within figure 5.2b the rectangular shaped irrigation networks are illustrated for the Indus basin. The blue cells represent river cells, whereas the other colours indicate individual irrigation networks. The black lines represent the OSM data.

## 5.2 Effect of the definition of the surface source water for irrigation networks

For the development of the irrigation networks, default river discharges are used. Here, the sensitivity of the definition of the river source has been evaluated for the average area of the irrigation networks, total irrigated surface area and the network lengths in terms of average length and maximum length. The river discharges were divided into three different classes, namely more than 100, 50 and 5 $m^3/s$ (Q100, Q50 and Q5).

Table 5.1 gives an overview of the average area of each irrigation network together with the total irrigated surface area fed by a river source. In general, when smaller minimum river discharges were used as source, more and smaller irrigation networks were created (figure 5.3). Larger discharges created networks that are more spread out. However, no characteristic shapes were identified. Selecting a different threshold affected the Citarum basin most, whereas the average area for Q5 is 137 $km^2$ compared to 851 $km^2$ for Q100. This implies an increase in area of 622% (Citarum basin) compared to 249% (the Netherlands), 201% (Indus basin) and 0% (Nile delta). The Nile delta has the biggest average irrigation networks, with an area of 1.498 $km^2$. The selected discharge threshold only affected the total irrigated areas of the Indus. Including smaller river discharges created more irrigation networks and as a consequence more irrigated area was estimated.

Second, the average network length was calculated, as the maximum distance to the boundary of the networks. Moreover, the maximum distance from the river to the boundary of the irrigation networks was calculated. Table 5.2 & 5.3 provide an overview of the estimated values. Overall, higher discharges indicated higher average maximum distances. The Nile delta calculated the highest average distance of 42 km. Selecting a different threshold affected the Citarum basin most, with 8 km (Q5) compared to 21 km (Q100). The maximum distance was calculated for the Indus basin, which was 189 km (Q100). Varying the minimum river discharge did not influence the Nile delta, since the Nile river is the only available surface water source within the area (figure 5.3).

Table 5.1: An overview of the average area of each irrigation network together with the total irrigated area fed by a river source [$km^2$].

| | **Average area of irrigation network** | | | **Total irrigated area fed by river source** | | |
|---|---|---|---|---|---|---|
| **Location** | Q5 | Q50 | Q100 | Q5 | Q50 | Q100 |
| **the Netherlands** | 244 | 525 | 605 | 27,002 | 27,002 | 27,002 |
| **Nile delta** | 1498 | 1498 | 1498 | 28,020 | 28,020 | 28,020 |
| **Indus basin** | 375 | 717 | 756 | 451,965 | 378,852 | 356,075 |
| **Citarum basin** | 137 | 429 | 851 | 4,430 | 4,430 | 4,430 |

Table 5.2: Average maximum distance and maximum distance from river to boundary irrigation network [km]

| | **Average length of irrigation network [km]** | | | **Maximum distance from river to boundary irrigation network [km]** | | |
|---|---|---|---|---|---|---|
| **Location** | Q5 | Q50 | Q100 | Q5 | Q50 | Q100 |
| **the Netherlands** | 12 | 16 | 20 | 53 | 82 | 118 |
| **Nile delta** | 42 | 42 | 42 | 136 | 136 | 136 |
| **Indus basin** | 18 | 26 | 28 | 91 | 150 | 189 |
| **Citarum basin** | 8 | 16 | 21 | 24 | 44 | 65 |

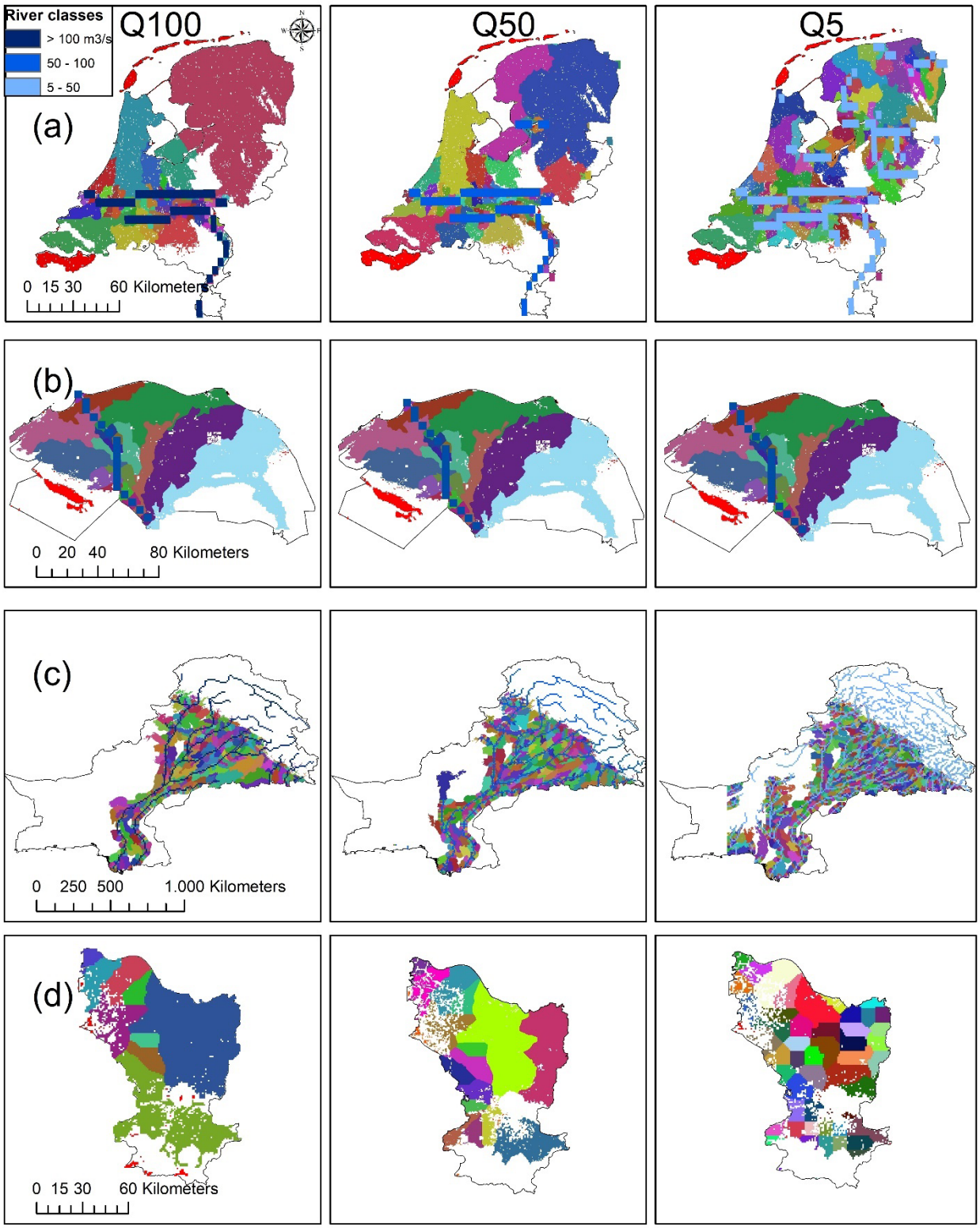


Figure 5.3: The OSM irrigation networks based on three different definitions of river source discharges, namely more than 100, 50 or 5 $m^3/s$. Networks are presented for (a) the Netherlands, (b) the Nile delta, (c) the Indus basin and (d) the Citarum basin. The Citarum river is not shown for better visualization of the irrigation networks within the Citarum basin.

## 5.3 Compare developed irrigation networks to GMIA

The OSM based irrigation networks were compared to reported irrigated surface areas from a previous study. Figure 5.4 shows a comparison of the OSM networks with the irrigation extent reported by the GMIA. The extent of irrigated surface areas are mostly in line with the reported values of the GMIA. In general, the GMIA reports a larger extent of irrigated land. Although the spatial resolution does not exactly correspond with each other for each study, they show good agreement for the Nile delta and the Upper Indus basin. However, in the southeastern part of the Indus, differences appear. These differences can be related to a lack of available OSM data and the maximum allowed spread of 30 km from an irrigation canal towards irrigated area. The differences in the GMIA for the Netherlands and the Citarum basin can be related to the elevation threshold.

In table 5.3 the total irrigated area fed by a river source is shown for both OSM and GMIA networks. In general, the OSM networks estimate higher values for total irrigated areas than the GMIA, however the GMIA reports higher values for the Citarum. There is a huge difference in irrigated surface area for the Netherlands; 28,807 $km^2$ (OSM) compared to 4,763 $km^2$ (GMIA).

Table 5.3: Total irrigated surface area [$km^2$] of the OSM networks compared to the reported AEI by the GMIA (Siebert *et al.*,2015)

| | **Nile delta** | **Indus basin** | **Citarum basin** | **the Netherlands** |
|---|---|---|---|---|
| **OSM data** | 28,020 | 356,075 | 4,430 | 27,002 |
| **GMIA** | 27,000 | 263,000 | 6,500 | 4,763 |

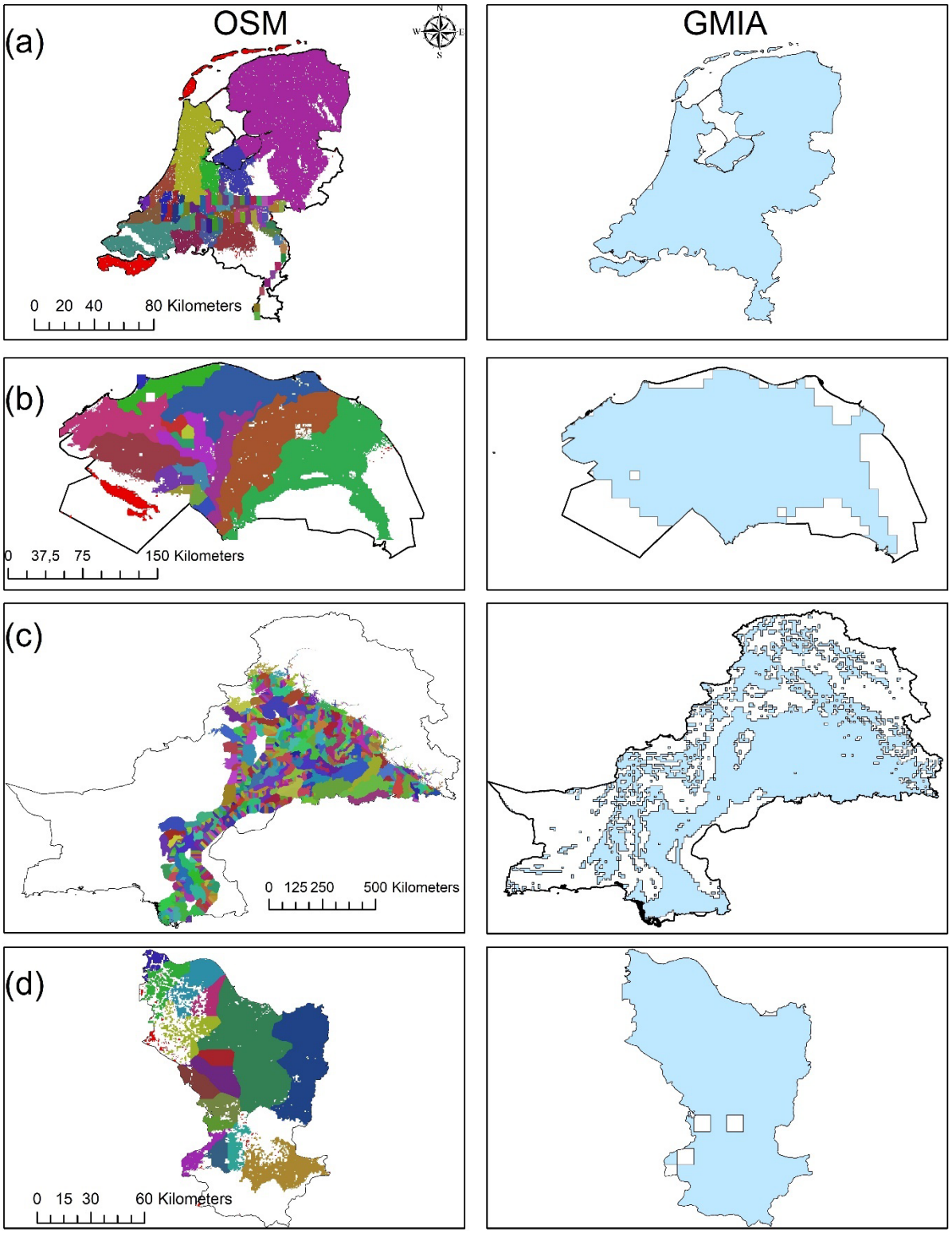


Figure 5.4: Comparison of the OSM networks with the GMIA reported area equipped for irrigation for (a) the Netherlands, (b) the Nile delta, (c) the Indus basin and (d) the Citarum basin.

## 5.4 Hydrological effects of the choice of irrigation network

Sixteen PCR-GLOBWB runs for the four cases and for the four networks (OSM, 60, 30 and 5') provided insight in the effect of the choice of irrigation network on hydrological parameters. Here, the effects on water demand, actual evapotranspiration and river discharge at the mouth are presented.

### 5.4.1 Water demand

To estimate the water demand, water withdrawals were simulated. This was separated into surface water, renewable groundwater and fossil groundwater. In table 5.4 the total withdrawals (irrigation, industry, livestock and households) are calculated in mm/year. Surface water (SW), renewable groundwater (RGW) and fossil groundwater (FGW) are presented as percentages of the total. Total water withdrawal shows to be affected by the choice of the irrigation networks. The 60' and OSM networks indicate an increase in total water withdrawal and surface water withdrawal compared to the 30' and 5' networks. However, the sensitivity in surface water withdrawal differed per study area. Surface water withdrawals in the Nile delta were more dependent on the choice of the irrigation networks compared to the other study areas. An increase between the 5' compared to OSM networks 40% to 94% (≈ factor 2) is observed.

The groundwater withdrawals (renewable groundwater and fossil groundwater) indicate an opposite trend compared to the surface water withdrawals; even though the total water withdrawals decrease. A decrease in total service area fed by a river (towards 5') implied an increase in groundwater withdrawal. The Nile delta shows largest increase from 8% to 60% (≈ factor 6).

Table 5.4: The actual evapotranspiration, the total abstraction, surface water abstraction (SW), renewable groundwater abstraction (RGW) and the fossil groundwater abstraction (FGW) for the raster-based 60, 30, 5' and OSM based networks [mm/year per $m^2$]. Only irrigated areas are included.

| **Location** | | **Actual Evapotran-spiration [mm/year per $m^2$]** | **Total abstraction [mm/year per $m^2$]** | **SW abstraction [% of total]** | **RGW abstraction [% of total]** | **FGW abstraction [% of total]** |
|---|---|---|---|---|---|---|
| | | | Total | Total | Total | Total |
| **the Netherlands** | 60' | 541 | 164 | 83% | 17% | 0% |
| | 30' | 536 | 160 | 75% | 24% | 1% |
| | 5' | 410 | 89 | 71% | 25% | 4% |
| | OSM | 539 | 176 | 81% | 19% | 0% |
| **Nile delta** | 60' | 550 | 407 | 92% | 8% | 0% |
| | 30' | 270 | 279 | 64% | 36% | 0% |
| | 5' | 90 | 56 | 40% | 47% | 13% |
| | OSM | 590 | 391 | 93% | 7% | 0% |
| **Indus basin** | 60' | 762 | 690 | 65% | 32% | 3% |
| | 30' | 690 | 560 | 63% | 32% | 5% |
| | 5' | 677 | 451 | 55% | 38% | 7% |
| | OSM | 701 | 660 | 64% | 33% | 1% |
| **Citarum basin** | 60' | 1180 | 352 | 81% | 19% | 0% |
| | 30' | 1271 | 343 | 80% | 20% | 0% |
| | 5' | 1241 | 201 | 72% | 28% | 0% |
| | OSM | 1270 | 297 | 91% | 9% | 0% |

### 5.4.2 Actual evapotranspiration

Figures 5.5 – 5.8 show the actual evapotranspiration (AET) simulated by PCR-GLOBWB. Table 5.4 shows the average AET in mm/year per $m^2$. AET values are shown for irrigated crops only. The choice of irrigation network affected the AET distribution for all study areas, except the Netherlands.

Comparing the different networks; the 60’ and OSM networks lead to the highest average AET. Although the choice of the irrigation network did not affect the AET distribution for the Netherlands very much, there are large differences observed within the Netherlands. Lowest AET values are observed in the western part of the country.

The choice of irrigation network mostly affected the AET distribution in the Nile delta (figure 5.6). The 30’ and 5’ networks cannot allocate water throughout the delta, resulting in significant water stress. Low AET values are observed at the fringes of the delta, which may be a reflection of the irrigated area, which is less at the fringes. Furthermore, the 60’ and 30’ maps show a high gradient over the cell boundary for the middle of the delta. These boundaries are a result of the different cell sizes that indicate individual irrigation networks. No water is allocated towards its adjacent cell and therefore less AET occurs in the eastern cell. This illustrates the shortcoming of the absence of the link between a river and irrigated areas very well.

For the Indus, high AET values are seen upstream for all maps. However differences arise in the southeastern part of the Upper Indus. The OSM networks show higher AET values compared to the other maps. Downstream, the choice of the irrigation network also affected the AET distribution. Severe water stress is observed for the 30’, 5’ and OSM networks. The 5’ and 30’ maps indicate sharp contrasts between the cell boundaries compared to the 60’ and the OSM maps.

In contrast to the other study areas, the 60’ irrigation networks for the Citarum indicate lowest average AET values for the entire area. The highest AET values have been estimated for the OSM and 30’ networks in the downstream area. However, the differences in AET between the different maps are very small.

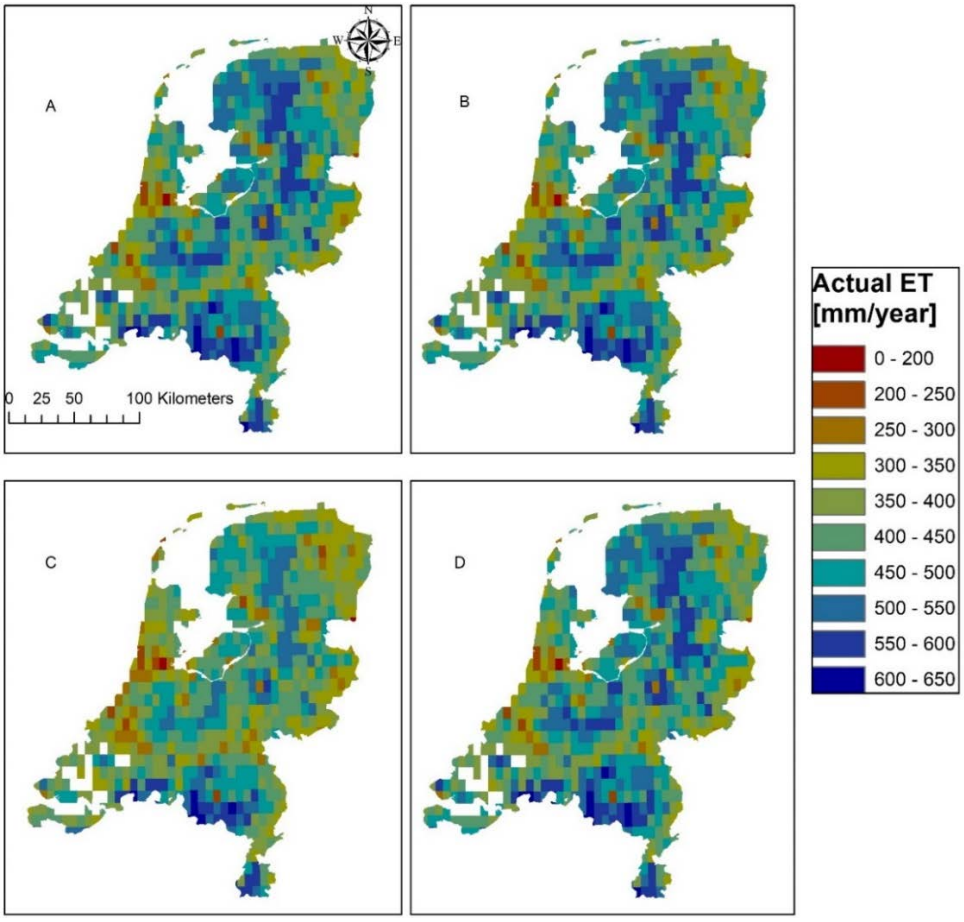


Figure 5.5: The actual evapotranspiration for the Netherlands for the (a) 60’, (b) 30’, (c) 5’ and (d) OSM networks in mm/year.

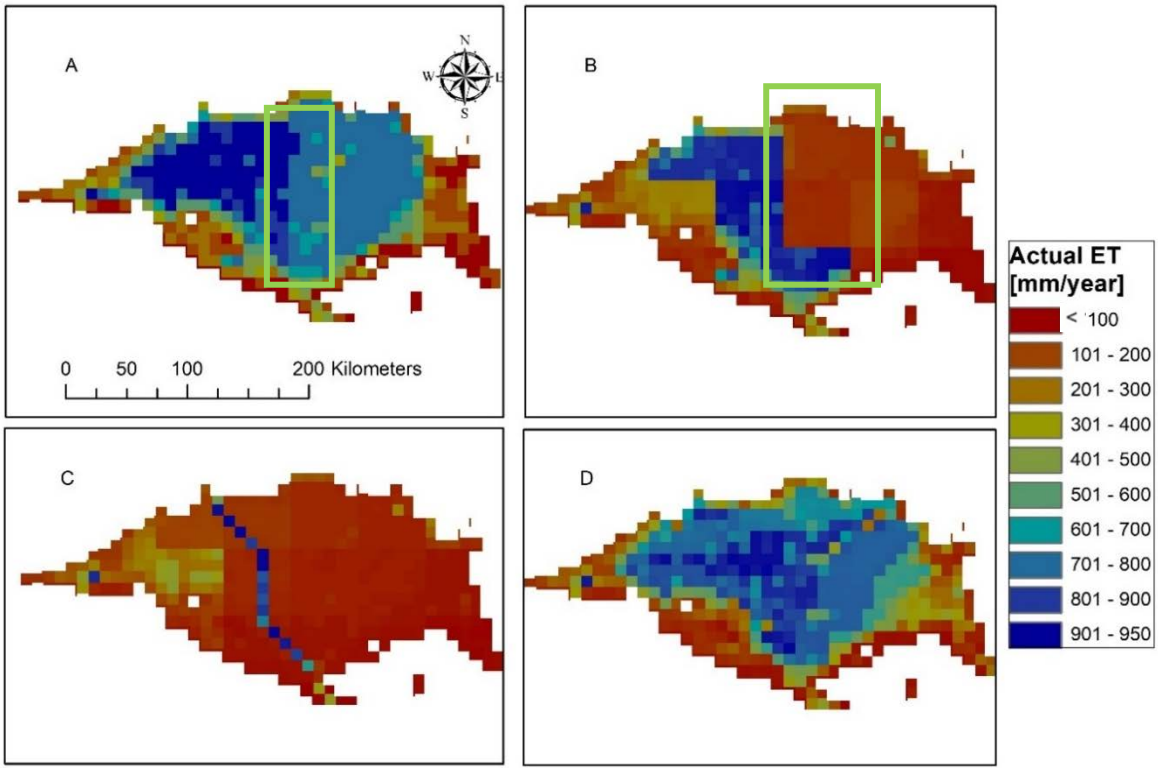


Figure 5.6: The actual evapotranspiration of the Nile (a) 60', (b) 30', (c) 5' and (d) OSM networks in mm/year. The green rectangles indicate the high gradient between the different irrigation networks. No water is allocated towards its adjacent cell and therefore large differences occur.

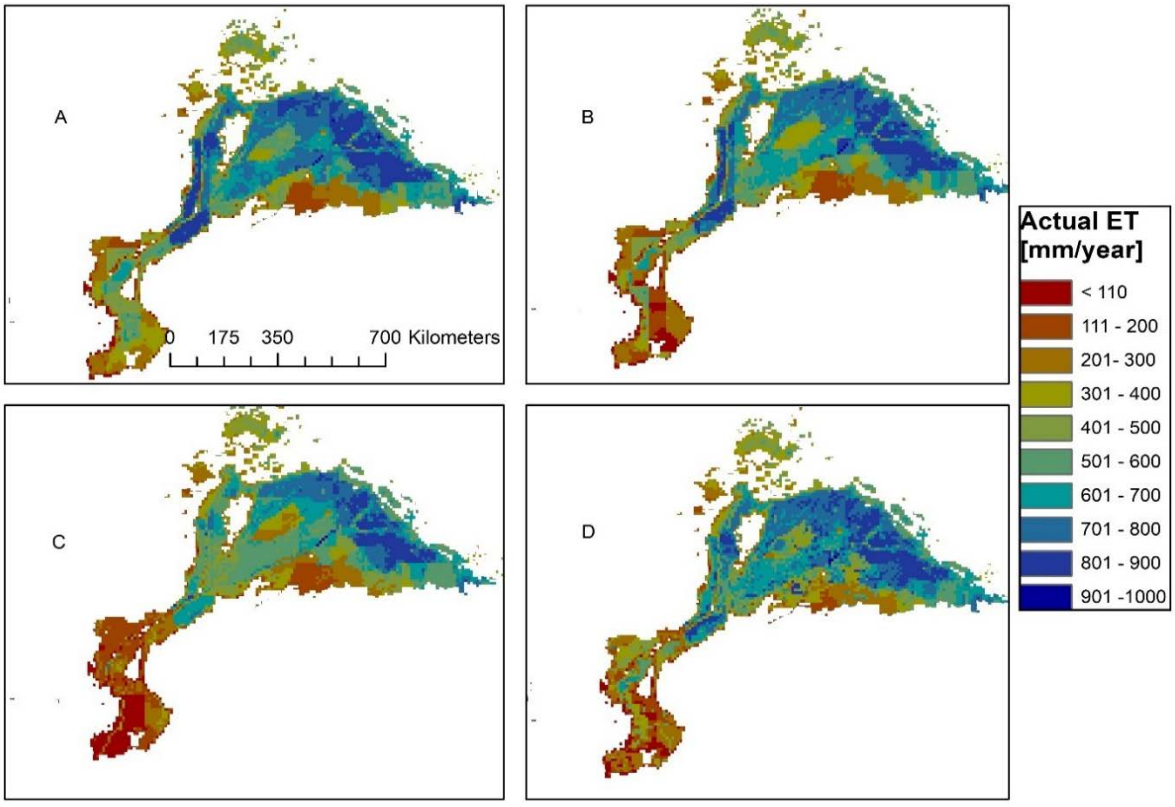


Figure 5.7: The actual evapotranspiration for the Indus basin for the (a) 60', (b) 30', (c) 5' and (d) OSM networks in mm/year.

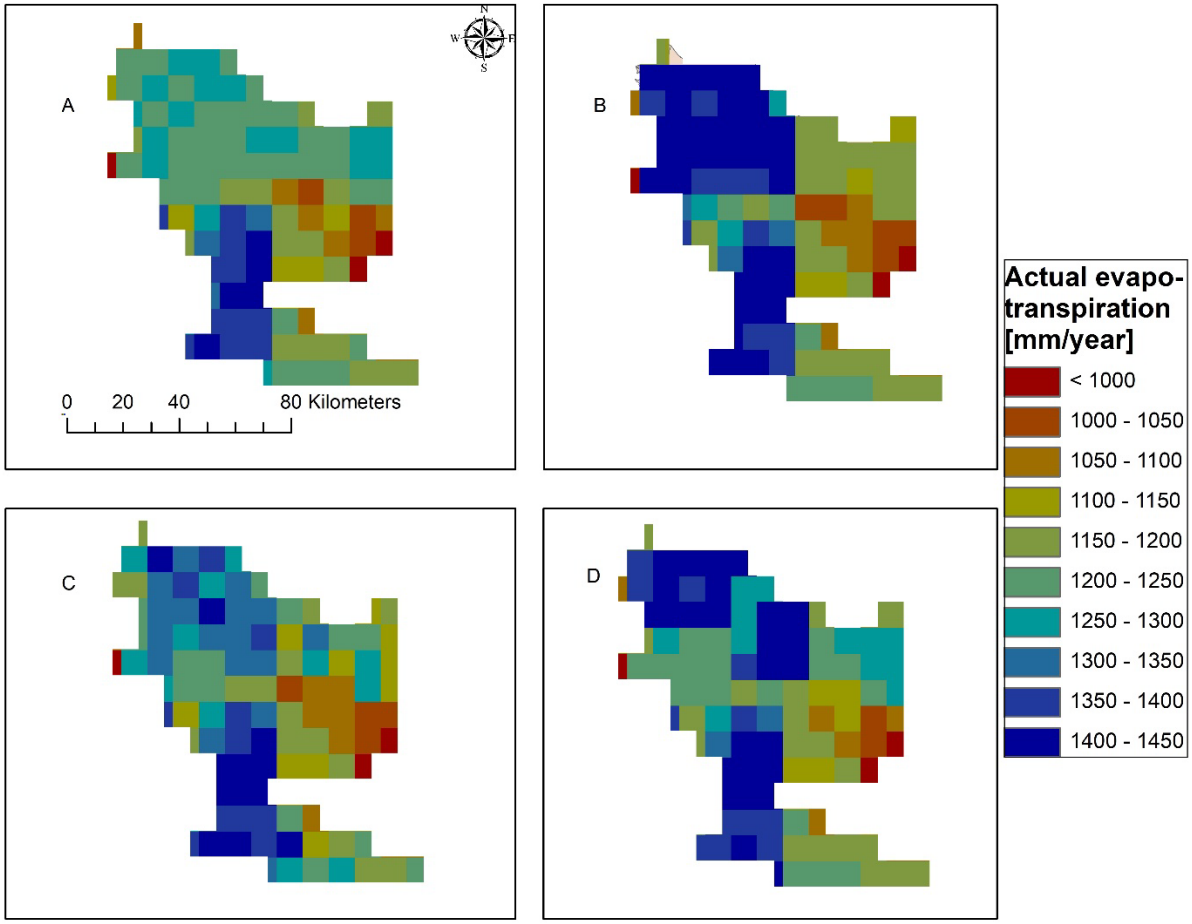


Figure 5.8: The actual evapotranspiration for the Citarum basin for the (a) 60', (b) 30', (c) 5' and (d) OSM networks in mm/year.

### 5.4.3 Discharge at river mouth

Average river discharges at the river mouth have been simulated and analyzed. Overall, the highest average discharges values were estimated for 5' networks (see table 5.5). The 30', OSM and 60' follow. Moreover, the difference between the OSM based and 60' maps are mostly very limited, 1% for both the Netherlands and the Nile delta and 2% for the Indus basin. Nonetheless, the Citarum basin has a large difference of 33%. The largest relative difference between the highest and smallest discharge is observed at the Indus, which highlights the need for a correct irrigation network.

Table 5.5: Discharges at the river mouth for all study areas. The discharges are in $m^3/s$. The discharges from the literature are derived from ([1]van der Most *et al.* (2009) [2] FAO AQAUSTAT [3]Memon and Thapa (2011) [4]Fulazzaky (2010)).

| Irrigation networks | the Netherlands | Nile delta | Indus basin | Citarum basin |
|---|---|---|---|---|
| **60'** | 2,878 | 4,246 | 1,933 | 239 |
| **30'** | 2,902 | 4,430 | 4,709 | 332 |
| **5'** | 3,005 | 5,075 | 5,509 | 351 |
| **OSM** | 2,891 | 4,284 | 1,985 | 318 |
| **Literature** | 2,300[1] | 2,900[2] | 1,955[3] | 80[4] |

## 5.5 Comparison water allocation fractions

To determine the accuracy of the simulations by PCR-GLOBWB, the simulated water allocation fractions of the 60' and OSM networks have been compared to each other. Subsequently, the OSM

fractions are compared to the reported fractions by the GMIA database. Surface water allocation maps are presented and a statistical comparison is performed. The fractions were separated into fractions of surface water, renewable groundwater and fossil groundwater allocations.

### 5.5.1 Fraction of water allocation maps

Figure 5.9 shows for each study area the surface water allocation fraction per 5' cell for OSM, 60' and GMIA irrigated surface areas. The fractions of the 60' and OSM networks are only shown for irrigated crops. Groundwater allocation maps are left out, since groundwater allocation is the one minus the surface water allocation and therefore the same patterns will be simulated. Groundwater allocation maps are shown in Appendix A.

Surface water allocation fractions show similar spatial variation to the AET for the Nile delta, the Indus basin and the Citarum basin. The 60' networks lead to highest average surface water allocation fractions, besides for the Citarum basin. The OSM and 60' networks for the Netherlands look near-identical, however they differ at the Meuse valley and the Veluwe due to the selected elevation threshold for the OSM networks. For both OSM and 60' networks, lower surface water allocation fractions are simulated for the western part of the Netherlands.

In general, the OSM networks performed better compared to the 60' networks in allocating water further away from the river. This is clearly seen for the Nile delta (figure 5.9b). For the Indus basin, the OSM networks indicate large amounts of groundwater use for both upstream and downstream compared to the 60' networks (figure 5.9c). Differences in surface water allocation for the Citarum are mainly seen downstream, whereas more surface water is allocated for the OSM (figure 5.9d).

On the right-hand side of figure 5.9 the reported fractions by the GMIA are shown. The simulated fractions for OSM networks and the reported data differ substantially. They vary spatially most notably in the Netherlands, the southwestern part of the Nile delta, the western part of the Citarum basin and downstream the Indus.

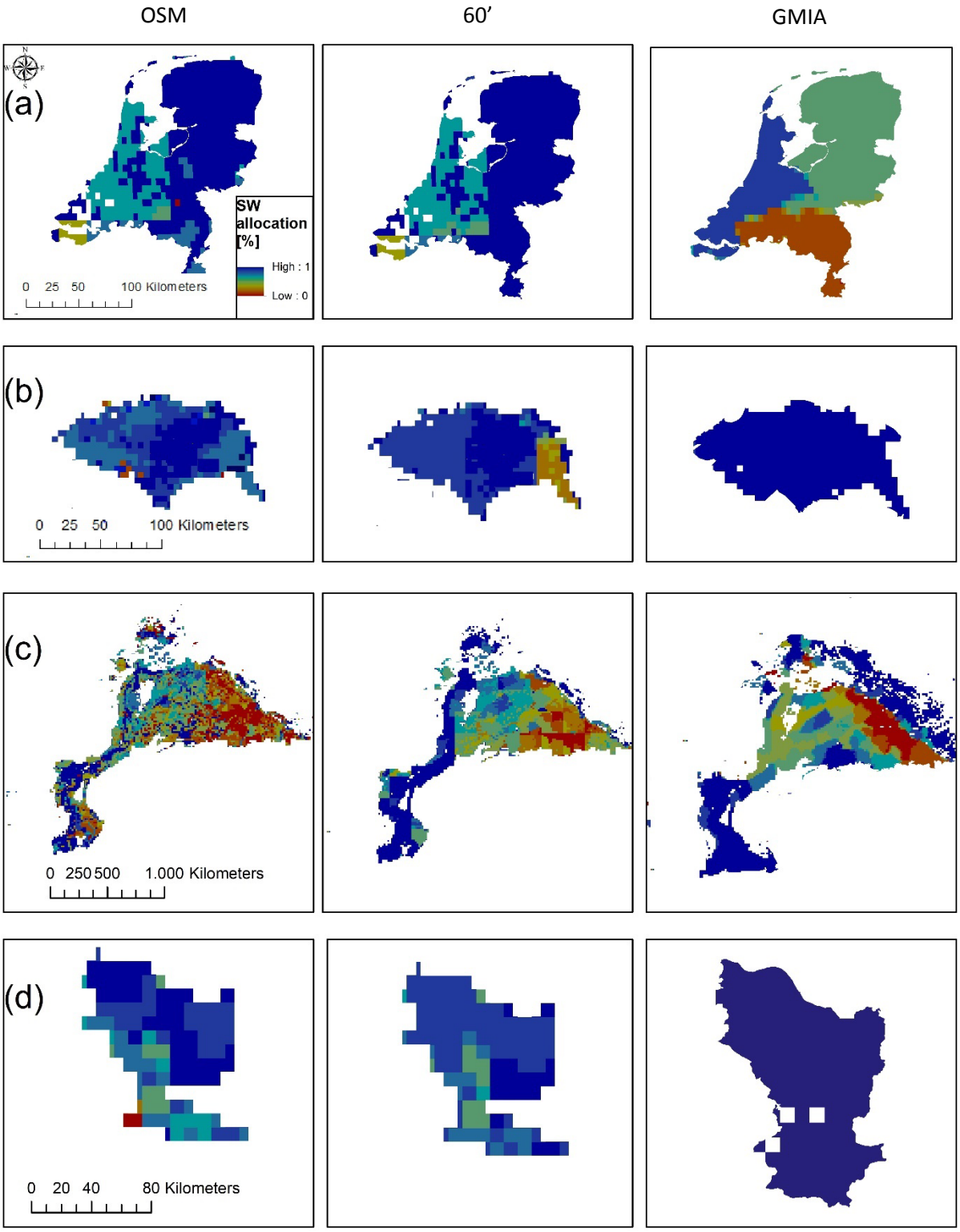


Figure 5.9: Comparison of simulated surface water allocation fractions to the reported values by the GMIA for (a) the Netherlands, (b) the Nile delta, (c) the Indus basin and (d) the Citarum basin. The reported fractions by the GMIA were obtained from the FAO AQUASTAT database.

## 5.5.2 OSM and 60' networks

Figure 5.10 shows the comparisons between the OSM and the 60' networks in plots. The fractions (%) of surface water and renewable groundwater from the OSM networks were plotted against the fractions of the 60' networks. The comparison shows that the OSM based irrigation networks simulated smaller average surface water allocation fractions compared to the 60' networks for the Netherlands, the Citarum basin and the Indus basin. However, for the Nile delta the points are more spread out. The renewable groundwater allocation fractions plots show that the OSM network estimated bigger groundwater allocation fractions for the Netherlands, the Indus basin and the Citarum basin. The Nile delta shows the same predisposition as its surface water fractions.

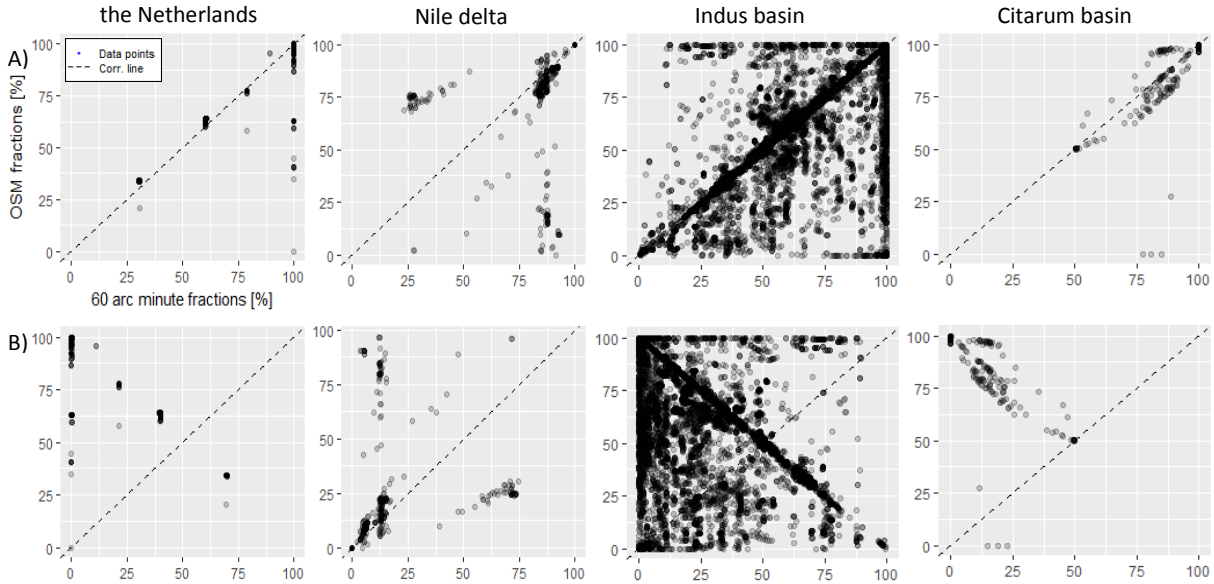


Figure 5.10: Comparison between the estimated fractions of water allocation for OSM based irrigation networks and the 60' raster-based irrigation networks for (a) surface water and (b) renewable groundwater for each study area, simulated by the PCR-GLOBWB model. The dashed lines represent the 1:1 correlation line.

## 5.5.3 Accuracy of OSM simulated water allocation

To estimate the accuracy of the simulated water allocation fractions, the OSM water fractions were compared to the fractions reported by the GMIA (figure 5.11 and table 5.6). The comparison show disagreement for surface water (CC ≤ 0.17 and NSE ≤ -0.77) and groundwater (CC ≤ 0.24 and NSE ≤ -1.4 for renewable groundwater and CC = NA and NSE = NA for renewable groundwater). The OSM networks tend to overestimate surface water fractions for the Netherlands (≈+80%) and the Indus basin (≈+30%) and tend the underestimate for the Nile delta (≈-10%) and the Citarum basin (≈-15%). Groundwater fractions were overestimated by PCR-GLOBWB for all study areas; Citarum basin (≈+400%), the Nile delta (≈+160%), the Netherlands (≈+60) and Indus basin (+50%).

To evaluate whether the OSM data improved the water distribution, the 60' surface water allocation fractions were compared to the GMIA. The comparison showed severe disagreement for both surface water and groundwater compared to the OSM networks for the Netherlands, the Nile delta and the Citarum basin. For detailed information see table 5.6.

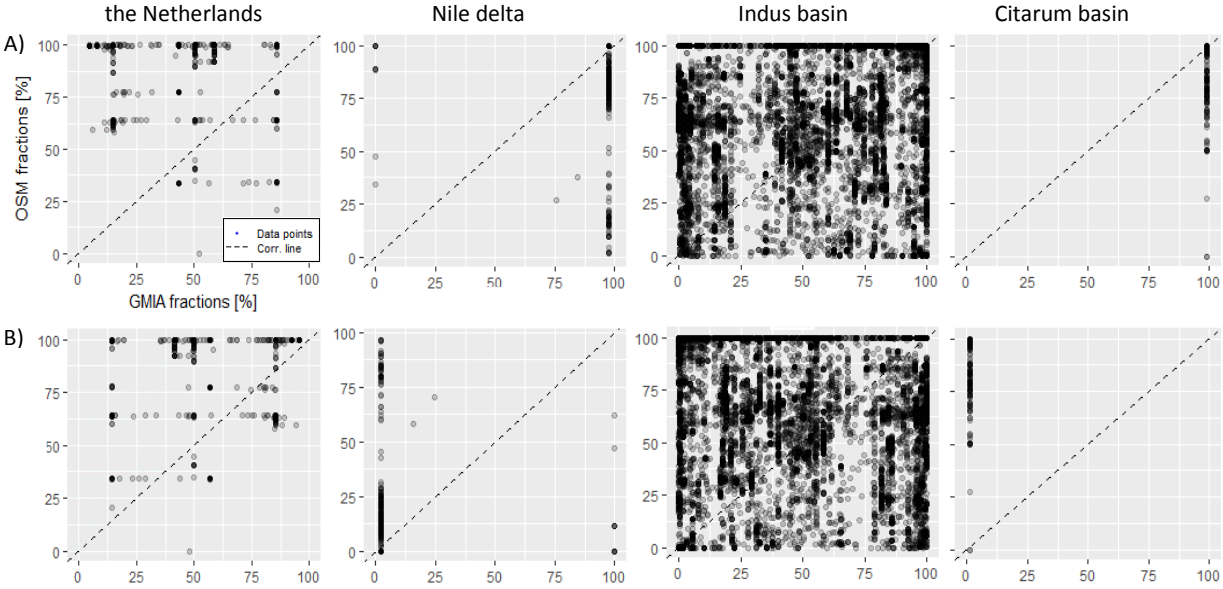


Figure 5.11: Comparison between the estimated fractions of water allocation for OSM based irrigation networks and the reported data for GMIA for (a) surface water and (b) renewable groundwater for each study area. The dashed lines represent the 1:1 correlation line.

Table 5.6: Validation statistics for simulated and reported water withdrawals by the GMIA per source for the Netherlands (N= 850), the Nile delta (N = 600), the Indus basin (N= 2300) and the Citarum basin (N=200). The Pearson correlation coefficient, NSE and Pbias have been presented.

| | | **the Netherlands GMIA** | | | **Nile delta GMIA** | | | **Indus basin GMIA** | | | **Citarum basin GMIA** | | |
|---|---|---|---|---|---|---|---|---|---|---|---|---|---|
| **Source of water** | | CC | NSE | PBias | CC | NSE | PBias | CC | NSE | PBias | CC | NSE | Bias |
| **Surface water** | 60' | 0.04 | -3.5 | 83 | -0.06 | - 4.0 | - 20 | 0.23 | -0.60 | 32 | 0.002 | -4.9 | -16 |
| | OSM | 0.05 | -2.9 | 78 | 0.17 | - 1.5 | - 11 | 0.11 | -0.77 | 40 | 0.07 | -4.8 | -15 |
| **Renewable groundwater** | 60' | 0.21 | -3.5 | 75 | -0.04 | - 3.7 | 340 | -0.01 | -1.1 | -66 | -0.01 | -5.9 | 500 |
| | OSM | 0.24 | -2.1 | 64 | - 0.04 | - 1.5 | 160 | -0.05 | -1.4 | 51 | 0.01 | -5.2 | 400 |
| **Fossil groundwater** | 60' | NA | NA | NA | NA | NA | NA | NA | NA | NA | NA | NA | NA |
| | OSM | NA | NA | NA | NA | NA | NA | NA | NA | NA | NA | NA | NA |

# 6. Discussion & limitations

The choice of an irrigation networks is likely to impact water withdrawal, actual evapotranspiration, river discharge and water allocation. This is because irrigation networks can be used as local water distributor to define a surface water service area (Hanasaki *et al.*, 2018). This study created a method to develop irrigation networks and link them to a river. OSM data and a global DEM were used to determine the shape and size of the networks.

## 6.1 Analyzing OSM irrigation networks

### 6.1.1 Performance irrigation networks

Irrigation networks were created based on OSM data and a global DEM. Average river discharges simulated by PCR-GLOBWB were linked to irrigation networks. This study showed that using OSM data, large irrigation networks can be created that are able to distribute river water over long distances. For the Netherlands, the irrigation networks coincide with the water distribution reported by Arnold (2009). Freshwater for the Northern provinces (Drenthe and Friesland) is mainly received from the IJssel, which originates from the Rhine (Arnold, 2009). The green network in figure 5.1a seems to be able to capture this surface water distribution. The northwestern part of the Netherlands is fed by the Rhine that carries water to North-Holland via the Amsterdam Rhine Canal (Arnold, 2009). This is also illustrated by the OSM networks (highlighted light blue in figure 5.1a). Furthermore, the areas that were assigned to be not connected to the river were reflected by the literature; the Wadden islands get its surface water from other sources, mostly groundwater (Speelman *et al.*, 2009) and the Scheldt provides water to Zeeuws Vlaanderen (Sevencoten and Icbs, 2000). The Scheldt, however is located outside the study area. It can be concluded that, besides some overestimations in the extent of the irrigation networks due to the elevation threshold, the irrigation networks perform well for the Netherlands.

Also the water distribution of the Nile delta showed to be in line with local surface water distributions (Roest, 1999; Oloo, 2010; Nofal *et al.*, 2015). Overall, the irrigation networks follow the irrigation canals shown in figure 3.3. The unconnected irrigated area in the southwest of the delta is probably fed by groundwater, since one of Egypt's groundwater reservoirs, Wadi El Natrun, is located underneath this area (Fattah, 2017).

An extensive irrigation canal network is built over the entire Indus basin (Magsi and Salman, 2012). Nonetheless, there is no good overview of the exact location of these canals available. Figure 3.4 represents the Indus basin with some of its main canals. A direct link between the OSM irrigation networks and the reported canals in figure 3.4 cannot be observed. However, downstream the OSM data represents the so called "Nara Canal" very well. Yet, it is not shown by the networks due to the selected river source. Figure 6.1 illustrates the OSM data at the location of the Nara Canal without a river source on the left side and with the selected river source on the right side. It can be seen that the river source overlaps and thus replaces the OSM irrigation canal. With a river as source, each river cell creates an individual irrigation network. This inaccuracy in river simulation is related to one of the input data layers for PCR-GLOBWB. For the standard parameterization of PCR-GLOBWB the drainage basin is defined using the drainage networks layers derived from HydroSHEDS (Lehner, Verdin and Jarvis, 2008). Flow of water is only allowed within basins; no flow of water is allowed across river basins. This indicates that the watershed divide, which determines the boundary between two river basins (Lehner, Verdin and Jarvis, 2008), may be exactly between these two simulated river sources (right through the Nara Canal). Therefore no water is distributed from the

eastern side towards the Indus river, resulting in an accumulation of water volumes flowing downstream and thus creating its own river.

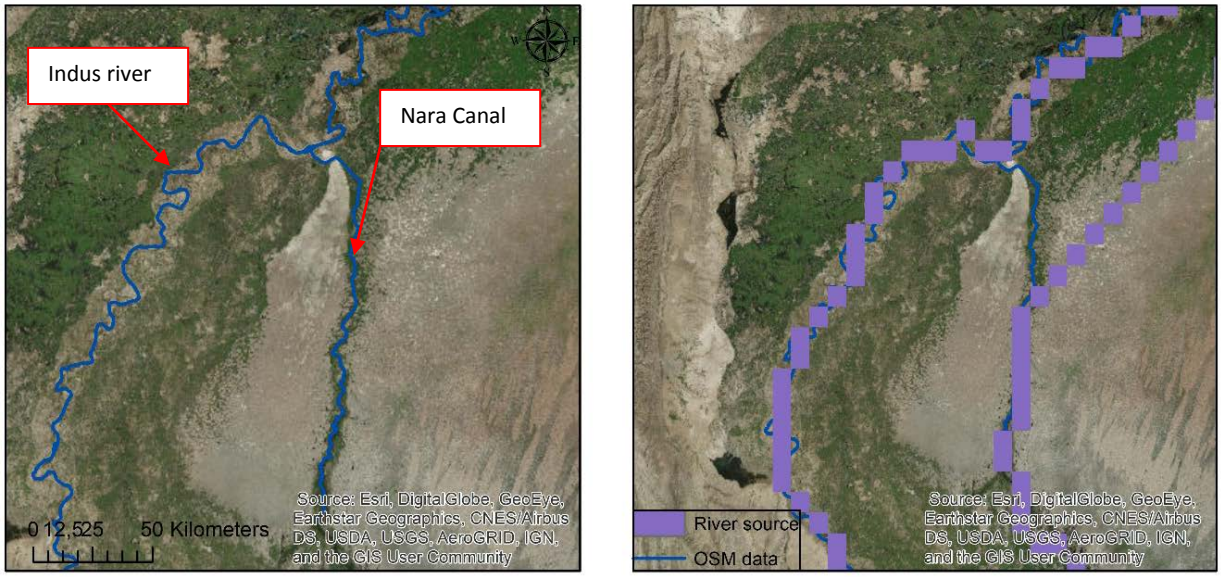


Figure 6.1: Left-hand side: the OSM water data is displayed for the Indus at the Nara Canal, which is located in the middle of the basin. Please note that only relevant OSM water data is shown. Right-hand side: the OSM data is displayed together with the river source.

For the Citarum basin it is hard to validate the created irrigation networks, since no regional data of existing irrigation canals is available. However, dams are often used to distribute water for irrigation purposes and therefore data of dams was used to validate (Ministry of Public Works Indonesia, 2007; Pawitan, Delinom and Taniguchi, 2015). A major dam is built in Jatiluhur (Fulazzaky, 2010), which is exactly at the location of the green area in the middle of the basin (figure 5.2c). Local studies, such as Pawitan, Delinom and Taniguchi (2015) and Fulazzaky (2010) mention that this dam is used as water storage for irrigation purposes and that small irrigation canals receive their water from it. This indicates that even for countries where the OSM data is limited, such as Indonesia, the OSM water data is capable of roughly simulating the water distribution.

### 6.1.2 Limitations and inaccuracies of irrigation networks

In this section we elaborate on some downsides to OSM irrigation networks. First, this study only included rivers as sources for irrigation networks and excluded lakes and reservoirs. This causes a different distribution of surface water in countries that rely on surface water from lakes. In the Netherlands for example the IJsselmeer is one of the main water suppliers for irrigation purposes (Arnold, 2009; Deltaris, 2014). Especially in the context of mapping of irrigation networks on a global scale; lakes and reservoirs are often used for storage of surface water for irrigation purposes (Brouwer *et al.,* 1988); Thachanamoorthy, 2008; Li, Huo and Xu, 2017). The HydroLAKES database can be used to identify lakes that can be used as source for irrigation networks.

Some of the inaccuracies in irrigation networks are caused by modeling errors. First, some irrigation networks were created at a higher elevation than the river source that fed the corresponding network. Examples of issue can be found in the Upper Indus and the upstream part of the Citarum (figure 6.2). These errors are mainly caused by the used spread zone function, which did not account for elevation difference. Consequently, unreliable networks were created. This would be

unexpected, since water must be pumped upwards, leading to high pumping costs. Due to this, these canals are likely to receive their water from another surface source, for instance lakes or rivers with a discharge lower than 5 $m^3/s$. Alternatively, they may represent small streams that originate upstream. Such information on OSM waterways, whether it is a stream or canal, could be added to the description of an OSM segment, which could then be used for further studies. However, this information is often absent.

Second, some irrigation networks show unnatural shapes and boundaries with adjacent networks due to the same spread zone operator. For example, the unnatural shaped networks appear on the southeastern side of the Indus basin (figure 5.2b). This occurs in places where limited or no OSM data is available. The performed spread zone function, used to create networks from the OSM water canals, creates a radial spread wherever OSM data is absent. Consequently, the shape of the irrigation networks is not dependent on local drain directions and thus unrealistic shapes can be created.

A couple of solutions have been considered to avoid this problem. First, elevation data can be used, e.g. the elevation of the cell on which the river relies can be used as maximum height, whereas spreading is only allowed to lower situated areas. This would be an accurate depiction of reality; irrigation canals often follow contour lines, which makes possible the use of gravity to move the water from the river to a network (Brouwer *et al.,* 1988). This might also create the expected concave or v-shaped irrigation networks (FAO, 1985). Second, in addition to the OSM data, the recently developed aqueduct database by Hanasaki *et al.* (2018) can be used for areas where OSM data is limited. This provides another source of data that determines the surface water distribution. However, the mentioned aqueduct project is still at an early stage and the database needs to be expanded in order to provide an accurate depiction of reality (Hanasaki *et al.*, 2018).

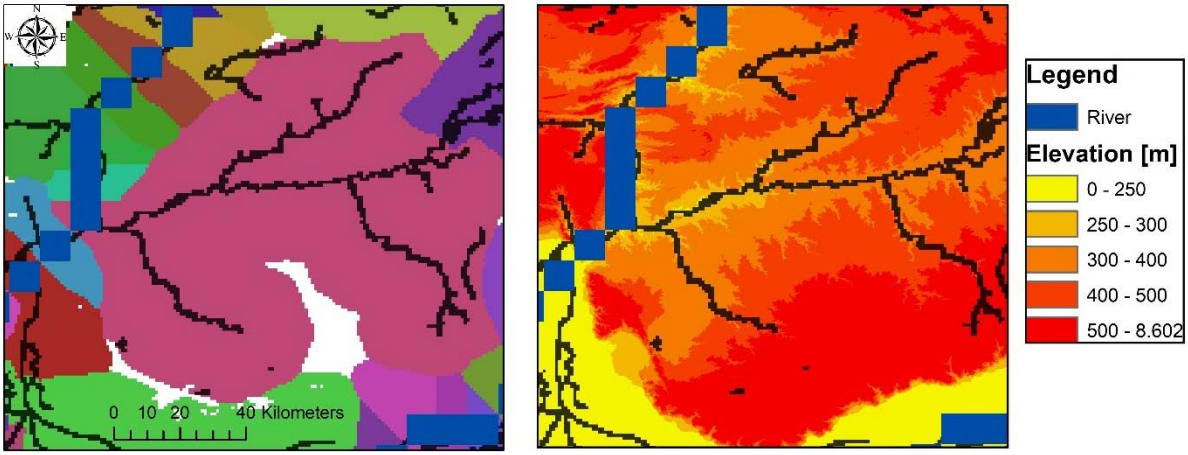


Figure 6.2: (a) Illustration of an irrigation network in the northwestern part of the Indus basin. (b) Represents the according DEM of the region. The large networks in the middle is used as example. This networks receives its water from the river source on the western side. However, looking at figure 6.2b it can be seen that the edges of the irrigation canals are located at a higher elevation than the water serving river.

Moreover, the irrigated areas fed by surface water are probably underestimated due to the elevation threshold, e.g. for the Indus basin and the Citarum basin. This study set a maximum height difference of 10 m between two adjacent cells, which represent a slope of ≈7% at the equator (explained in chapter 4.2). These regions are well known for their terraced paddy fields (Ministry of Public Works, 2007; Fulazzaky, 2010; Nüsser, Schmidt and Dame, 2012). Terraced irrigation allows for

slopes of 25% (FAO, 1985; Brouwer *et al.*, 1988). Selecting a different threshold, for example 20 m that equals a slope of ≈14%, may simulate more reliable results in mountainous regions.

## 6.2 Effect of the definition of the source of surface water on irrigation networks

Analysis of the river discharge has shown that the definition of the river discharge as source has influence on the created irrigation networks. Small discharges created more and smaller networks. the Netherlands, the Indus and the Citarum are dependent on the definition of the source, whereas the Nile delta is not. The Nile river is the only available river source within the area and therefore the chosen discharge does not influence the networks. However, the differences may be only arising because the access to a source becomes limited whenever a minimum discharge is set higher. This is because setting a higher discharge as threshold results in reduced river sources. Since the total surface areas did not change, except from the Indus, larger average irrigation networks were created as a results.

In general, the chosen default discharges showed, for these cases, the best results in terms of the maximum network length. Q100 for the Indus estimated a maximum length of 189 km, which concurs with the results of Qureshi *et al.* (2008) that stated some irrigation networks can be more than 200 km in length. Moreover, the maximum length for the Nile delta was estimated to be 132 km. This is in accordance with the Nubaria Canal, one of Egypt's largest canals that has a length of 130 km (Samuel, 2014). However, these estimated maximum lengths may be higher for the Indus if the river discharge did not overlap the Nara canal (illustrated in figure 5.2) and probably other irrigations, which was discussed in Chapter 6.1.1.

## 6.3 Evaluating OSM networks to GMIA

The created OSM based irrigation networks were compared to the AEI reported by the GMIA. Also the total irrigated surface areas were compared. The results showed that the OSM data is capable to construct irrigation networks. A good agreement in reported extent was observed for the Nile delta and the Indus basin. Overall, the GMIA presents a larger extent of irrigated areas. This can be attributed to the resolution size of the GMIA: irrigated surface area is reported as percentage AEI per 5' cell. So, even though only a small fraction (≥ 1%) of the land area has been irrigated, this whole 5' cell is assigned as irrigated surface area (Siebert *et al.*, 2015). As a consequence, only showing the extent of irrigated areas on 5' cells and not accounting for the percentages AEI of each cell, the GMIA maps overestimates the irrigated extent. This also explains the large differences in the extent and the reported irrigated areas by the GMIA for the Netherlands. However, a real validation of the irrigated surface areas remains difficult. The GMIA has many uncertainties in the reported AEI. It is mainly based on national census statistics, but in developing countries there is often a lack of available information. In these countries, such as Indonesia (poor quality) and Pakistan (fair quality) (Siebert *et al.*, 2013) the reported area is based on many assumptions, which may cause unreliable estimations (Thenkabail *et al.*, 2008). Statistics seem to largely underestimate the irrigated areas in India and Pakistan and slightly overestimate for the Nile delta (Thenkabail *et al.*, 2008; Meier, Zabel and Mauser, 2017). This may be due to the presence of unrecorded illegal wells, boreholes and irrigation canals (Salmon *et al.*, 2015).

Total irrigated surface areas showed a good agreement with the reported AEI by the GMIA for the Nile delta. The Citarum showed acceptable differences. Major differences were observed for

the Netherlands (27,702 $km^2$ for OSM and 4702 $km^2$ for GMIA) and the Indus (356,075 $km^2$ for OSM and 263,000 $km^2$ for GMIA). The differences for the Netherlands are likely caused by the inequality in the definition of irrigated surface area. This study estimated potential irrigated areas, which is defined as the area of land that is potentially irrigable (FAO, 1985). Existing crop extents for example were not accounted for. The FAO reported the AEI, which is defined as the area equipped to provide water to the crops (FAO, 1985). This may be an explanation for the large differences for the Netherlands; a country with limited irrigation (Arnold, 2009). The differences for the Indus, however are more likely to be caused by the prescribed underestimation of the national statistics (Meier, Zabel and Mauser, 2017).

## 6.4 Estimation of the effect of the choice of irrigation networks

### 6.4.1 Water demand

The total water withdrawal for irrigated areas was simulated by the PCR-GLOBWB model. Water withdrawal was divided into surface water, renewable groundwater and fossil groundwater. Surface water withdrawal indicated to be dependent on the choice of the irrigation networks. The 30' and 5' irrigated areas showed significant underestimation of the surface water withdrawal. This indicates that the water demand is not met for the 30' and 5' networks. The 60' and OSM based networks showed larger surface water withdrawals. Using PCR-GLOBWB, first surface water is abstracted and in cases where no surface water is available, groundwater is used (Wada, Van Beek and Bierkens, 2012). Improving the irrigation networks caused an increase in surface water availability (Hanasaki *et al.*, 2018), because the OSM irrigation networks are able to distribute water over a longer distance. This explains the increases in surface water withdrawal. This effect is best seen in arid climate, such as the Nile delta (see table 5.4). Surface water is limited and the availability is totally dependent on the Nile river (Roest, 1999). The estimated surface water withdrawals for the 60' and OSM are accordance with the reported green water consumption by Rost *et al.* (2008), whereas the 30' and 5' show underestimations. Good agreement of these numbers in may indicate good irrigation networks.

The water withdrawal calculated by PCR-GLOBWB is based on all water demands (irrigation, industrial, livestock and domestic). The comparison between the different irrigation networks is thus based on total water abstractions. Improving the area served also increases water withdrawals by the other sectors. This might cause a overestimation of the influence of the choice of networks on the irrigation water withdrawals.

Furthermore, the total water withdrawal and thus the irrigation water withdrawal may be underestimated for the Indus basin and Citarum basin. This may be due to the overestimation of the irrigation efficiency. In the default parameterization of PCR-GLOBWB the irrigation efficiency is set to 71% (Sutanudjaja *et al.*, 2017). Surface irrigation (basin, border and furrow irrigation) is the most common type of irrigation in these regions, with an approximate efficiency of 60% (Brouwer *et al.*, 1988). However, irrigation efficiencies within the Nile delta are increasing rapidly. The network is built, such that irrigation water used upstream can be reused downstream (Roest, 1999). Efficiencies around 80% are estimated in some region in the delta (Gaafar, El-agha and Rap, 2016) and therefore water withdrawals may be overestimated for the Nile delta. The over- or underestimation of the irrigation efficiency may also influence the AET, the discharge and the allocation.

### 6.4.2 Actual evapotranspiration

This study illustrated that the choice of an irrigation network influenced the AET distribution over an area. Significant water stress was observed for both 5' and 30' maps. The 60' and OSM networks showed approximately the same results with highest average AET values (figure 5.5-5.8 and table 5.4). This is related to the connectivity of these networks with the surface water. They distribute water over most of the study area (figure 5.9) and if the area is supply limited, the additional surface water leads to additional AET. The changes in AET are most significant in the Nile delta. This is not evident for the Netherlands, due to lower sun power and large amount of available surface water (KNMI, 2017). However, the Citarum basin shows differences, even though the amount of surface water is evident. This can be related to the size of the study area. The 60' irrigation network indicates less evaporation compared to the other maps, due to the cell size of a 60' cell. One 60' cell is 111 km by 111 km, which is larger than the study area itself and therefore water from the Citarum river can also be distributed to other areas outside the study area. This causes a loss in water availability and thus less AET. The high AET values downstream the Citarum basin for the 30' networks compared to the OSM based networks can be related to urban areas (figure 5.9b&d). In contrast to the 30' networks, the OSM networks consider urban areas and therefore no water is allocated towards these cells, which results in less AET.

Several studies (Rost *et al.,* 2008; FAO, 2012a) report the same distribution of AET compared to the simulated values for OSM networks for Nile delta, the Indus basin and the Citarum basin. However, for the Netherlands the patterns differ. The KNMI and the FAO (2016) report overall higher evaporation values in the western part of the Netherlands, whereas PCR-GLOBWB simulated vice versa. Since AET is highly dependent on the surface water availability (Siebert *et al.*, 2015), the limited amount of surface water allocated towards the western part of the Netherlands may be the reason (figure 4.9). However, the spatial differences in AET may also be related to urban areas. This study computed AET for irrigated crops only, however the irrigated crops extent in PCR-GLOBWB is based on FAOSTAT (FAO, 2012c) irrigated areas. They report the area that is actually irrigated per cell on a 5' resolution. As a consequence, If only 1 ha of this 5' cell is irrigated, this study assumed that the whole cell was irrigated area. There might be small irrigated areas at the edges of a urban area, causing a urban area to be indicated as irrigated area.

### 6.4.3 Discharge at river mouth

Different average discharges at the mouth of the river were simulated and compared. The discharges at the mouth of the river were effected by the water distribution within the study area. The 60' and OSM irrigation networks cause more river water to be distributed towards the irrigation canals and thus resulted in a lower discharge at the river mouth. These networks estimated average discharges similar or closer to the reported discharges in the literature (table 4.5). Discharges are highly overestimated for the 5' and 30' networks, which is caused by the smaller size of the total irrigated surface areas fed by a river source. However, the 60' networks for the Citarum simulated relative small discharges compared to the OSM networks. Again, this is evaluated by the size of the study area, which is explained in Chapter 6.4.2. The discharge at the river mouth of the Indus decreases enormous for the OSM and 60' networks compared to the 30' and 5' networks. This implies that most water is used mid- and downstream, since the irrigated crops in Upper Indus are mostly fed by groundwater (Wada, Van Beek and Bierkens, 2012; Cheema, Immerzeel and Bastiaanssen, 2014).

Overall, the simulated discharge estimates show best results for the Netherlands and the Indus. As in all hydrological assessments, imprecise discharge generations can be a result from meteorological input data (Biemans *et al.*, 2009). In the Netherlands, the CRU data set, on which the

meteorological forcing is based, has a higher station availability that causes more accurate results (Sutanudjaja *et al.*, 2017). The small overestimation in discharge for the Netherlands may be a results of the underestimation of AET in the western part. For the Nile delta and the Citarum basis, large overestimation occurs. Probably due to overestimation of precipitation and underestimation of open water evaporation (van Beek and Bierkens, 2008). Still, regarding the meteorological reliability for the discharge estimates, the simulations by PCR-GLOBWB for the OSM and 60' networks for the Indus and the Netherlands show reliable results compared to the literature.

## 6.5 Evaluating the comparison water fractions against Global Map Irrigated Areas

### 6.5.1 Fraction of water allocation maps

Surface and groundwater water allocation fractions have been simulated by the PCR-GLOBWB model and spatial maps have been presented (figure 5.9). In general, compared to the AET the same distribution is observed for the Indus basin, the Citarum basin and the Nile delta. This is in line with the expectations, since surface water mainly determines the water uses and thus the irrigation water uses (Wada, Wisser and Bierkens, 2014). Although OSM networks for the Indus have shown that their performance in allocating water further away from a river source is improved compared to the 60' networks, still large groundwater allocation fractions are observed in the Upper Indus. This might be explained by the groundwater availability upstream. Extensive groundwater reservoirs are simulated by many GHMs (Wada *et al.*, 2010; Wada, van Beek and Bierkens, 2011) and reported by local studies (Nüsser, Schmidt and Dame, 2012; Cheema, Immerzeel and Bastiaanssen, 2014). Due to these groundwater reservoirs, irrigated crops are mostly fed by groundwater instead of surface water. This also explains why the choice of the network did not affect the AET distribution in the Upper Indus. However, the OSM networks at downstream part of the Indus basin show significant differences in surface water allocation compared to the 60' networks and the GMIA. These differences are probably caused by resampling of the OSM networks to a bigger resolution. The OSM networks were created on a 30 arcseconds resolution, whereas the current version of PCR-GLOBWB allows a finest resolution of 5'. Resampling causes a loss of accuracy, which in this case means that the irrigation networks might become unconnected to the river (figure 6.3). As a consequence, no river water is allocated towards these networks an therefore groundwater is used and a significant water stress is observed (figure 5.7). This is not seen at other study areas, however, it might become problematic, when mapping globally.

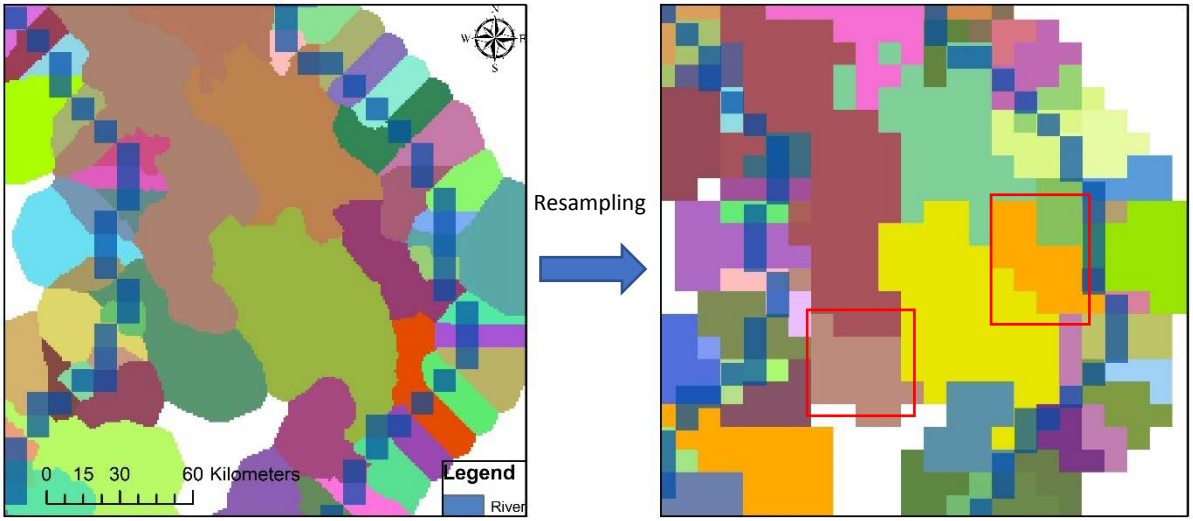

Figure 6.3: Left-hand side: the irrigation networks for the downstream part of the Indus basin at a 30 arcseconds resolution. Right-hand side: the irrigation networks after resampling of the original data to a 5' resolution. The red squares indicate examples of areas the became unconnected to the river source.

For the Netherlands, differences in surface water allocation fractions were observed in the western part of the country. These estimates do not reflect the surface water withdrawals reported by the Dutch government and local authorities (Arnold, 2009). Within PCR-GLOBWB surface water and groundwater allocation is simulated based on daily baseflow that is established by the long-term average discharge and the number of available upstream and local water reservoirs (Wada, Wisser and Bierkens, 2014). Simulated baseflow is used to interpret the extrable groundwater volumes. This assumption might be realistic in arid regions that mainly use groundwater to meet the demands. However, groundwater withdrawal is managed in many developed countries and this water management, for example pumping regulations, is not accounted for in PCR-GLOBWB (Wada, Wisser and Bierkens, 2014). Therefore it might overestimate the amount of groundwater used in areas that mainly rely on surface water, even though groundwater is available (e.g., the Netherlands).

### 6.5.2 OSM and 60' networks

The irrigation networks based on 60' areas simulated higher average fractions of surface water allocation compared to the OSM based irrigation networks. However, the 60' irrigation networks have the tendency to overestimate the water served surface area. This implies that some cells receive surface water, yet no link with a river is present. This is well illustrated for the Nile delta, whereas no other river source is nearby and the 60' networks do not estimate higher average surface water allocation (figure 5.10). For the renewable groundwater volume fractions, the OSM estimated larger average fractions. A possible explanation could be that due to the elevation threshold for the OSM networks, some areas will receive less surface water. The resulting gap to meet the water demand is then met by groundwater (Sutanudjaja *et al.*, 2017). As a consequence, the fraction of groundwater that is been allocated increases. Furthermore, the 60' networks might simulate larger availabilities of groundwater. Consequently, if the groundwater withdrawal for both 60' and OSM network is approximately the same, then the fraction of groundwater allocation decreases. This may could the explanation for the Citarum where the OSM networks show higher average groundwater allocation (figure 4.10), yet smaller groundwater withdrawals are estimated (table 5.4)

### 6.5.3 Accuracy of fraction of water allocation

The OSM volume fractions per water source for each cell, simulated by the PCR-GLOBWB model, have been validated against the data reported by the GMIA. These two were in disagreement with each other (CC ≤ 0.17 and NSE ≤ -0.77). One of the main reasons could be the difference in the extent of irrigated areas. PCR-GLOBWB reports the allocation fractions to some extent which does not have to be the same for the GMIA. This can be seen in the southeast of the Indus basin (figure 5.9), whereas the GMIA reported a greater extent. This might lead to comparisons of cells with no data values to cells with data values, resulting in a bad correlation.

As already captured in Chapter 6.3 the GMIA has many uncertainties in AEI, and so does the water source for irrigation. In most countries, data on water fractions is limited (Siebert *et al.*, 2013; Meier, Zabel and Mauser, 2017). It has many assumptions and one of its major assumptions that might bias the comparison for groundwater fractions is the fact that in some countries the AEI with groundwater was indicated as 100 or 0 percent (Siebert *et al.*, 2013). Subnational data was not used in these countries. This has been recognized for the renewable groundwater, whereas the GMIA only reported 0 values for entire study areas. Second, the GMIA reports that areas with integrated use of groundwater and surface water were assigned with 50 percent to AEI with groundwater and 50 percent to AEI with surface water whenever there was no data on this ratio (Siebert *et al.*, 2015). These assumptions are likely to cause inaccuracies in the irrigation water uses per water source (Salmon *et al.*, 2015).

Moreover, the reference years of the estimated fraction of water source of irrigation can be different between both PCR-GLOBWB and the GMIA (Siebert *et al.*, 2013). The GMIA presents reference irrigated area maps around 2005 and for some countries only information around 1995 is available. This study estimated irrigated areas around 2010. Taking these uncertainties into account, a validation of surface water allocation (per source) remains difficult due to a lack of reliable information in many regions of the world ( Siebert *et al.*, 2013; Wada, Wisser and Bierkens, 2014).

However, a general positive correlation is seen using OSM data compared to the raster-based 60' networks. This is not observed for the Citarum basin. This may be related to the map quality of the GMIA. Very poor map quality is reported for Indonesia (Siebert *et al.*, 2013).

# 7. Conclusions

OSM data and a global DEM were used to create irrigation networks that were linked to a river source. This study showed that using OSM data, large irrigation networks can be created that are able to distribute river water over long distances. OSM data was capable of constructing irrigation networks that followed the local water distribution quite well. Areas that were indicated as irrigated areas, but were not connected a river source were most likely fed by groundwater.

The definition of the surface water source showed to affect the irrigation networks. Setting a low threshold for minimum discharge, such as 5 $m^3/s$, simulated more and smaller irrigation networks compared to higher discharges. No characteristic shapes were identified as a result of changing the minimum discharge threshold. The Nile delta, however, was not affected, since the Nile was the only selected surface water source within this area. Largest length of an irrigation canal was estimated for the Indus (183 km). These canals are probably larger if the accuracy of the selected river discharge is improved.

The created networks showed to be in good agreement with the extent of irrigated areas reported by the GMIA for the Nile delta and the Indus basin. The main differences for the Citarum basin and the Netherlands occurred to the selected elevation threshold. The total irrigated surface area of the OSM networks were comparable to the areas reported by the GMIA. However, significant overestimation was estimated for the Netherlands.

The simulation by the PCR-GLOBWB model showed to be dependent on the choice of the irrigation networks for all four parameters; water demand, actual evapotranspiration, discharge at the river mouth and fraction of water allocation. The OSM networks showed to improve the water distribution and therefore more surface water is available compared to the 30’ and 5’ networks. This resulted in an increase in total withdrawal, which were mostly caused by the increase surface water withdrawal. This indicated that water demands were not met for the 30’ and 5’ networks. However the water withdrawals may be under- or overestimated due to the default irrigation efficiency. Actual evapotranspiration showed a more reliable spatial distribution for the OSM data based irrigation networks. This was best seen in arid regions, such as the Nile delta. Discharge at the river mouth was highly overestimated for 30’ and 5’ maps and slightly overestimated using the 60’ and OSM based irrigation networks.

Surface water allocations fractions are probably overestimated by the 60’ networks due to the overestimation of the network size. It does not account for elevation and therefore water might be allocated towards higher located regions. The OSM networks showed an improvement for the Nile delta and the Citarum. For the Netherlands, however, several factors that determine the water allocation within PCR-GLOBWB might cause an underestimation of surface water allocation towards the western part of the country. Resampling of the OSM networks caused an accuracy loss that resulted in sever water stress in the downstream part of the Indus. The simulated volume fractions per water source for each cell were in bad agreement with the Global Map of Irrigated Areas for both Pearson correlation coefficient and Nash-Sutcliffe efficiency. Surface water fractions were overestimated for the Indus and the Netherlands and underestimated for the Nile delta and the Citarum. However, this can partly be explained by the uncertainties of the GMIA. However, a general positive trend in correlation is seen using OSM data compared to the raster-based 60’ networks. This indicates that the OSM networks may be an improvement of the currently used allocation scheme.

# 8. Recommendations

First of all, to improve the method based on OSM data, a regional DEM can be used to determine local drain directions. Using these LLD affects the water distribution from the river towards the irrigation canals and from the irrigation canals towards the irrigated fields. This affects the shape and extent of the irrigation networks and avoids unnatural shapes and boundaries between the networks. This may results in concave (in deltas) or v-shaped networks (in mountainous areas), which are expected.

Second, the used urban area data can be improved. This study used OSM data for buildings to determine urban area. However, a good quality map of the urban extent would increase the quality of the irrigation networks. This can also be provided by the OSM database, whereas the density of the data is increasing every day (Haklay, 2010). Alternatively, global land cover maps based on remote sensing can be used, e.g. GlobCover (Bontemps *et al.*, 2011) or Global Land Cover (GLC) (Latham *et al.*, 2014).

Third, using different river source data. The current LDD allows no bifurcation of the river network and therefore only the main streams are computed. Improving a LLD to make bifurcations possible, would increase the quality of the river discharge as source. Furthermore, in this study only rivers are included to function as source for the irrigation networks. However, lakes for example can also function as surface water source for irrigation purposes. Using a different database as the river source, such as data from the Worldbank 2 data based on SRTM Plus elevation (http://www.naturalearthdata.com/downloads/) or HydroSHEDS recently released HydroLAKES (Lehner and Messager, 2017), and combine this with OSM data would improve the irrigation networks.

Fourth, this study developed a method to create irrigation networks based on four case studies. Subsequently, irrigation networks can be mapped globally.

Last but not least, improvement of the accuracy and completeness of the OSM would increase the quality of the irrigation networks. Whenever the OSM is complete, some of the previously mentioned recommendation are then mainly accounted for.

# 9. References


Allam M.N., El Gamal F., H. M. (2005) 'Irrigation Systems Performance in Egypt', *Series A – Mediterranean Seminars, No. 52, Irrigation systems performance*, 98, p. 85–98.

Allen, R. G. *et al.* (1998) 'Crop evapotranspiration - Guidelines for computing crop water requirements - FAO Irrigation and drainage paper 56', *Irrigation and Drainage*, p. 1–15. doi: 10.1016/j.eja.2010.12.001.

Arnold, G. (2009) 'Waterhuishouding en waterverdeling in Nederland', *Ministerie van Verkeer en Waterstaat, Directoraat-Generaal Water en Rijkswaterstaat, Waterdienst* , p. 43. Available at: http://edepot.wur.nl/3254

Asawa, L. A. (2008) 'Irrigation and Water Resources Engineering', pp. 3–7. doi: 10.1017/CBO9781107415324.004.

Barrington-Leigh, C. and Millard-Ball, A. (2017) 'The world's open-source street map is more than 80% complete', *Plos One*, 12(8), p. e0180698. doi: 10.1371/journal.pone.0180698.

Van Beek, L. P. H. 'Forcing PCR-GLOBWB with CRU data', Tech. rep., Department of Physical Geography, Utrecht University, Utrecht, The Netherlands, http://vanbeek.geo.uu.nl/suppinfo/vanbeek2008.pdf, 2008.van Beek, L. P. H. and

Van Beek, L.P.H., Bierkens, M. F. P. (2008) 'The Global Hydrological Model PCR-GLOBWB: Conceptualization, Parameterization and Verification', *Department of Physical Geography*, p. 53. Available at: http://vanbeek.geo.uu.nl/suppinfo/vanbeekbierkens2009.pdf.

van Beek, L. P. H., Wada, Y. and Bierkens, M. F. P. (2011) 'Global monthly water stress: 1. Water balance and water availability', *Water Resources Research*, 47(7). doi: 10.1029/2010WR009791.

Biemans, H. *et al.* (2009) 'Effects of Precipitation Uncertainty on Discharge Calculations for Main River Basins', *Journal of Hydrometeorology*, 10(4), p. 1011–1025. doi: 10.1175/2008JHM1067.1.

Biswas, A. K. (1983) 'Long-distance water transfer: a Chinese case study and international experiences. Tycooly International Publishing Ltd.', Chapter 2(3), p. 1–16, ISBN-10: 0907567525

Bontemps, S. *et al.* (2011) 'GLOBCOVER 2009 Products Description and Validation Report', *ESA Bulletin*, 136, p. 53. doi: 10013/epic.39884.d016.

Brouwer, C. *et al.* (1988) 'Irrigation water management: irrigation methods', *Training manual*, 9(5), pp. 5–7, p 14-20. Available at: http://www.fao.org/docrep/s8684e/s8684e00.htm

Cheema, M. J. M., Immerzeel, W. W. and Bastiaanssen, W. G. M. (2014) 'Spatial quantification of groundwater abstraction in the irrigated indus basin', *Groundwater*, 52(1), p. 25–36. doi: 10.1111/gwat.12027.

Delrieu, G. *et al.* (2005) 'The Catastrophic Flash-Flood Event of 8–9 September 2002 in the Gard Region, France: A First Case Study for the Cévennes–Vivarais Mediterranean Hydrometeorological Observatory', *Journal of Hydrometeorology*, 6(1), p. 34–52. doi: 10.1175/JHM-400.1.

Deltaris (2014) 'Irrigatiewater - Locatie beregeningsonttrekkingen uit grondwater en oppervlaktewater', p. 1–5. Available at: https://data.overheid.nl/data/dataset/irrigatiewater-locatie-beregeningsonttrekkingen-uit-grondwater-en-oppervlaktewater.

Doll, P. and Siebert, S. (2002) 'Global modeling of irrigation water requirements', *Water Resources Research*, 38(4), p. 1–10. doi: 10.1029/2001WR000355.

Droogers, P. *et al.* (2012) 'Modeling water resources trends in Middle East and North Africa towards 2050', *Hydrology and Earth System Sciences Discussions*, 9(4), p. 4381–4416. doi: 10.5194/hessd-9-4381-2012.

FAO (1985) 'Land evaluation for irrigated agriculture'.

FAO (2007) *Gridded Livestock of the World*, *Organization*. doi: 10.1017/CBO9781107415324.004.

FAO (2011) 'Indus river basin', *Aquastat*, p. 1–14.

FAO (2012a) 'Food and Agricultural Organisation of the United Nations (FAO AQUASTAT) - Information System on Water and Agriculture TABLE 5 (from report " Irrigation water requirement and water withdrawal by country " , November 2012)' , p. 4446.

FAO (2012b) 'Food and Agriculture Organization of the United Nations: FAOSTAT statistics database. Global map of yearly actual evapotranspiration - 5 arc minutes', p. 2018. Available at: http://www.fao.org/geonetwork/srv/en/main.home.

FAO (2012c) *Food and Agriculture Organization of the United Nations: FAOSTAT statistics database*. doi: 9789251073179.

FAO (2016) 'Food and Agricultural Organisation of the United Nations (FAO AQUASTAT) - Information System on Water and Agriculture', p. 1–8. Available at: http://www.fao.org/nr/water/aquastat/main/index.stm.

Farr, T. *et al.* (2007) 'The shuttle radar topography mission', *Reviews of Geophysics*, 45(2005), p. 1–33. doi: 10.1029/2005RG000183.1.

Fattah, M. (2017) 'Evaluation of Water Resources in Wadi El Natrun Western Desert, Egypt', (1), p. 329–349. doi: 10.22161/ijeab/2.1.42.

Fipps, G. and Dainello, F. J. (2015) 'Vegetable Growers Handbook Chapter V Irrigation', p. 41-60 ISBN: 978-0-471-73828-2

Fulazzaky, M. A. (2010) 'Water quality evaluation system to assess the status and the suitability of the Citarum river water to different uses', *Environmental Monitoring and Assessment*, 168(1–4), p. 669–684. doi: 10.1007/s10661-009-1142-z.

Gaafar, I., El-agha, D. E. and Rap, E. (2016) 'Irrigation Efficiency and the Nile Delta Water Balance', (October 2017). doi: 10.13140/RG.2.2.24418.43208.

Global Administrative Areas (GADM) (2017). Assessed on [06-11-17] at: https://gadm.org/maps.html

De Graaf, I. E. M. *et al.* (2014) 'Dynamic attribution of global water demand to surface water and groundwater resources: Effects of abstractions and return flows on river discharges', *Advances in Water Resources*. Elsevier Ltd, 64, pp. 21–33. doi: 10.1016/j.advwatres.2013.12.002.

Gupta, H. V. *et al.* (2009) 'Decomposition of the mean squared error and NSE performance criteria: Implications for improving hydrological modelling', *Journal of Hydrology*. Elsevier B.V., 377(1–2), p. 80–91. doi: 10.1016/j.jhydrol.2009.08.003.

Haddeland, I. *et al.* (2014) 'Global water resources affected by human interventions and climate change', *Proceedings of the National Academy of Sciences*, 111(9), p. 3251–3256. doi: 10.1073/pnas.1222475110.

Haklay, M. (2010) 'How good is volunteered geographical information? A comparative study of OpenStreetMap and ordnance survey datasets', *Environment and Planning B: Planning and Design*,

37(4), pp. 682–703. doi: 10.1068/b35097.

Hanasaki, N. *et al.* (2008) 'An integrated model for the assessment of global water resources – Part 1: Model description and input meteorological forcing', *Hydrology and Earth System Sciences*, 12(4), p. 1007–1025. doi: 10.5194/hess-12-1007-2008.

Hanasaki, N. *et al.* (2018) 'A global hydrological simulation to specify the sources of water used by humans', *Hydrology and Earth System Sciences*, 22(1), p. 789–817. doi: 10.5194/hess-22-789-2018.

Harding, D. J. and Carabajal, C. C. (2005) 'ICESat waveform measurements of within-footprint topographic relief and vegetation vertical structure', *Geophysical Research Letters*, 32(21), p. 1–4. doi: 10.1029/2005GL023471.

HOT Humanitarion OpenStreetMap Team (2016) 'Explore How the World is Mapped with OSM Analytics', p. 2016–2019. Assessed on [19-02-18] at: https://hotosm.org/updates/2016-04-28_explore_how_the_world_is_mapped_with_osm_analytics.

Hunger, M. and Doll, P. (2008) 'Value of river discharge data for global-scale hydrological modeling', *Hydrology and Earth System Sciences*, 12(3), p. 841–861. doi: 10.5194/hess-12-841-2008.

IPCC (2014) 'Climate Change 2014: Synthesis Report', *Contribution of Working Groups I, II and III to the Fifth Assessment Report of the Intergovernmental Panel on Climate Change. In: Core Writing Team, Pachauri RK, Meyer LA (eds) IPCC, Geneva, Switzerland, 151 p.*, p. 1–112. doi: 10.1017/CBO9781107415324.

Kabat, P. *et al.* (2004) 'Vegetation, water, humans, and the climate : a new perspective on an interactive system', *Global change--the IGBP series,* p. 566 doi: 10.1007/978-3-642-18948-7.

Karssenberg, D. *et al.* (2010) 'A software framework for construction of process-based stochastic spatio-temporal models and data assimilation', *Environmental Modelling and Software*. Elsevier Ltd, 25(4), p. 489–502. doi: 10.1016/j.envsoft.2009.10.004.

Khanal, P. R. (2003) 'Participation and governance in Local water Management', *Wageningen University, Netherlands. Irrigation and Water Engineering group*, pp. 1–9. Available at: http://centralasia.iwlearn.org/dokumenty/project-docs-ru/component-tajikistan-ru/national-training-materials/files/Khanal.Participation and governance in Local water Management.pdf.

Kharagpur (2012) 'Design of Irrigation Canals', p. 1–28. ISBN-10: 1845938747

Latham, J. *et al.* (2014) 'Global Land Cover SHARE (GLC-SHARE) Database Beta-Release Version 1.0-2014', *Food and Agric. Organ. of the UN, …*, p. 1–39. Available at: http://www.fao.org/uploads/media/glc-share-doc.pdf.

Lehner, B. and Messager, M. (2017) 'HydroLAKES. Technical Documentation Version 1.0', (December), p. 16. doi: 10.1038/ncomms13603.

Lehner, B., Verdin, K. and Jarvis, A. (2008) 'HydroSHEDS Technical Documentation', p. 1–27. Available at: http://hydrosheds.cr.usgs.gov.

Li, X., Huo, Z. and Xu, B. (2017) 'Optimal allocation method of irrigationwater from river and lake by considering the fieldwater cycle process', *Water (Switzerland)*, 9(12). doi: 10.3390/w9120911.

Magsi, H. and Salman, A. (2012) 'The Indus water distribution in Sindh, Pakistan : management, impacts and conflicts', *Agricultural Journal*, 7(6), p. 382–387. doi: 10.3923/aj.2012.382.387.

Martel, M. *et al.* (2018) 'Simulation of actual evapotranspiration from agricultural landscapes in the

Canadian Prairies', *Journal of Hydrology: Regional Studies*. Elsevier, 15(December 2017), p. 105–118. doi: 10.1016/j.ejrh.2017.11.010.

McDonald, R. I. *et al.* (2014) 'Water on an urban planet: Urbanization and the reach of urban water infrastructure', *Global Environmental Change*, 27(1), p. 96–105. doi: 10.1016/j.gloenvcha.2014.04.022.

Meier, J., Zabel, F. and Mauser, W. (2017) 'Extending global irrigation maps – going beyond statistics', *Hydrology and Earth System Sciences Discussions*, (April), p. 1–16. doi: 10.5194/hess-2017-156.

Memon, J. A. and Thapa, G. B. (2011) 'The Indus irrigation system, natural resources, and community occupational quality in the delta region of Pakistan', *Environmental Management*, 47(2), p. 173–187. doi: 10.1007/s00267-010-9569-0.

van der Most, H. *et al.* (2009) 'Towards sustainable development of deltas , estuaries and coastal zones Trends and responses : executive summary', *Aquaterra conference*, p. 39.

MPWI (2007) 'Ministry of Public Works Indonesia: Integrated Citarum Water Resources Management Project (Financed by the Technical Assistance Special Fund)', *Report on Roadmap and Program Development*, (January 2007).

Nash, J. E. and Sutcliffe, J. V (1970) 'River Flow Forecasting Through Conceptual Models Part I-a Discussion of Principles*', *Journal of Hydrology*, 10, p. 282–290. doi: 10.1016/0022-1694(70)90255-6.

Nofal, E. R. *et al.* (2015) 'Delineation and modeling of seawater intrusion into the Nile Delta Aquifer: A new perspective', *Water Science*. National Water Research Center, 29(2), p. 156–166. doi: 10.1016/j.wsj.2015.11.003.

National Programme On Technology Enhanced Learning, (2016) 'Lesson 3: Canal Systems for Major and Medium Irrigation'.

Nüsser, M., Schmidt, S. and Dame, J. (2012) 'Irrigation and development in the upper indus Basin: Characteristics and recent changes of a socio-hydrological system in central Ladakh, India', *Mountain Research and Development*, 32(1), p. 51–61. doi: 10.1659/MRD-JOURNAL-D-11-00091.1.

Oloo, a (2010) 'The quest for cooperation in the Nile Water Conflicts: The case of Eritrea', *African Sociological Review / Revue Africaine de Sociologie*, 11(1), p. 95–105. doi: 10.4314/asr.v11i1.51447.

OSM (2015) 'OpenStreetMap Data Extracts', assesses on [20-09-2017] at: http://download.geofabrik.de/)

Pawitan, H., Delinom, R. and Taniguchi, M. (2015) 'The human-environment sustainability in Indonesia : case of the Citarum basin', (November 2016). Available at: https://www.researchgate.net/publication/286238800.

Portmann, F. T., Siebert, S. and Döll, P. (2010) 'MIRCA2000-Global monthly irrigated and rainfed crop areas around the year 2000: A new high-resolution data set for agricultural and hydrological modeling', *Global Biogeochemical Cycles*, 24(1), doi: 10.1029/2008GB003435.

Qureshi, A. S. *et al.* (2008) 'Managing salinity and waterlogging in the Indus Basin of Pakistan', *Agricultural Water Management*, 95(1), p. 1–10. doi: 10.1016/j.agwat.2007.09.014.

Roest, C. W. J. (1999) 'Regional water distribution in the Nile Delta of Egypt', *ILRI Workshop: water and food security in (semi-) arid ares*, (Figure 1), p. 61–82. Available at: http://agris.fao.org/agris-search/search/display.do?f=2001/NL/NL01032.xml;NL2001002127.

Salmon, J. M. *et al.* (2015) 'Global rain-fed, irrigated, and paddy croplands: A new high resolution map derived from remote sensing, crop inventories and climate data', *International Journal of Applied Earth Observation and Geoinformation*. Elsevier B.V., 38, p. 321–334. doi: 10.1016/j.jag.2015.01.014.

Samuel, M. G. (2014) 'Limitations of navigation through Nubaria canal , Egypt', *Journal of Advanced Research*. Cairo University, 5(2), p. 147–155. doi: 10.1016/j.jare.2013.01.006.

Samuelsen, A., Hansen, C. and Wehde, H. (2015) 'Tuning and assessment of the HYCOM-NORWECOM V2.1 biogeochemical modeling system for the North Atlantic and Arctic oceans', *Geoscientific Model Development*, 8(7), p. 2187–2202. doi: 10.5194/gmd-8-2187-2015.

Schaphoff, S. *et al.* (2018) 'LPJmL4 - A dynamic global vegetation model with managed land - Part 1: Model description', *Geoscientific Model Development*, 11(4), p. 1343–1375. doi: 10.5194/gmd-2017-146.

Sevencoten, F. V. A. N. and Icbs, V. (2000) 'De internationale commmissie voor de bescherming van de Schelde', Referatenboek 4de Scheldesymposium: De sterke schouders van het Scheldebekken (deel I) Brussel : VZW Water, Energie en Leefmilieu, 1998. - p. 338-342 Themanummer van: Water : tijdschrift over waterproblematiek, Jrg. 17, 103.

Shiklomanov, I. A. (2000) 'Appraisal and assessment of world water resources', *Water International*, 25(1), pp. 11–32. doi: 10.1080/02508060008686794.

Siebert, S. *et al.* (2010) 'Groundwater use for irrigation - A global inventory', *Hydrology and Earth System Sciences*, 14(10), p. 1863–1880. doi: 10.5194/hess-14-1863-2010.

Siebert, S. *et al.* (2013) 'Update of the digital global map of irrigation areas to version 5', *Rheinische Friedrich-Wilhelms-Universituy, Bonn, Germany and Food and Agriculture Organization of the United Nations, Rome, Italy*, p. 171. doi: 10.13140/2.1.2660.6728.

Siebert, S. *et al.* (2015) 'Historical Irrigation Dataset (HID)', *Hydrology and Earth System Sciences*, 19, pp. 1521–1545. doi: 10.13019/M20599.

Siebert, S. and Döll, P. (2008) 'The Global Crop Water Model (GCWM): Documentation and first results for irrigated crops', *Frankfurt Hydrology Paper*, (07), p. 42. doi: 10.13140/2.1.1218.8809.

Sitch, S. *et al.* (2003) 'Evaluation of ecosystem dynamics, plant geography and terrestrial carbon cycling in the LPJ dynamic global vegetation model', *Global Change Biology*, 9(2), p. 161–185. doi: 10.1046/j.1365-2486.2003.00569.x.

Speelman, H. *et al.* (2009) 'De ontwikkeling van het waddengebied in tijd en ruimte', 2017 (November 2015), p. 108. Available at: http://eems.pbworks.com/w/file/fetch/39541216/2009-02_De_ontwikkeling_van_het_waddengebied_in_tijd_en_ruimte.pdf.

Sutanudjaja, E. H. *et al.* (2017) 'PCR-GLOBWB 2: a 5 arc-minute global hydrological and water resources model', *Geoscientific Model Development Discussions*, (December), p. 1–41. doi: 10.5194/gmd-2017-288.

Thenkabail, P. *et al.* (2008) 'A Global Irrigated Area Map (GIAM) Using Remote Sensing at the End of the Last Millennium, Water Management', doi: 10.13140/RG.2.1.4945.0087.

UNEP (2000) 'Global Perspectives: United Nations Environment Programme (UNEP), Global Environmental Outlook 2000, Earthscan, London, 1999.', p. 2–3.

United Nations (2013) 'The Millennium Development Goals Report', *United Nations*, p. 68. doi: ISBN

978-92-1-101284-2.

Vorosmarty, C. J. *et al.* (2005) 'Millennium Ecosystem Assessment Volume 1: Conditions and Trends, chap. 7: Freshwater ecosystems, Island Press, Washington DC, USA, 165–1115 207, 2005.

Wada, Y. *et al.* (2010) 'Global depletion of groundwater resources', *Geophysical Research Letters*, 37(20), p. 1–5. doi: 10.1029/2010GL044571.

Wada, Y., van Beek, L. P. H. and Bierkens, M. F. P. (2011) 'Modelling global water stress of the recent past: on the relative importance of trends in water demand and climate variability', *Hydrology and Earth System Sciences*, 15(12), p. 3785–3808. doi: 10.5194/hess-15-3785-2011.

Wada, Y., Van Beek, L. P. H. and Bierkens, M. F. P. (2012) 'Nonsustainable groundwater sustaining irrigation: A global assessment', *Water Resources Research*, 48(1). doi: 10.1029/2011WR010562.

Wada, Y., Wisser, D. and Bierkens, M. F. P. (2014) 'Global modeling of withdrawal, allocation and consumptive use of surface water and groundwater resources', *Earth System Dynamics*, 5(1), p. 15–40. doi: 10.5194/esd-5-15-2014.

Weber, P. and Haklay, M. (2008) 'User-Generated Street Maps', p. 12–18. doi: 10.1109/MPRV.2008.80.

Xiao, X. *et al.* (2006) 'Mapping paddy rice agriculture in South and Southeast Asia using multi-temporal MODIS images', *Remote Sensing of Environment*, 100(1), p. 95–113. doi: 10.1016/j.rse.2005.10.004.

Yamazaki, D. *et al.* (2017) 'A high-accuracy map of global terrain elevations', *Geophysical Research Letters*, 44(11), pp. 5844–5853. doi: 10.1002/2017GL072874.

Yuan, F. *et al.* (2017) 'Assessment of GPM and TRMM multi-satellite precipitation products in streamflow simulations in a data sparse mountainous watershed in Myanmar', *Remote Sensing*, 9(3). doi: 10.3390/rs9030302.

# Appendix A

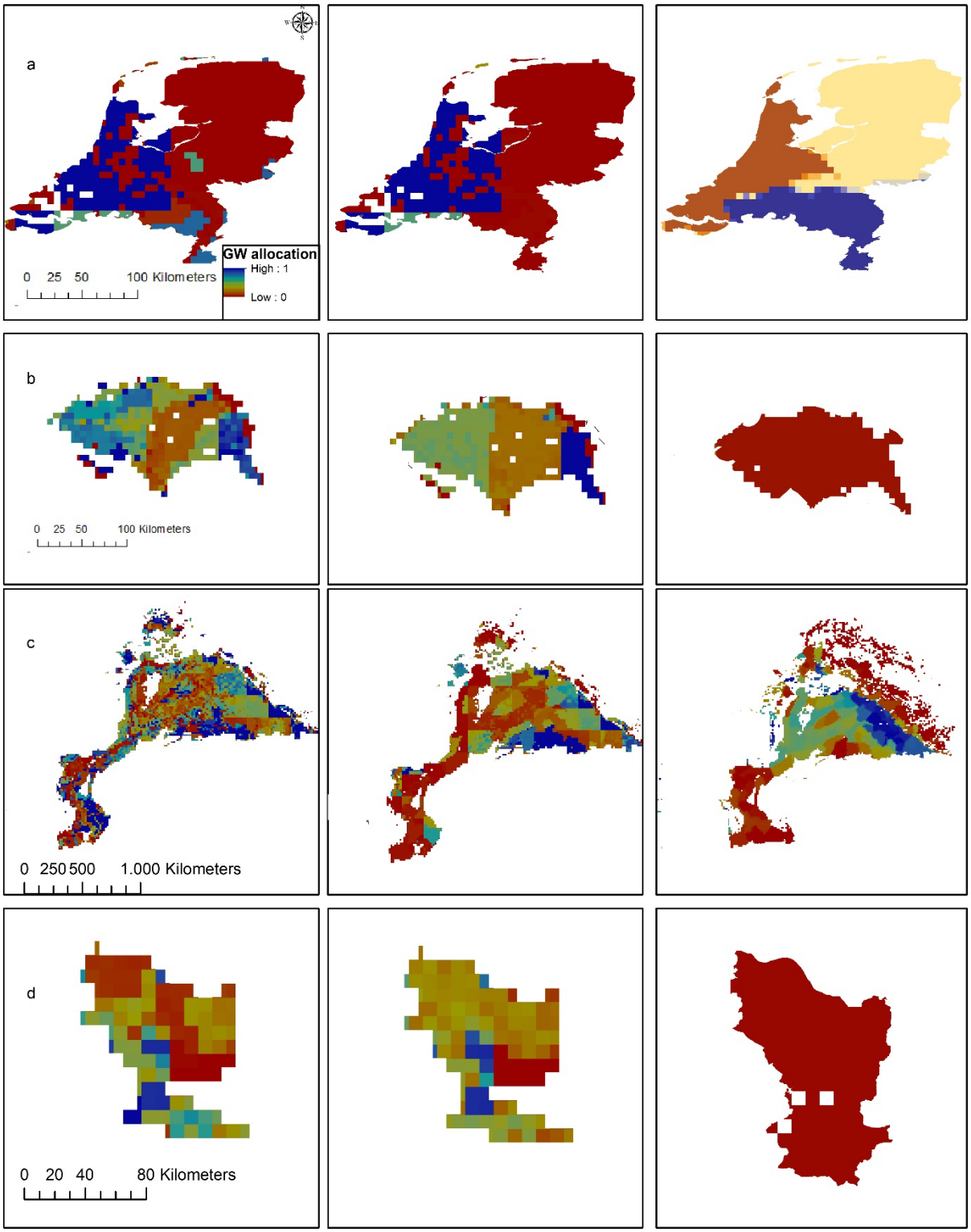


Figure A1: Comparison of simulated groundwater allocation fractions to the reported values of the GMIA for (a) the Netherlands, (b) the Nile delta, (c) the Indus basin and (d) the Citarum basin. The reported fractions of the GMIA were obtained from the FAO AQUASTAT database.

# Appendix B

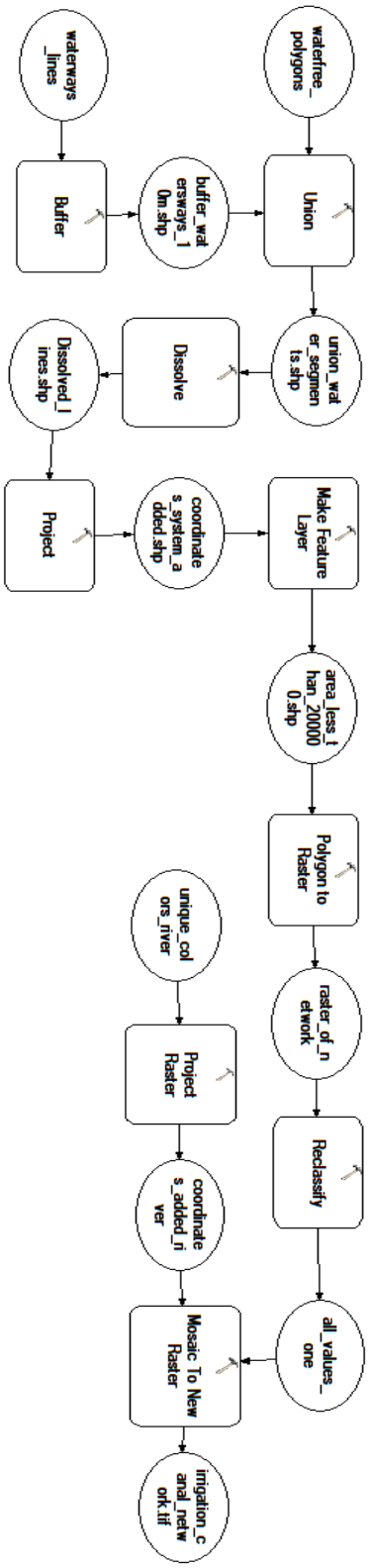


Figure B1, modelling framework extracting irrigation canal network, within ArcGIS.

# Appendix C

## The modeling code

Author: Masterthesis Ian van Zaanen
Studentnumber: 5960819
1th supervisor: dr. Menno Straatsma
2nd supervisor: dr. Rens van Beek

```
"""
import pcraster as pcr
import numpy as np
import numpy.ma as ma
import os, glob, string, subprocess, time, datetime, math, random
import geopandas as pd
import sys
import pandas as pd

#%% import maps and set workspace
root_dir = os.getcwd()
input_dir = os.path.join(root_dir, 'Documents\Universiteit\Masterthesis\Network\Input')
scratch_dir = os.path.join(root_dir, 'scratch')

#%% Chapter 4.1 Develop irrigation networks (also modelbuilder provided in Appendix A)
#Import arcpy module
import archook #The module which locates arcgis
archook.get_arcpy()
import arcpy

#check spatial analyst

if arcpy.CheckExtension("Spatial") == "Available":
  arcpy.AddMessage("Checking out Spatial")
  arcpy.CheckOutExtension("Spatial")
else:
  arcpy.AddError("Unable to get spatial analyst extension")
  arcpy.AddMessage(arcpy.GetMessages(0))
  sys.exit(0)
#overwrite
arcpy.env.overwriteOutput = True

# Local variables:
boundary = r'C:\\Users\\Ian\\Documents\\Universiteit\\Masterthesis\\Network\\scratch\\clip_boundary.tif'
waterways = r'C:\\Users\\Ian\\Documents\\Universiteit\\Masterthesis\\Arcgis_thesis\\Egypte\\waterways.shp'
buffer_waterways = "C:\\Users\\Ian\\Documents\\Universiteit\\Masterthesis\\Network\\scratch\\buffer_waterways.shp"
water_free = r'C:\Users\Ian\Documents\Universiteit\Masterthesis\Arcgis_thesis\Egypte\water_free.shp'
union_shp = "C:\\Users\\Ian\\Documents\\Universiteit\\Masterthesis\\Network\\scratch\\union.shp"
union_Dissolve_shp = "C:\\Users\\Ian\\Documents\\Universiteit\\Masterthesis\\Network\\scratch\\union_Dissolve.shp"
union_Dissolve_Project_shp =
"C:\\Users\\Ian\\Documents\\Universiteit\\Masterthesis\\Network\\scratch\\union_Dissolve_Project.shp"
union_Project_shp__2_ = union_Dissolve_Project_shp
area_300000 = "area_300000"
rasterize = "C:\\Users\\Ian\\Documents\\Universiteit\\Masterthesis\\Network\\scratch\\area_raster.tif"
area30000 = "C:\\Users\\Ian\\Documents\\Universiteit\\Masterthesis\\Network\\scratch\\area300000_1"
irrigation_canals.tif = area30000
```

```
# Process: Buffer
arcpy.Buffer_analysis(waterways, buffer_waterways, "15 Meters", "FULL", "ROUND", "NONE", "", "PLANAR")

# Process: Union
arcpy.Union_analysis("C:\\Users\\Ian\\Documents\\Universiteit\\Masterthesis\\Network\\scratch\\buffer_waterways.shp
#;water_free #", union_shp, "ALL", "", "GAPS")

# Process: Dissolve
arcpy.Dissolve_management(union_shp, union_Dissolve_shp, "osm_id", "", "MULTI_PART", "DISSOLVE_LINES")

# Process: Project
arcpy.Project_management(union_Dissolve_shp, union_Dissolve_Project_shp,
"PROJCS['World_Mollweide',GEOGCS['GCS_WGS_1984',DATUM['D_WGS_1984',SPHEROID['WGS_1984',6378137.0,298.257
223563]],PRIMEM['Greenwich',0.0],UNIT['Degree',0.0174532925199433]],PROJECTION['Mollweide'],PARAMETER['False_Ea
sting',0.0],PARAMETER['False_Northing',0.0],PARAMETER['Central_Meridian',0.0],UNIT['Meter',1.0]]", "", "",
"NO_PRESERVE_SHAPE", "", "NO_VERTICAL")

# Process: Add Geometry Attributes
arcpy.AddGeometryAttributes_management(union_Dissolve_Project_shp, "AREA", "", "SQUARE_METERS",
"PROJCS['World_Mollweide',GEOGCS['GCS_WGS_1984',DATUM['D_WGS_1984',SPHEROID['WGS_1984',6378137.0,298.257
223563]],PRIMEM['Greenwich',0.0],UNIT['Degree',0.0174532925199433]],PROJECTION['Mollweide'],PARAMETER['False_Ea
sting',0.0],PARAMETER['False_Northing',0.0],PARAMETER['Central_Meridian',0.0],UNIT['Meter',1.0]]")

# Process: Make Feature Layer
arcpy.MakeFeatureLayer_management(union_Project_shp__2_, area_30000, "\"POLY_AREA\" > 30000", "", "osm_id
osm_id VISIBLE NONE;POLY_AREA POLY_AREA VISIBLE NONE")

# Process: Polygon to Raster
arcpy.PolygonToRaster_conversion(area_30000, "FID", area_raster1, "MAXIMUM_COMBINED_AREA", "NONE", "15")

# Process: Reclassify
arcpy.Reclassify_3d(area_raster1, "VALUE", "0 54 1;54 146 1;146 210 1;210 267 1;267 760 1;760 1207 1;1207 1414 1;1414
1990 1;1990 4147 1", area30000, "DATA")

# Process: Project Raster
arcpy.ProjectRaster_management(clip_dem0, clip_dem0_ProjectRaster1_tif,
"PROJCS['World_Mollweide',GEOGCS['GCS_WGS_1984',DATUM['D_WGS_1984',SPHEROID['WGS_1984',6378137.0,298.257
223563]],PRIMEM['Greenwich',0.0],UNIT['Degree',0.0174532925199433]],PROJECTION['Mollweide'],PARAMETER['False_Ea
sting',0.0],PARAMETER['False_Northing',0.0],PARAMETER['Central_Meridian',0.0],UNIT['Meter',1.0]]", "NEAREST",
area30000, "", "",
"GEOGCS['GCS_WGS_1984',DATUM['D_WGS_1984',SPHEROID['WGS_1984',6378137.0,298.257223563]],PRIMEM['Greenwi
ch',0.0],UNIT['Degree',0.0174532925199433]]")

# Process: Mosaic To New Raster
arcpy.MosaicToNewRaster_management("C:\\Users\\Ian\\Documents\\Universiteit\\Masterthesis\\Network\\scratch\\cli
p_dem0_ProjectRaster1.tif;C:\\Users\\Ian\\Documents\\Universiteit\\Masterthesis\\Network\\scratch\\area300000_1",
scratch, "irrigation_canals.tif", "", "8_BIT_UNSIGNED", "", "1", "FIRST", "FIRST")

###### tif raster to PCraster file
e = os.path.join(input_dir,'file.tif')
print os.path.isfile(e)
#tranlate DEM from tif file to map (pcraster format)
cmd = 'gdal_translate -ot Float32 -of PCRaster %s file.map' % e
print cmd
subprocess.call(cmd, shell=True)
```

```
###### irrigation area
#read rivernetwork from ArcGIS and give same id's as river source

rivernetwork = pcr.readmap('riversMap.map')
ordinal_map = pcr.ordinal(rivernetwork)
spreadzonemap_rivers = pcr.spreadzone(ordinal_map,0,1)
rivermap_colors = pcr.ifthen(spreadzonemap_rivers > 0, spreadzonemap_rivers)
pcr.report(rivermap_colors, 'riverMap_color.map')

#calculate the area equipped for irrigation based on elevation differences (dem)
 '''
 maximum difference of 10 m in elevation is used to calculate what area is
 equipped for irrigation
 '''
dem = pcr.readmap('dem.map')
changesouth = dem - pcr.shift(dem, 1, 0)
changewest = dem - pcr.shift(dem, 0, -1)
changeeast = dem - pcr.shift(dem, 0, 1)
changenorth = dem - pcr.shift(dem, -1, 0)
change = pcr.ifthenelse(pcr.pcror(pcr.pcror(changesouth > 2, changewest > 2), pcr.pcror(changeeast > 2, changenorth > 2)),
pcr.scalar(1), 0)
pcr.aguila(change)

#### merge area equipped for irrigation with the coloured river network
cmd = 'gdal_warp -cutline elev.tif -crop_to_cutline -dstalpha riverMap_color.tif river_AOI_elev.tif'
  print cmd
  subprocess.call(cmd, shell=True)

###### irrigation networks according to the area equipped for irrigation
irrAreaSource = pcr.readmap('river_AOI_elev.map')
ordinalmap = pcr.ordinal(irrAreaSource)
spreadzoneSource1 = pcr.spreadmaxzone(ordinalmap,0,1,0.2)
spreadzoneSource = pcr.ifthen(spreadzoneSource1 > 0, spreadzoneSource1)
pcr.aguila(spreadzoneSource)
pcr.report(spreadzoneSource, 'IrrMap_AOI.map')

##################################AOI#############################################
AOI = 'nile'

if AOI == 'nile':
  dem = pcr.readmap('dem_nile.map')
  rivers_1km = pcr.readmap('egypt_network1000.map')
  irrAreaSource = pcr.readmap('irrArea_nile1km_withsource.map')

if AOI == 'indus':
  dem = pcr.readmap('dem_indus.map')
  rivers_1km = pcr.readmap('indus_network1000.map')
  irrAreaSource = pcr.readmap('irrArea_indus1km_withsource.map')

if AOI == 'netherlands':
  dem = pcr.readmap('dem_ned.map')
  rivers_1km = pcr.readmap('ned_network1000.map')
  irrAreaSource = pcr.readmap('irrArea_ned1km_withsource.map')

if AOI == 'indonesia':
  dem = pcr.readmap('dem_indo.map')
```

```
 rivers_1km = pcr.readmap('indo_network1000.map')
 irrAreaSource = pcr.readmap('irrArea_indo1km_withsource.map')

#%% Chapter 4.2 calculate average area of irrigation networks
zones = pcr.readmap('IrrMap_AOI.map')
extent = pcr.ifthen(zones > 0, pcr.scalar(1))
total = pcr.maptotal(extent)
pcr.aguila(zones)
area = pcr.areatotal(extent, pcr.nominal(zones))

zones_a1D = pcr.pcr2numpy(zones, -9999).flatten()
dist_a1D = pcr.pcr2numpy(extent, -9999).flatten()

data = {'zones' : zones_a1D,
   'dist' : dist_a1D}
df = pd.DataFrame(data)
df = df[(df.zones > 0) & (df.dist > 0)]
grps = df.groupby('zones').max()

print grps.mean()
print grps.max()
print grps.head()

#### Calculate the average maximum disstance and maximum distance
pcr.setclone('dem.map')
river = pcr.readmap('rivers_1km.map')
irrigationSystem = pcr.readmap('IrrMap_AOI.map')

cellLength = pcr.scalar(6.9)
pcr.setglobaloption('unitcell')
clone = pcr.cover(pcr.ifthen(pcr.boolean(river), pcr.boolean(1)), pcr.boolean(1))
distCollector = pcr.ifthen(clone == 0, pcr.scalar(1))
canalIDs = np.sort(np.unique(pcr.pcr2numpy(irrigationSystem, -9999)))
for ID in canalIDs[1:]:
 pcrID = pcr.nominal(int(ID))
 selectedSystem = pcr.nominal(irrigationSystem) == pcrID
 points  = pcr.ifthen(selectedSystem, river)
 extent  = pcr.ifthen(selectedSystem, pcr.boolean(0))
 points  = pcr.cover(points, pcr.scalar(extent))
 friction = pcr.ifthenelse(selectedSystem, cellLength, cellLength**2)
 IDDistance = pcr.spread(pcr.nominal(points), 0, friction)
 distCollector = pcr.cover(distCollector, IDDistance)
pcr.aguila(IDDistance)
pcr.aguila(distCollector)

zones_a1D = pcr.pcr2numpy(irrigationSystem, -9999).flatten()
dist_a1D = pcr.pcr2numpy(distCollector, -9999).flatten()
data = {'zones' : zones_a1D,
   'dist' : dist_a1D}
df = pd.DataFrame(data)
df = df[(df.zones > 0) & (df.dist > 0)]
grps = df.groupby('zones').max()

print grps.max()
print grps.mean()
print grps.head()
```